

**A STUDY ON SHAPE AND PHASE TRANSITION
IN HOT ROTATING NUCLEI**

A THESIS

Submitted by

K. M. MOHAMMED RAFIC

(REG.NO:10473)

PHYSICS

in partial fulfillment of the requirements for the award of degree of

DOCTOR OF PHILOSOPHY



MANONMANIAM SUNDARANAR UNIVERSITY

TIRUNELVELI - 627 012

JANUARY 2019

MANONMANIAM SUNDARANAR UNIVERSITY

TIRUNELVELI - 627 012

CERTIFICATE

The research work embodied in the present Thesis entitled “**A STUDY ON SHAPE AND PHASE TRANSITION IN HOT ROTATING NUCLEI**” has been carried out in the Department of Physics, Manonmaniam Sundaranar University, Tirunelveli. The work reported herein is original and does not form part of any other thesis or dissertation on the basis of which a degree or award was conferred on an earlier occasion or to any other scholar.

I understand the University’s policy on plagiarism and declare that the thesis and publications are my own work, except where specifically acknowledged and has not been copied from other sources or been previously submitted for award or assessment.

K. M. MOHAMMED RAFIC

RESEARCH SCHOLAR

Dr. T. R. RAJASEKARAN

SUPERVISOR

Professor

Department of Physics

M.S.University

Tirunelveli -12

ACKNOWLEDGEMENT

First and foremost I thank God Almighty for the blessings that he has showered upon me during this research and indeed throughout my life.

I wish to record my deep sense of gratitude and profound thanks to my research supervisor **Dr. T. R. Rajasekaran**, Professor, Department of Physics, Manonmaniam Sundaranar University, Tirunelveli-12, for his keen interest, inspiring guidance, constant encouragement with my work during all stages, to bring this thesis into fruition.

I am extremely indebted to **Dr. B. Sundarakannan**, Professor and Head, **Dr. S. Shailajha**, Assistant Professor, **Dr. K. Mohanraj**, Assistant Professor, **Dr. V. Sabarinathan**, Assistant Professor, Department of Physics, Manonmaniam Sundaranar University, Tirunelveli-12, for their valuable suggestions and support during the course of my research work.

I express my deepest of gratitude to my co-research scholars **Dr. N. Boomadevi, Dr. J. Dhivya Saranya, Mr. G. Ram Kumar, Mr. S. Sounder and Miss. L. Agnes** for all their tremendous efforts who dedicated their time and energy for my sake.

I am greatly indebted and thankful to **Miss. A. Muhila Suba Janani**, for her continuous and unwavering support from the very beginning of my research work.

Finally, I express my very heartfelt gratitude to my family members for their valuable support throughout the course of my research work.

K. M. Mohammed Rafic

CONTENT

Chapter No.	Title	Page No.
CHAPTER I		
INTRODUCTION		
1.1	Yrast line	2
1.2	Moment of inertia	3
1.3	Pairing	4
	1.3.1 Effects of pairing correlation	5
1.4	Objective of the present study	6
1.5	Scope of the thesis	7
CHAPTER II		
STATISTICAL THEORY OF HOT ROTATING NUCLEI		
2.1	Introduction	17
2.2	Statistical formalism	20
2.3	Inclusion of pairing correlation in statistical formalism	22
2.4	Nuclear models	24
	2.4.1 Biaxially deformed single particle levels	24
	2.4.2 Triaxially deformed single particle levels	33
CHAPTER – III		
NUCLEAR SHAPE TRANSITIONS		
3.1	Introduction	37
3.2	Finite temperature Hartree-Fock-Bogoliubov Cranking method	39
3.3	Finite temperature Strutinsky method	40
3.4	Relativistic mean field theory	42
3.5	Monte Carlo method	43
3.6	Landau theory of phase transition	44
3.7	Jacobi transition	44
CHAPTER IV		
SHAPE TRANSITIONS IN Te AND Se ISOTOPES		
4.1.	Introduction	46
4.2	Determination of structural properties	48
	4.2.1 Excitation energy	49

4.2.2	Level density parameter	49
4.2.3	Spin cut off parameter	50
4.2.4	Rotational energy	50
4.2.5	Kinematical moment of inertia	50
4.2.6	Neutron emission probability	50
4.2.7	Single nucleon separation energy	51
4.3	Results and discussions	51
4.4	Conclusion	80

CHAPTER V

PHASE TRANSITION IN HOT ROTATING NUCLEI

5.1	Introduction	82
5.2	Significance of phase transitions	86
5.3	Results and discussion	91
5.4	Conclusion	101

CHAPTER VI

A COMPARATIVE STUDY OF NUCLEAR STRUCTURE

PROPERTIES WITH AND WITHOUT PAIRING

CORRELATIONS

6.1	Introduction	102
6.2	Pairing phase transition	105
6.3	Formalism	107
6.4	Results and discussion	107
6.5	Conclusion	123

CHAPTER VII

SUMMARY AND CONCLUSION	124
-------------------------------	-----

REFERENCES	126
-------------------	-----

LIST OF PUBLICATIONS	146
-----------------------------	-----

REPRINT OF PUBLICATIONS	
--------------------------------	--

BIO-DATA	
-----------------	--

LIST OF FIGURES

Figure No.	Title	Page No.
1.1	Schematic illustration of various phenomenon observed in yrast line.	2
1.2	Compound nucleus reactions and yrast line.	5
2.1	Nilsson diagram for protons and neutrons. Single-particle energies as a function of deformation δ are shown for Z or $N \leq 50$. The even and odd parity levels are denoted by solid and dashed lines respectively. The labeling of levels are by asymptotic quantum numbers $\Omega[Nn_zm]$.	32
2.2	Polar plot of nuclear deformation for rotation around x-axis.	35
2.3	Polar plot of nuclear deformation for rotation around y-axis.	36
2.4	Polar plot of nuclear deformation for rotation around z-axis.	36
4.1	The shape evolution of ^{110}Te , ^{114}Te , ^{116}Te , ^{122}Te , ^{124}Te and ^{130}Te as a function of the angular momentum $M(\hbar)$ at the temperature $T = 0.5$ MeV. The dot refers to the free energy minimized with respect to deformation parameters ε and γ for a particular range of angular momentum M .	52
4.2	Excitation energy E^* (MeV) for ^{124}Te and ^{126}Te as a function of the angular momentum M (\hbar) at the temperature $T = 0.5$ MeV. Results are compared with available experimental data and with shell model.	53
4.3	Comparison of calculated and experimental excitation energy E^* (MeV) for ^{74}Se .	53
4.4	Excitation Energy E^* (MeV) as a function of angular momentum M (\hbar) for various temperatures T (MeV) for Te isotopes.	54
4.5	Excitation Energy E^* (MeV) as a function of angular momentum M (\hbar) for various temperatures for Se isotopes.	55

4.6	The level density parameter a (MeV^{-1}) as a function of angular momentum M (\hbar) with various temperatures T (MeV) for Te nuclei.	57
4.7	Level density parameter a (MeV^{-1}) as a function of angular momentum $M(\hbar)$ for various temperatures T (MeV) for Se nuclei.	58
4.8	Spin cut-off factor σ^2 as a function of angular momentum M (\hbar) at various temperatures $T(\text{MeV})$ for ^{110}Te , ^{114}Te , ^{116}Te , ^{122}Te , ^{124}Te and ^{130}Te nuclei.	60
4.9	Spin cut-off parameter σ^2 as a function of angular momentum M (\hbar) for various temperatures T (MeV) for Se nuclei.	61
4.10	Rotational energy E_{rot} (MeV) as a function of angular momentum M (\hbar) for ^{110}Te , ^{114}Te , ^{116}Te , ^{122}Te , ^{124}Te and ^{130}Te nuclei.	64
4.11	Angular momentum M (\hbar) as a function of rotational frequency ($\omega\hbar/\text{MeV}$) for (a) ^{120}Te at $T = 1.0$ MeV and (b) ^{124}Te at $T = 2.5$ MeV . The open circles represent the experimental value [Hossain 2015].	66
4.12	Moment of Inertia (\hbar^2/MeV) as a function of angular momentum M (\hbar) for (a) ^{120}Te and (b) ^{124}Te with same description as in fig.5.	70
4.13	The neutron separation energy S_n (MeV) as a function of angular momentum M (\hbar) with various temperatures T (MeV).	72
4.14	The proton separation energy S_p (MeV) as a function of angular momentum M (\hbar) with various temperatures T (MeV).	74
4.15	Neutron emission spectrum for various angular momenta as a function of neutron energy (MeV) for ^{110}Te , ^{114}Te , ^{116}Te , ^{122}Te , ^{124}Te and ^{130}Te nuclei.	76
4.16	The neutron separation energy S_n (MeV) as a function of temperature T (MeV) with various angular momenta M (\hbar) for ^{110}Te , ^{114}Te , ^{116}Te , ^{122}Te , ^{124}Te and ^{130}Te nuclei.	78
4.17	The proton separation energy S_p (MeV) as a function of temperature with various angular momenta M (\hbar) for ^{110}Te , ^{114}Te , ^{116}Te , ^{122}Te , ^{124}Te and ^{130}Te nuclei.	79

5.1	The S-shape nuclear specific heat capacity (C_V) as a function of temperature T (MeV) and angular momentum M (\hbar) for ^{141}Ce .	92
5.2	The S - shape nuclear specific heat capacity (C_V) as a function of temperature T MeV and angular momentum M (\hbar) for ^{142}Ce .	92
5.3	The difference in specific heat capacity (ΔC_V) as a function of temperature T (MeV) and angular momentum M (\hbar) for ^{141}Ce and ^{142}Ce isotopes [$\Delta C_V = C_V^{even} - C_V^{odd}$].	93
5.4	The S - shape nuclear specific heat capacity (C_V) as a function of temperature T (MeV) and angular momentum M (\hbar) for (a) ^{141}Ba and (b) ^{142}Ba isotopes.	94
5.5	The S - shape nuclear specific heat capacity (C_V) as a function of temperature T (MeV) and angular momentum M (\hbar) for (a) ^{141}Xe and (b) ^{142}Xe isotopes.	95
5.6	The difference in specific heat capacity (ΔC_V) as a function of temperature T (MeV) and angular momentum M (\hbar) for ^{141}Ba and ^{142}Ba isotopes [$\Delta C_V = C_V^{even} - C_V^{odd}$].	96
5.7	The difference in specific heat capacity (ΔC_V) as a function of temperature T (MeV) and angular momentum M (\hbar) for ^{141}Xe and ^{142}Xe isotopes [$\Delta C_V = C_V^{even} - C_V^{odd}$].	96
5.8	The nuclear specific heat capacity (C_V) as a function of temperature T (MeV) and angular momentum M (\hbar) for ^{145}Nd .	97
5.9	The nuclear specific heat capacity (C_V) as a function of temperature T (MeV) and angular momentum M (\hbar) for ^{146}Nd .	97
5.10	The difference in specific heat capacity (ΔC_V) as a function of temperature T (MeV) and angular momentum M (\hbar) for ^{145}Nd and ^{146}Nd isotopes [$\Delta C_V = C_V^{even} - C_V^{odd}$].	98
5.11	The nuclear specific heat capacity (C_V) as a function of temperature T (MeV) and angular momentum M (\hbar) for ^{150}Sm .	99
5.12	The nuclear specific heat capacity (C_V) as a function of temperature T (MeV) and angular momentum M (\hbar) for ^{151}Sm .	100

5.13	The difference in specific heat capacity (ΔC_V) as a function of temperature T (MeV) and angular momentum M (\hbar) for ^{150}Sm and ^{151}Sm isotopes [$\Delta C_V = C_V^{odd} - C_V^{even}$].	100
6.1	Pairing gap Δ (MeV) as a function of temperature T (MeV) for (a) ^{161}Dy and (b) ^{162}Dy isotopes.	109
6.2	Pairing gap Δ (MeV) as a function of temperature T (MeV) for (a) ^{171}Yb and (b) ^{172}Yb isotopes.	110
6.3	Excitation energy E^* (MeV) as a function of temperature with inclusion of pairing and without pairing for (a) ^{161}Dy and (b) ^{162}Dy isotopes.	113
6.4	Excitation energy E^* (MeV) as a function of temperature with inclusion of pairing and without pairing for (a) ^{171}Yb and (b) ^{172}Yb isotopes.	114
6.5	Entropy (S) as a function of temperature T (MeV) with inclusion of pairing and without pairing for (a) ^{161}Dy and (b) ^{162}Dy isotopes.	116
6.6	Entropy (S) as a function of temperature T (MeV) with inclusion of pairing and without pairing for (a) ^{171}Yb and (b) ^{172}Yb isotopes.	117
6.7	Level density parameter a (MeV^{-1}) as a function of temperature T (MeV) with inclusion of pairing and without pairing for (a) ^{161}Dy and (b) ^{162}Dy isotopes.	118
6.8	Level density parameter (MeV^{-1}) as a function of temperature with inclusion of pairing and without pairing for (a) ^{171}Yb and (b) ^{172}Yb isotopes.	119
6.9	S- shape heat capacity (C_V) as a function of temperature T (MeV) with inclusion of pairing and without pairing for (a) ^{161}Dy and (b) ^{162}Dy isotopes.	121
6.10	S- shape heat capacity (C_V) as a function of temperature T (MeV) with inclusion of pairing and without pairing for (a) ^{171}Yb and (b) ^{172}Yb isotopes.	122

LIST OF TABLES

Table No.	Title	Page No.
4.1	Comparison of level density parameter as a function of angular momentum M (\hbar) for the isotopes ^{110}Te , ^{114}Te , ^{116}Te , ^{122}Te , ^{124}Te and ^{130}Te for temperatures $T=1\text{MeV}$ and $T=3\text{ MeV}$.	59
4.2	Comparison of spin cut off parameter (σ^2) as a function of angular momentum M (\hbar) and temperature for the Te isotopes.	63
4.3	Comparison of rotational energy (MeV) as a function of angular momentum M (\hbar) and temperature for the Te isotopes.	65
4.4	Comparison of rotational frequency as a function of angular momentum and temperatures calculated from STHRN method with the available IBM – 1 model and experimental data [Hossain 2015] for the Te isotopes.	69
4.5	Comparison of moment of inertia as a function of angular momentum M (\hbar) and temperatures calculated from STHRN method with the available IBM – 1 model and experimental data [Hossain 2015] for the isotopes ^{120}Te , ^{122}Te and ^{124}Te .	71
4.6	Comparison of neutron separation energy (MeV) as a function of angular momentum M (\hbar) and temperature for the Te isotopes.	73
4.7	Comparison of proton separation energy (MeV) as a function of angular momentum M (\hbar) and temperature for the Te isotopes.	75
6.1	Neutron and proton pairgap as a function of temperature for ^{161}Dy , ^{162}Dy , ^{171}Yb and ^{172}Yb nuclei.	111

CHAPTER I

INTRODUCTION

The study on the structure of nuclei with high angular momentum and high thermal energy has been an important area of investigation in nuclear physics. With the advent of heavy ion fusion reactions [Ramamurthy 1970, Nix 1972, Cerny 1974, Ansari 1976, Hua 2002, Henss 1988, Bernstein 1995, Svensson 2001, Yu 1999, Simpson 1988 and Lagergren 2001], nuclei can be imparted with very high angular momentum and excitation energy. In a complete fusion evaporation reaction, the projectile nucleus carrying a large kinetic energy and angular momentum fuses with the target nucleus to become a fused composite nucleus. After the particle emission, the residual nucleus is left with fairly high excitation energy and orbital angular momentum. This stage where the nucleus is bound to particle is called only entry state [Herskind 1986] subsequent to which the cooling of the residual takes place through γ rays.

- a) One way is to align the spin vectors of individual nucleons resulting in an irregular nuclear level structure. This happens in the case of weakly deformed nuclei.
- b) Another way is by way of collective rotation about an axis normal to the nuclear symmetry axis resulting in a regular level structure and this happens for well deformed nuclei.

Normally most of the states are a mixture of these modes. Thus, the introduction of high angular momentum and excitation energy opens the possibility of perturbing the nucleus and observe the changes of energies of quantum states as well as the properties of nucleus itself. Interplay of temperature and spin with the final compound system reached in these heavy ion fusion reactions, together with the

deformation degrees of freedom [Nix 1972] sets the stage for interesting problems such as phase and shape transition, shape coexistence and super-deformation. Some phenomena are given below:

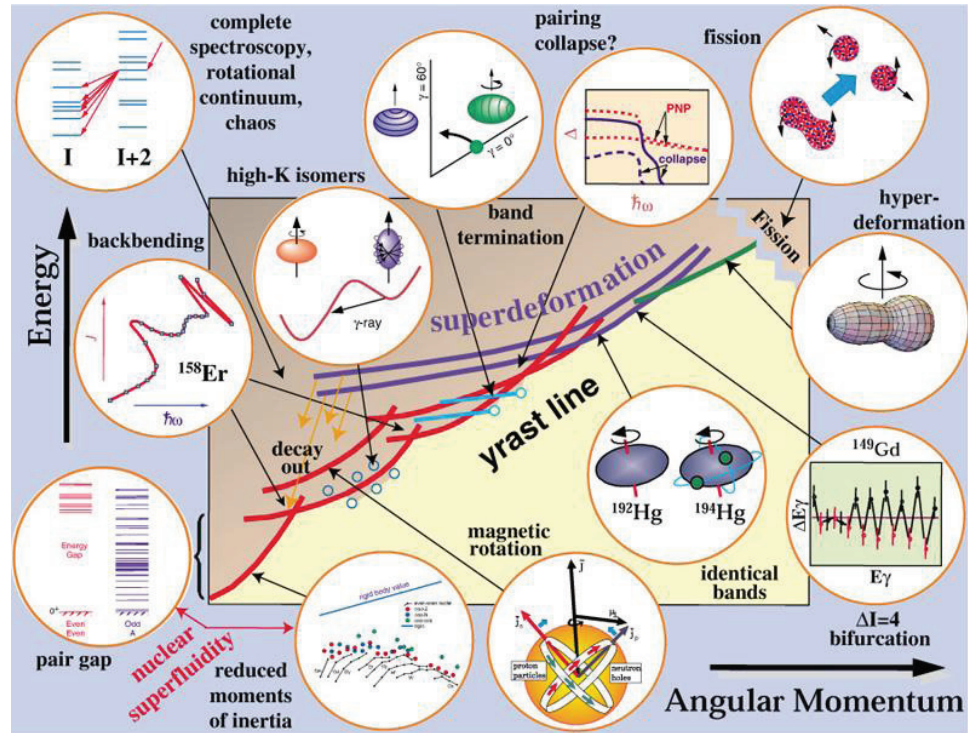


Fig.1.1: Schematic illustration of various phenomenon observed in yrast line.

1.1 Yrast line

The yrast line connects the states with the lowest energy for each angular momentum value. Consequently no states exist below this line. Above the yrast line moving up in energy and temperature, new classes of phenomena may be explored [Szymanski 1983]. Examples include the phase transitions, quasi – continuum and rotational damping, giant resonances, the melting of shell structure and the transition from order to chaos.

1.2 Moment of inertia

Fast nuclear rotation leads to strong modification and mixing of single particle orbital in nuclei. The sequence of energy levels and their distances in the rotational band depend essentially on one parameter, the nuclear moment of inertia. Investigations on the shape of energy versus spin have given a lot of information about the effect of high angular momentum upon the structure and deformation of nuclei. When the nucleus rotates it is found that the moment of inertia does change with spin. Hence for a rotating nucleus, the rotational energy spectra can be discussed in terms of two spin – dependent moments of inertia defined by Bohr and Mottelson [Bohr 1975], which is related to first – order ($j^{(1)}$) and second – order derivatives ($j^{(2)}$) of excitation energy with respect to aligned angular momentum (M).

Back-bending is a paradigm of structural changes in a nucleus under rotation. A sudden increase of a nuclear moment of inertia in the yrast rotational band at some critical angular momentum or rotational frequency discovered a few decades ago [Johnson 1971] continues to attract considerable attention. There is a general notion that this phenomenon is a result of the rotational alignment of angular momenta of a nucleon pair occupying a high – j intruder orbital near the Fermi surface. The moment of inertia of a classical rotor depends both on the shape and the flow pattern of its matter. Many of the low lying levels in a rotational band are described in terms of a nucleus with constant moment of inertia (j). But at high spin the value of j will be considerably increased. The larger j could be a reflection of a larger deformation or of a considerable reduction in the number of nucleons paired off. The effect of j is an indirect evidence for an energy gap caused by pairing.

1.3 Pairing

Pairing correlations and related superfluid properties are the robust features of quantum many – body systems and have gained a lot of interest recently. The Cooper phenomenon is a primary reason for the thriving of pairing [Cooper 1956]. The occurrence of pairing correlation in nuclei is well supported by a number of experimental evidences such as the zero spin for the ground state of all even – even nuclei (≈ 1 MeV) that to the odd mass nuclei, observation of lower value of measured moment of inertia compared to the rigid body values, the observation of low value of binding energies of the odd – even and odd – odd nuclei compared to the mean binding energy of the two nearby even – even nuclei etc. Indeed questions of phase transitions [Chomaz 2005], interplay with other collective modes [Bahri 1998], continuum effects [Barranco 2001] and thermodynamic properties of small systems are important in present day science and technology.

Pairing correlations in nuclei are the result of the short range character of the effective particle – particle force which favors pairs of identical nucleons coupled to zero angular momentum. This can be explained in a graceful manner by the BCS approach initially invented for infinite systems in the theory of superconductivity, and employed to finite nuclei by Bohr, Mottelson and Pines [Bohr 1958] and also by Belyaev [Belyaev 1965]. Analogous to the superconductor where one notices a phase transition to a normal conductor for a sufficiently high magnetic field and for increasing temperature, it has been expected that for nuclear superfluidity, an overall pairing collapse at higher angular momenta should take place allied with the breaking of individual pairs by the Coriolis force and also by higher temperature in which the increasing excitation energy allows the population of unpaired configuration.

1.3.1 Effects of pairing correlation

The structural properties of the nuclei get modified in the presence of pairing interaction, as they afford further binding force to the nuclei. Under the influence of this force, the nucleons persist in scattering with their paired partners depending upon the availability of the nearby vacant orbits around the Fermi surface. Thus the unoccupied orbits also play a vital role in the nuclear dynamics. If a single particle energy level lies above the Fermi surface then it acts more like a particle state while the one below is like a hole state. This gives rise to quasi – particle states or orbits, [Bardeen 1957] i.e. a mixture of particle and hole states, near the Fermi surface rather than pure particle (above the Fermi level) and pure hole (below the Fermi level) states, which are the solutions of the overall nuclear Hamiltonian including the pairing interaction. Accordingly, these correlations reduce the moment of inertia as compared to the rigid rotor value and the nucleus is said to be in the superfluid phase.

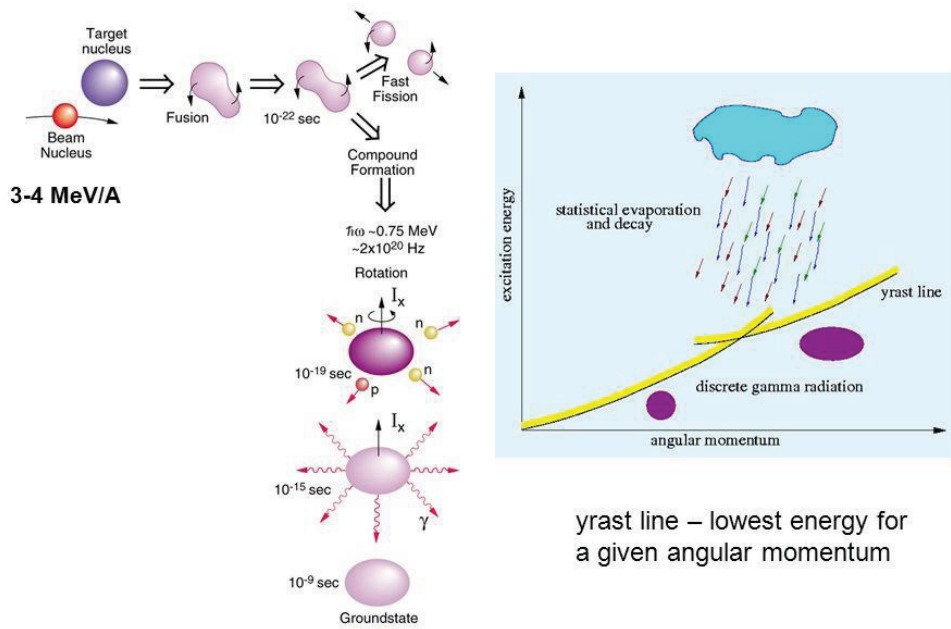


Fig.1.2 Compound nucleus reactions and yrast line

As the spin of the nucleus increases, the effect of pairing decreases since when the nucleus rotates, the individual nucleon experiences centrifugal and Coriolis forces. The Coriolis forces tend to counteract the pairing force and consequently, the pairing force reduces with the increasing rotational frequency. At some critical value of the rotational frequency, the Coriolis forces become as strong as the pairing correlation results in a sudden increase in the moment of inertia known as backbending [Stephens 1972]. Consequently, the energy level spacing deviates from the $M(M+1)$ rule resulting in an increase in moment of inertia having value nearly equal to that of the rotating rigid body. The yrast region contains sequence of rotational bands parallel to the line, as indicated by A in fig. 1.2. With the increase of the angular momentum, the centrifugal forces produce an effect comparable to the shell structure effect. This will tend to make the prolate shape gradually changes into a triaxial shape and exhibits many more collective states. The changes in the yrast region result in a crossing band structure indicated by B in fig.1.2. Further increase in the angular momentum results into an oblate deformation of the nucleus, indicated by C in fig.1.2. The total angular momentum in this case is aligned along with the symmetry axis rather than the perpendicular axis as in the case of the prolate nuclei. Finally, before the nucleus undergoes fission, it passes through another phase of triaxial shapes, where again the collective bands are observed to exist [Andersson 1976]. In this triaxial region, a very large increase in the moment o inertia is observed and is known as giant backbending.

1.4 Objective of the present study

Of the many achievements of the nuclear theory, a prominent one is its ability to explain the occurrence of a variety of shapes and its ability to predict the location of nuclear shapes in the whole of the nuclear chart. With the advent of highly

sophisticated experimental techniques and faster computation capabilities, the theoretical investigations have ultimately led to a more realistic and transparent analysis of nuclear structure changes in the entire mass region. Although studies of nuclear shapes of hot rotating nuclei have been carried out in terms of measurement of giant dipole resonance (GDR) built on excited states, alpha-gamma angular correlations, rotational damping and so on, studies of ground state deformation with temperature seem to be insufficient in some cases and hence this present study, which is a study of thermal and rotational response to nuclear properties, has been undertaken. In particular, the present study focuses on phase transition and shape evolutions in the framework of the statistical theory.

1.5 Scope of the thesis

This thesis studies the nuclear shapes under the framework of statistical theory of hot rotating nuclei with the incorporation of deformation, collective and non-collective rotational degrees of freedom, shell effects and pairing correlations (BCS formalism). Pairing – phase transition from super fluid to normal state and shape-phase transition such as deformed to spherical shape, prolate to oblate shapes with increasing temperature and angular momentum are observed. The interplay of different degrees of freedom and their effect on the behaviour of the nuclei that are of particular interest are investigated with specific focus to the following nuclear structure properties level density parameter, nucleon separation energies, moment of inertia, spin cut off parameter and nuclear specific heat.

Level densities are very crucial in all the statistical model calculations since they help determining the nuclear reaction rates. Thermal energy produces changes in the shape of the nucleus which is closely linked to phase transition associated with level density. We have used statistical theory to investigate the above mentioned

nuclear structure parameters. One of the achievements of this theory is its explanation for asymptotic fission which is because of the shell structure of nuclei and its application in the studies reported in this thesis gives a strong support of its use. Ramamurthy et al. [Ramamurthy 1970] prescribed a statistical method which is equally efficient as the Strutinsky's method in extracting shell correction of liquid drop energies. Thus statistical theory proved to yield microscopic as well as macroscopic details. Also the statistical theory proved to be successful in describing heavier nuclei, with their collective and non-collective degrees of freedom and energy levels that are more closely spaced. If the excitation energy is high enough, the levels that are overlapped will be excited and the number of energy levels becomes so high that an individual treatment is impossible. Statistical theory circumvents this problem and gives a good description. A successful application of statistical theory has been brought about by the meticulous development of the theory by many [Bethe 1936, Ericson 1960, Ignatyuk 1969, Moretto 1973 and Rajasekaran 1988].

The basic ingredient of the statistical theory is a suitable shell model level scheme generated for various nuclear deformations. Two types of parameterizations are practiced. One is on the basis of expanding the harmonic oscillator frequencies and the other is on the basis of expanding the nucleus surface in terms of spherical harmonics where Wood-Saxon potential is used. In this thesis, we have given due care in choosing the various parameters involved in the deformed harmonic oscillator Hamiltonian for hot rotating nuclei. Triaxial deformations are assumed in the diagonalization of the Hamiltonian as needed by situation.

Nuclei that are formed in collisions can attain very high spin. There are two ways of attaining angular momentum states in the statistical theory, namely, Statistical Theory of Hot Rotating Nuclei (STHRN) and Cranked Nilsson Model

(CNM). The first method was formulated by Moretto [Moretto 1971]. In this method, triaxially deformed single particle levels are used and lagrangian multipliers are used to project out different angular momentum states of the system from the grand partition function [Feynmann 1972, Eisenberg 1975 and Parthia 1972].

The nuclear rotational motion is provided by the cranking model introduced by Inglis in 1954 [Inglis1954], the nucleons move in a cranked Nilsson potential with the deformation given by ϵ and γ . The cranking is done about one of the principal axes and the cranking frequency is given by ω . As the statistical theory inputs the microscopic single particle levels [Nilsson 1969] corresponding to the deformed Nilsson harmonic oscillator potential [Scholes 2004 and Miller 1989], the results show the shell structure effect of the system at different deformation. Methods of obtaining biaxial, triaxial, energy eigen values and Cranked-Nilsson-Strutinsky approach are explained in this thesis.

Chapter II deals with the theoretical background of this thesis, elaborating on the statistical theory. It outlines the ways of producing angular momentum states used in the calculation of nuclear properties on the basis of a shell model level sequence with and without pairing correlation. Statistical theory applies a rigorous treatment of high spin states by including rotation in the thermodynamic potential. This might be one of the ways to treat the very high spin nuclei formed in highly excited states in a cogent manner. The determination of the grand partition function [Nilsson 1969, Jing-Ye-Zhang 1989, Langanke 1991 and Pathira 1972] is one of the usual procedures in statistical mechanics which basically describes the average behavior of the compound nucleus and its decay. The lagrangian multipliers in the grand partition function are fixed by the conservation of proton number, neutron number, total angular momentum and the total energy of the system. The calculation of the

occupation probability in each single particle level is also done. Statistical definitions are used for the calculation of entropy, excitation energy, level density parameter and nuclear level density etc.

The shape is one of the fundamental properties of the nucleus, along with its mass and radius. It is governed by the interplay of macroscopic, liquid drop like properties of the nuclear matter and microscopic shell effects. In a nucleus with the partially filled shells the valence nucleons tend to polarize the core towards a deformed mass distribution. The deformation can be described by a multipole expansion with the quadrupole deformation being the most important deviation from spherical shape. Such quadrupole shapes can either have axial symmetry, in which one distinguishes elongated (prolate) and flattened shapes (oblate), or the deformation can be without axial symmetry resulting in different elongations along the two or three axes of the system, referred to as biaxial or triaxial shape respectively.

In some areas of the nuclear chart, the shape is very sensitive to the structural effects and can change from one nucleus to its neighbor. In addition to the shape changes with the proton or neutron number, the shape can also change with excitation energy or angular momentum within the same nucleus. Such changes cause the rearrangement of the orbital configurations of the nucleons or by the dynamic response of the nuclear system to rotation. In some cases configurations corresponding to different shapes coexist at similar energies. The wave functions of such states can then mix according to the laws of quantum mechanics.

Cohen et al. [Cohen 1979] have predicted that the nucleus undergoes shape changes with increasing angular momentum by assuming the nucleus as a structure less and charged liquid drop subjected to Coulomb and surface forces. The behavior of nucleus with increasing spin in the different regions of deformation was studied by

Bohr and Mottelson [Bohr 1975]. Neergard et al. [Neergard 1976], Anderson et al. [Anderson 1976] and Bengtsson et al. [Bengtsson 1975] have investigated nuclei by employing Strutinsky's prescription, which have yielded good results for the deformation behavior of the nuclei at high spins. Different methods are available for studying shape transition in nuclei which are given below.

1. Finite temperature Hartree – Fock Bogoliubov Cranking methods
2. Finite Temperature Strutinsky Method
3. Relativistic mean field theory
4. Monte Carlo method
5. Landau Theory of Phase Transition
6. Jacobi Transition

The mean field theories, both relativistic and non-relativistic, such as finite temperature Hartree – Fock Bogoliubov cranking theory (FTHBCS) [Goodman 1983] or finite temperature cranked Strutinsky methods (FTCS) [Alhassid 1988] have been used to study structural changes in hot rotating nuclei. A systematic study of temperature dependence of the shapes and pairing gaps of some isotopes in the rare earth region was made in the relativistic Hartree – Fock Bogoliubov theory (RHFB). As we have already mentioned the major objective of this present study to investigate the behavior of the fused compound nuclear system found in fusion reactions at high excitation angular momentum states. These behaviors have been studied by many theoretical formalism are presented in chapter III

Chapter IV describes the evaluation of the structural properties of hot rotating nuclei such as level density parameter, single neutron separation energy and single proton separation energy using statistical theory of hot rotating nuclei. These parameters are extracted as a function of angular momentum, temperature and

deformation parameter. Nuclei are finite quantum systems, having uniquely transitional features. In nuclei, two types of phase transition such as: (i) pairing phase transition (superfluid to normal fluid) and (ii) shape-phase transition (deformed to spherical shape) occur. The second type of phase transition is also called as quantum phase transitions and these have also been extended to excited state, which has a qualitative change in the properties of the system as a function of the excitation energy [Iachello 2011]. The shape of the nucleus is determined using the deformation parameter at various temperature and angular momenta. To have a complete and comprehensive picture of shape transitions and other intrinsic properties of nuclei, a systematic study of thermodynamic properties using statistical approach has been done.

Numerical results obtained using the formalism given in chapter II for the Te and Se isotopes are presented in this chapter. The dependence of nuclear temperature and spins on the excitation energy, nuclear level density parameter and spin cut off parameter is studied for the nuclei considered in this text. The hodograph of the nuclei drawn shows the shapes of the nuclei as a function of angular momentum, temperature and deformation. The excitation energies extracted are compared with available experimental data and shell model results. It is seen that the calculated parameters as a function of angular momentum, temperature, deformation parameter ϵ and γ should experience an abrupt change for these heavier systems beyond angular momentum $M \approx 12\hbar$ for Te isotopes and $M \approx 8\hbar$ for Se isotopes. This abrupt fall causes a minimum in the parameter values and it corresponds to a shape transition from collective prolate to non collective oblate. It is also seen that the values of the rotational frequency and kinematic moment of inertia show very good agreement with the available experimental data.

The analogy of back-bending phenomenon to a behavior of superconductors in magnetic field is prompting researchers to apply Landau theory of phase transitions to nuclei [Goodman 1983]. It is a common property of rotating classical fluids that beyond a certain angular momentum, the equilibrium shape changes abruptly from a slightly flattened configuration to a triaxial shape rotating about its shortest axis. With increasing angular momentum, this configuration elongates very rapidly and eventually fissions at a characteristic angular momentum. The original discovery of such a transition from oblate to triaxial shapes was made in 1934 by Jacobi, in the context of rotating, idealized, incompressible, gravitating masses.

In 1996, the oblate to triaxial shape transition was found to take place in the more realistic nuclear Thomas – Fermi model under the assumption of synchronous rotation i.e., all the mass elements rotate with a common angular velocity. Shell effects can produce sharp deviations from average binding energies and shapes, more over, the assumption of synchronous rotation is known to be strongly violated at low angular momenta where pairing effects are important.

Conventional superdeformed nuclei owe their elongation to shell effects, and are conserved down to relatively low angular momenta. On contrary, the existence of Jacobi like configuration is due to the centrifugal force, and without help from shell effects, such shapes would appear only at very high angular momentum, but they should then occur over a wide range of nuclei rather than in the small pockets characteristic of the effects driven by the shell structure. Thus phase transition arises as a result of competition between three different factors: a pairing like force, a monopole interaction and finite temperature effects and rich variety of situations thus ensues. In this thesis, a statistical approach has been employed for a precise understanding of the phase transitions in finite nuclei.

In the modern classification scheme, phase transitions are divided into two broad categories, named similarly to the Ehrenfest classes. The first-order phase transitions are those that involve a latent heat. During such a transition, a system either absorbs or releases a fixed amount of energy and many important phase transitions fall in this category, including the solid/ liquid/gas transitions. The second class of phase transitions are the continuous phase transitions, also called second – order phase transitions. Examples superfluid transition. Lev Landau gave a phenomenological theory of second order phase transitions and can be applied to nuclear systems. Examples of nuclear phase transitions are given below:

(i) The emergence of superfluidity in nuclei when temperature or angular momentum reaches a critical value.

(ii) The breaking of axial symmetries in the ground state as regards the deformed to spherical transition.

In recent years [Kargar 2013, Dhivya 2016, Sofia 2017 and Danilo 2013] a lot of effort has been made to describe the behavior of paired small systems such as atomic nuclei. The investigation on specific heat is important since it plays a significant role within the determination of the phase transition in finite nuclei. Several authors [Algin 2008, Alhassid 2000, Dukelsky 1991, Rossingoli 1998, Ngyen 1990 and Bhaduri 1988] have investigated the existence of phase transition in finite nuclei. The change in the nuclear shape induced by thermal excitation is related to this phase transition. Danilo [Danilo 2013] have discussed the pairing phase transition from specific heat capacity (C_V) in hot nuclei by finite – temperature variation after projection BCS approach (FT – VAP). The pairing correlations existing in nuclei are counteracted by interactions induced in nuclear rotation. The gradual decreasing of gap parameter with respect to temperature, followed by a

sudden decrease is interpreted as a rapid breaking of nucleon Cooper pairs and also the suppression of pairing correlation. This is often related with the S shape heat capacity.

Chapter V describes the importance of pairing phase transition of the method of evaluating the specific heat capacity C_V as a function of angular momentum (M) and temperature (T). In the framework of statistical theory one important tool to study the phase transition is the specific heat. The specific heat is recognized as a quantity which indicates the occurrence of phase transition. The nuclear specific heat of a fused compound system formed in heavy ion collision can be estimated if the excited states spectrum is well-known. Elementary examples of this are stated by Pathria [Pathria 1972], including the free particle, the harmonic oscillator and rigid rotor. The behavior of nuclear specific heat at high temperature directly yields the information about the relevant degrees of freedom in the spectrum of Dulong and Petit's law. Tanabe, Goodman, Cole, Miller and others [Tanabe 1981, Goodman 1984, Cole 1989, Miller 1989, Dukelseky 1991, Civitarese 1990 and Bhaduri 1998] have emphasized the role of nuclear specific heat in the determination of important properties of the nuclei. One motivating feature is the peak structure in specific heat which endorses the existence of phase transition. The occurrence of phase transition is predicted in three rare nuclei along with their isotopes such as $^{141, 142}\text{Ce}$, $^{145, 146}\text{Nd}$ and $^{150, 151}\text{Sm}$. The results of our calculations on specific heat capacity shows a predominant appearance of a hump in the low temperature region which is considered as the suppression of pairing correlation and it is an indication of phase transition. It is also noted that the occurrence of the peak in the specific heat at low temperature is a contribution of the ground state rotational band [Huang 2002].

In chapter VI of this thesis, a comparative study of the influence of pairing on the nuclear structure properties are given. For illustrative purpose calculations have been carried out for heavier nuclear systems like $^{161,162}\text{Dy}$ and $^{171,172}\text{Yb}$. It is found that there is no much difference in the values of both with and without pairing correlation in the parameters such as excitation energy, entropy, level density parameter and heat capacity at very low temperature. However there is a remarkable difference in their values at high temperature.

In chapter VII , a brief summary and conclusion are drawn.

CHAPTER II

STATISTICAL THEORY OF HOT ROTATING NUCLEI

2.1 Introduction

In heavy ion reactions, one of the main interests is the formation of fused systems in excited states. The behavior of these excited compound systems provide important and interesting problem in understanding the structure of the nucleus. At the low excitation energy the nucleus is excited to levels, characterized by energy, spin and parity. These levels are discrete and the level density can be determined by direct counting. However, at higher excitation energies, the nuclear level density increases so rapidly that it is practically impossible to study the transition between the levels and hence statistical approach is more appropriate one to employ the average behavior of the compound nucleus. Fused compound systems are described as thermodynamical system of fermions with several degrees of freedom like temperature, angular momentum, deformation, collective and non-collective rotations, fluctuations etc. [Blatt 1979]. For such a complicated system, the statistical theory of nuclei is developed by several nuclear researchers [Bethe 1936, Ericson 1960, Ignatyuk 1969, Nilsson 1969 and Rajasekaran 1988 & 2008]. A number of phenomenological extensions were made and statistical approaches have been developed for the present work. The statistical theory is used for extracting information about many nuclear properties and level density by determining the excitation energy as a function of angular momentum and temperature for finite nuclear systems. More significantly, low energy nuclear structure properties show a strong dependence on the nuclear pairing force [Moller 1992]. In calculations of low-lying quasiparticle energies and other quantities that depend on the low energy microscopic structure of the nucleus, it is therefore crucial to consider the pairing

effects. A sophisticated pairing model and an appropriate choice of pairing model parameters are both important for obtaining realistic results. A microscopic study based on the BCS Hamiltonian is made by incorporating the effects of pairing interaction within the framework of the statistical theory [Moretto 1971].

Depending on the system under study, one can choose among different kinds of statistical ensembles in order to derive thermodynamic quantities. The thermodynamic quantities derived within different ensembles give the same results in the thermodynamic limit. On the other hand, the choice of a specific ensemble may change results significantly for small systems. For example, the caloric curves derived within the microcanonical and canonical ensembles coincide for large systems; but the two caloric curves depart from each other for small systems [Schiller 2005 and Tavukcu 2002]. The microcanonical ensemble is commonly accepted as the appropriate ensemble to use in investigating atomic nuclei, as the nuclear force has a short range and the nucleus does not share its excitation energy with its surroundings. However some thermodynamic quantities such as temperatures and heat capacities may have large fluctuations and negative values when derived within the microcanonical ensemble. On the other hand, the canonical ensemble averages too much over structural changes of the system. Therefore, it is difficult to choose an appropriate ensemble for a small system. Apart from that, we use grand-canonical ensemble to study the thermodynamic properties of the system.

Statistical descriptions of many-body quantum systems are based on the grand-canonical ensemble average which contains all the information about the statistical average of energy, angular momentum and entropy that determine the phase space of the system. The main assumption for statistical analysis is the microscopic equilibrium which means that all the states with the same excitation energy are

equally populated. The Lagrangian multipliers in the grandpartition function are fixed by the conservation of the energy, number of particles and angular momentum of the system. We have also treated the system with constant angular momentum, which is possible within restricted configuration spaces. Ignatyuk [Ignatyuk 1969] performed the calculations with pairing correlations and in his work only constant values of Nilsson parameters [Nilsson 1969] are used for all the shells. Strutinsky [Strutinsky 1967] has given an expression for thermodynamical potential of rotating nuclei and shell correction at a finite temperature. Civitarese has [Civitarese 1983] investigated the temperature dependence of level density parameter with BCS formalism [Civitarese 1990] but neglected the effect of angular momentum. Rajasekaran [Rajasekaran 1988, 2003 & 2008] has studied the dependence of both temperature and angular momentum on level density parameter and separation energy.

There are two ways of generating the angular momentum in nuclei [Hamamota 1983]:

- i) by introducing the z projection of the angular momentum as a constant of motion through the Lagrangian multiplier occurring in the Fermi distribution corresponding to the single-particle spins by assuming the cranking frequency $\omega = 0$.
- ii) by discarding the Lagrangian multiplier corresponding to the single-particle spins in the Fermi distribution function but adjusting and fine tuning the cranking frequency term ω in the Nilsson Hamiltonian itself.

The former method which we have used is valid only for the rotation around the symmetry axis but cannot be applied to nuclei rotating about an axis perpendicular to the symmetry axis since the spin projection m_z is not a good quantum number in this case. The Lagrangian multiplier and the collective frequency of rotation of the system

should be equal to one another as long as the single-particle spin projections along the symmetry axis are good quantum numbers. For axially symmetric shapes of the nuclei, the single-particles spin projections m_z are good quantum numbers while for triaxial deformations the single-particle spin projections m_z are not good quantum numbers as the matrix elements for triaxially deformed system connects states of different m_z [Huizenga 1972]. Moretto [Moretto 1973] has exemplified that the laboratory fixed z – axis can be made to coincide with the body fixed z' - axis and it is possible to identify and substitute M for the total angular momentum I . In the quantum mechanical limit the z component M of the total angular momentum is $M = M_N + M_Z \rightarrow I + 1/2$. This chapter describes the formulation of statistical theory used in the estimation of nuclear properties on the basis of a shell model level sequence with and without the inclusion of pairing correlation.

2.2 Statistical formalism

In the grand-canonical partition function, the statistical properties of the system are given by,

$$Q = \sum_i \exp(-\beta E_i + \alpha_Z Z_i + \alpha_N N_i + \lambda M_i), \quad (2.1)$$

where the Lagrangian multipliers α_N , α_Z , β and λ that conserve the proton number, neutron number, angular momentum along the space fixed z -axis and total energy for a given temperature $T = 1/\beta$ are fixed by the following equations [Rajasekaran 2008]:

$$\langle N \rangle = \frac{\partial \ln Q}{\partial \alpha_N}, \quad (2.2)$$

$$\langle Z \rangle = \frac{\partial \ln Q}{\partial \alpha_Z}, \quad (2.3)$$

$$\langle M \rangle = \frac{\partial \ln Q}{\partial \lambda}, \quad (2.4)$$

$$\text{and } \langle E \rangle = -\frac{\partial \ln Q}{\partial \beta}. \quad (2.5)$$

The corresponding equations in terms of single - particle levels for protons ϵ_i^Z with the spin projections m_i^Z and neutrons ϵ_i^N with the spin projection m_i^N are

$$\langle N \rangle = \sum_i n_i^N = \sum_i \{1 + \exp[-(\alpha_N + \lambda m_i^N - \beta \epsilon_i^N)]\}^{-1}, \quad (2.6)$$

$$\langle Z \rangle = \sum_i n_i^Z = \sum_i \{1 + \exp[-(\alpha_Z + \lambda m_i^Z - \beta \epsilon_i^Z)]\}^{-1}, \quad (2.7)$$

$$\langle M \rangle = \sum_i n_i^N m_i^N + \sum_i n_i^Z m_i^Z, \quad (2.8)$$

$$\langle E(M, T) \rangle = \sum_i n_i^N \epsilon_i^N + \sum_i n_i^Z \epsilon_i^Z. \quad (2.9)$$

where, n_i^N and n_i^Z are occupational probabilities of the i^{th} shell corresponding to neutron and proton. The above coupled non-linear equations have to be solved to determine the Lagrangian multipliers for a given temperature T.

The entropy is calculated using the relation,

$$S = -\sum_i n_i^N \ln n_i^N + (1 - n_i^N) \ln(1 - n_i^N) - \sum_i n_i^Z \ln n_i^Z + (1 - n_i^Z) \ln(1 - n_i^Z). \quad (2.10)$$

The spin cut-off parameter σ^2 is computed using the following expression

$$\sigma^2 = \frac{1}{4} \sum m_i^{N^2} \text{sech}^2 \left[\frac{1}{2} (\beta \epsilon_i^N - \alpha_N + \gamma m_i^N) \right] + \frac{1}{4} \sum m_i^{Z^2} \text{sech}^2 \left[\frac{1}{2} (\beta \epsilon_i^Z - \alpha_Z + \gamma m_i^Z) \right]. \quad (2.11)$$

The excitation energy E^* is obtained using the relation

$$E^* = E - E_0 \quad (2.12)$$

where, E is the total energy and E_0 is the ground state energy of the system.

The free energy of the system contains all the thermodynamic information and is computed as,

$$F = E - TS. \quad (2.13)$$

2.3 Inclusion of pairing correlations in statistical formalism

By incorporating the effect of pairing correlations in the statistical formalism, the grand canonical partition function is described as [Rajasekaran 2011],

$$\ln Q_{pair} = -\beta \sum_k (\epsilon_k^Z - \mu_Z - E_k^Z) + \sum_k \ln \{1 + \exp[-\beta(E_k^Z - \lambda m_k^Z)]\} - \beta \Delta_Z^2 / G_Z \quad (2.14)$$

where, $E_k^Z = [(\epsilon_k^Z - \mu_Z)^2 + \Delta_Z^2]^{1/2}$ is the proton quasiparticle energy, G_Z the pairing strength and Δ_Z the gap parameter. The quantity β is the reciprocal of the temperature ($\beta = 1/T$) and μ_Z the proton chemical potential.

The particle number equations for protons, the equations for angular momentum and energy are given below:

$$Z_{pair} = \sum_k \left[1 - \left\{ (\epsilon_k^Z - \mu_Z) \tanh \frac{\beta}{2} (E_k^Z - \lambda m_k^Z) / 2E_k^Z \right\} \right], \quad (2.15)$$

$$M_{pair}^Z = \sum_k \{ m_k^Z / [1 + \exp \beta (E_k^Z - \lambda m_k^Z)] \}, \quad (2.16)$$

$$E_{pair}^Z = \sum_k \epsilon_k^Z \left\{ 1 - (\epsilon_k^Z - \mu_Z) \tanh \frac{\beta}{2} (E_k^Z - \lambda m_k^Z) / 2E_k^Z \right\} - \Delta_Z^2 / G_Z \quad (2.17)$$

The gap parameter Δ_Z is obtained as a function of β , λ_Z , and μ_Z by solving the gap equation

$$\sum_k \tanh \frac{\beta}{2} (E_k^Z - \lambda m_k^Z) / 2E_k^Z = 2 / G_Z. \quad (2.18)$$

The entropy S^Z of the system is then determined as

$$S_{pair}^Z = \sum_k \ln \{ 1 + \exp[-\beta(E_k^Z - \lambda m_k^Z)] \} + \sum_k \beta \{ (\epsilon_k^Z - \lambda m_k^Z) / (1 + \exp[-\beta(E_k^Z - \lambda m_k^Z)]) \} \quad (2.19)$$

Equations (2.11) and (2.14) are solved for particular values of β and λ to obtain μ_Z and Δ_Z . A similar set of equations for neutrons also exist. The pairing gap parameter Δ is an important aspect in the statistical formalism and it is a measure of

the pairing correlation. The Δ value is very sensitive to the number of levels taken for pairing calculations especially when the system is excited. The total energy E , total angular momentum M and total entropy S are obtained as,

$$E_{pair} = E_{pair}^N + E_{pair}^Z, \quad (2.20)$$

$$M_{pair} = M_{pair}^N + M_{pair}^Z \quad (2.21)$$

$$\text{and } S_{pair} = S_{pair}^N + S_{pair}^Z. \quad (2.22)$$

The spin cut-off parameter σ^2 is derived as,

$$\sigma_{pair}^2 = \frac{1}{2} \sum_k m_k^{N^2} \text{sech}^2 \frac{1}{2} \beta E_k^N + \frac{1}{2} \sum_k m_k^{Z^2} \text{sech}^2 \frac{1}{2} \beta E_k^Z. \quad (2.23)$$

The excitation energy E_{pair}^* and free energy F_{pair} of the system are given by,

$$E_{pair}^* = E_{pair} - E_{pair}^0, \quad (2.24)$$

$$F_{pair} = E_{pair} - TS_{pair}. \quad (2.25)$$

where, E_{pair} is the total energy of the system for a given temperature and E_{pair}^0 is the ground state energy of the system. In the statistical formalism, the equilibrium shape of the nucleus at given angular momentum and temperature has been obtained by minimizing the free energy as a function of deformation. The basic ingredient to the statistical theory is a suitable microscopic shell model level scheme generated for various nuclear deformations and are discussed in subsequent sections.

2.4 Nuclear models

The basic satisfactory microscopic ingredient to the statistical theory is a suitable shell model level scheme generated for various nuclear deformations. The nuclear deformation is a feature which depends more upon the details of the shell structure than upon the smooth nuclear properties. Therefore it is of utmost importance to study the thermodynamic properties of the nucleus corresponding to different deformations. Shell model level scheme obtained by diagonalising the Nilsson and cranked Nilsson Hamiltonian and both are used in different circumstances of the present work. Considerable attention has been devoted to choose the various parameters involved in the deformed harmonic oscillator Hamiltonian [Irvine 1972 and Sulaksono 2005]. The purpose of this chapter is to predict procedure of obtaining energy levels by biaxially deformed and triaxially deformed oscillator potentials.

2.4.1 Biaxially deformed single particle levels

The generalization of the phenomenological shell model to deformed nuclear shapes was first given by [Nilsson 1969], and this version is often referred to the Nilsson model. Hence, the single particle energy eigenvalues are generated using the Nilsson Hamiltonian for biaxially deformed nuclei. The principal idea is to make the oscillator constants different in the different spatial directions:

$$V(r) = \frac{1}{2}m(\omega_X^2 X'^2 + \omega_Y^2 Y'^2 + \omega_Z^2 Z'^2). \quad (2.26)$$

Here X', Y', Z' are the coordinates of the particle in body fixed axes and ω_X, ω_Y and ω_Z are the oscillation frequencies along X, Y and Z axis (space fixed). Hence the Hamiltonian including the spin orbit coupling term $(\vec{l} \cdot \vec{s})$ and the centrifugal term (\vec{l}^2) leads,

$$H_N = H_{ON} + Cl \cdot \vec{s} + D\vec{l}^2 \quad (2.27)$$

In this deformed shell model the following assumptions are made,

- a) Constancy of surface potential
- b) Volume conservation and
- c) Axial symmetry

By the first assumption:

Surface potential of a spherically symmetric potential = Surface potential of the Nilsson model.

$$\frac{1}{2}m\omega_o^2(R_o^2) = \frac{1}{2}m(\omega_x^2 X'^2 + \omega_y^2 Y'^2 + \omega_z^2 Z'^2), \quad (2.28)$$

where, $\eta\omega_o = (41/A^{1/3})$ MeV is the oscillator constant for the equivalent spherical nucleus.

The condition of incompressibility of nuclear matter requires that the volume of the ellipsoid should be the same as that of the sphere, implying $R^3 = XYZ$, and this impose a condition on the oscillator frequencies,

$$\omega_x + \omega_y + \omega_z \approx \omega_o^3 = const. \quad (2.29)$$

Now assume axial symmetry around the z axis, i.e., $\omega_x = \omega_y$, and a small deviation from the spherical shape given by a small parameter δ .

$$\omega_x^2 = \omega_y^2 = \omega_o^2 \left(1 + \frac{2}{3}\delta\right), \quad (2.30)$$

$$\omega_z^2 = \omega_o^2 \left(1 - \frac{4}{3}\delta\right). \quad (2.31)$$

For the incompressibility condition to hold generally we require ω_o to be function of the deformation:

$$\omega_0(\delta) = \omega_0^0 \left[\left(1 + \frac{2}{3}\delta^2\right) \left(1 - \frac{4}{3}\delta\right) \right]^{\frac{-1}{6}}. \quad (2.32)$$

In equation (2.24),

$$H_{ON} = \frac{\hbar^2}{2m} \left(\frac{\partial^2}{\partial X'^2} + \frac{\partial^2}{\partial Y'^2} + \frac{\partial^2}{\partial Z'^2} \right) + \frac{1}{2} m (\omega_X^2 X'^2 + \omega_Y^2 Y'^2 + \omega_Z^2 Z'^2). \quad (2.33)$$

The deformation parameter δ is defined by,

$$\delta = \frac{R_Z - R_X}{R_o}. \quad (2.34)$$

$$\left. \begin{aligned} \delta = 0 &\rightarrow R_X = R_Y = R_Z \rightarrow \textit{spherical} \\ \delta > 0 &\rightarrow R_X = R_Y < R_Z \rightarrow \textit{prolate} \\ \delta < 0 &\rightarrow R_X = R_Y > R_Z \rightarrow \textit{oblate} \end{aligned} \right\} \quad (2.35)$$

Changing the coordinate scale by,

$$\begin{aligned} X &= \sqrt{\frac{m\omega_o}{\hbar}} X', \\ Y &= \sqrt{\frac{m\omega_o}{\hbar}} Y' \textit{ and} \\ Z &= \sqrt{\frac{m\omega_o}{\hbar}} Z'. \end{aligned} \quad (2.36)$$

In H_{ON} , we have

$$H_{ON} = \frac{\hbar^2}{2m} \left(\frac{m\omega_o}{\hbar} \nabla^2 \right) + \frac{1}{2} m \left(\omega_X^2 \frac{\hbar}{m\omega_o} X^2 + \omega_Y^2 \frac{\hbar}{m\omega_o} Y^2 + \omega_Z^2 \frac{\hbar}{m\omega_o} Z^2 \right), \quad (2.37)$$

$$H_{ON} = H_o + \frac{1}{3} \hbar \omega_o \delta (r^2 - 3Z^2), \quad (2.38)$$

where, $H_o = \frac{1}{2} \hbar \omega_o (-\nabla^2 + r^2)$ is the spherical harmonic oscillator potential,

$r^2 - 3Z^2$ is the quadrupole deformation operator and is related to the spherical

harmonics by $r^2 Y_{20} = \frac{1}{4} \sqrt{\frac{\pi}{5}} (3Z^2 - r^2)$.

Therefore,

$$r^2 - 3Z^2 = -4 \sqrt{\frac{5}{\pi}} \hbar \omega_o \delta r^2 Y_{20}. \quad (2.39)$$

Substituting equation (2.35) in equation (2.34), we get

$$H_N = H_0 - \frac{4}{3} \sqrt{\frac{5}{\pi}} \hbar \omega_0 \delta r^2 Y_{20}. \quad (2.40)$$

Therefore, $H_{ON} = H_0 + H_\delta$, thus the total Hamiltonian given by equation (2.27) becomes,

$$H_N = H_0 + H_d + C \vec{l} \cdot \vec{s} + D \vec{l}^2 \quad (2.41)$$

The \vec{l}^2 term is introduced phenomenologically to lower the energy of the single particle states closer to the nuclear surface in order to correct for the steep rise in the harmonic-oscillator potential there. κ and μ may be different for protons and neutrons and also depend on the nucleon and number. The Hamiltonian may be diagonalized in the basis of the harmonic oscillator using either spherical or cylindrical coordinates depending on the application. The energy levels in the spherical basis are given by,

$$\varepsilon = \eta \omega_0 \left(N + \frac{3}{2} \right), \quad (2.42)$$

with the principle quantum number $N = 2(n_r - 1) + l$, radial quantum number n_r , angular momentum quantum number l , and projection m . In the cylindrical basis they are replaced by,

$$\varepsilon = \eta \omega_z \left(n_z + \frac{1}{2} \right) + \eta \omega_\rho (2n_\rho + |m| + 1). \quad (2.43)$$

where, n_z is the number of quanta in the z direction, n_ρ is that of radial excitations, and m is again the angular momentum projection on the z axis. For the spherical shape the levels will be grouped according to the principle quantum number N (with the splitting by the spin-orbit force then determined through the total angular momentum j), but the behavior with deformation depends on how much of the excitations is in the z direction. For prolate deformation, the potential becomes

shallower in this direction, and the energy contributed by n_z excitations decreases. The cylindrical quantum numbers are thus helpful in understanding the splitting for small deformations. For very large deformations, on the other hand, the influence of the spin-orbit and \vec{l}^2 terms becomes less important and one may classify the levels according to the cylindrical quantum numbers. It has thus become customary to label the single-particle levels with the set $\Omega^\pi[Nn_zm]$. The projection of total angular momentum Ω , and the parity π are good quantum numbers while N , n_z and m are only approximate and may be determined for a given level only by looking at its behavior near the spherical state.

Thus, the single particle energies ε_i and spin projections m_i as a function of deformation parameter δ are obtained by diagonalizing the Nilsson Hamiltonian in cylindrical basis. Calculations are carried out by varying deformation parameter δ values from -0.6 to 0.6 in steps of 0.1. Figure 2.1 show the resulting generated single particle energy levels as functions of deformation. At first sight this Nilsson diagram appears to be a confusing mixture of intersecting levels, yet a number of interesting features can be observed. The highly degenerate spherical levels split up into the individual state pairs characterized by $\pm\Omega$ and the parity, which is determined by the orbital angular momentum in the case of a spherical shape. For the spherical levels the magic numbers and the conventional nomenclature for orbital and total angular momentum are also indicated.

The projection $|\Omega|$ and the parity are indicated for all the levels arising from spherical multiplets below the magic number 82. The way in which the levels diverge can be understood quite easily: states with a larger projection should have smaller quantum number n_z , so that for oblate deformation, where the frequency in the z direction increases, they are lowered with respect to the other states and the opposite

happens for prolate deformation. This systematic behavior of the levels is made more complicated by avoided energy level crossings. As a general rule, levels with the same quantum number numbers should never cross if they are plotted as functions of a single parameter. Thus degeneracy should always be caused by a symmetry which produces additional quantum numbers to distinguish the states. If two levels with the same quantum numbers get close to each other, they are repelled. For example in fig.2.1, the $1/2^-$ level coming from the $f_{5/2}$ spherical multiplet below magic number 40. Going towards negative deformations it is first repelled by the $1/2^-$ level from the $p_{1/2}$ state above and then by the one from the $p_{3/2}$ below. It is not, however, forbidden from crossing the $9/2^+$ coming from the above. This type of level diagram is essential for understanding many of deformed nuclei.

To evaluate the matrix elements corresponding to the above Hamiltonian, we choose the uncoupled basis $|Nl\lambda\Sigma\rangle$.

where,

N – Harmonic oscillator principal quantum number, $N = 0, 1, 2, \dots$

l – Orbital angular momentum quantum number, $l = N, N-2, N-4, \dots$

λ – Projection of l , $\lambda = -l$ to l in steps of unity.

Σ – Projection of intrinsic angular momentum, $\Sigma = \pm 1/2$.

The projection of total angular momentum is given by $\Omega = \lambda + \Sigma$ is a good quantum number.

Diagonal matrix element:

$$\langle Nl\lambda\Sigma | H_o | Nl\lambda\Sigma \rangle = (N + 3/2)\hbar\omega_o, \quad (2.44)$$

$$\langle Nl\lambda\Sigma | \vec{l}^2 | Nl\lambda\Sigma \rangle = l(l + 1)\hbar^2, \quad (2.45)$$

$$\langle Nl\lambda\Sigma | l_z | Nl\lambda\Sigma \rangle = \lambda\hbar, \quad (2.46)$$

$$\langle Nl\lambda\Sigma | r_z | Nl\lambda\Sigma \rangle = \Sigma\hbar, \quad (2.47)$$

To find the matrix element of $H_N = H_0 + H_d + C\vec{l} \cdot \vec{s} + D\vec{l}^2$,

Matrix element of H_0 :

$$\langle N'l'\lambda'\Sigma' | r^2 Y_{20} | Nl\lambda\Sigma \rangle = \langle N'l' | r^2 | Nl \rangle \langle l'\lambda' | Y_{20} | l\lambda \rangle \delta_{\Sigma\Sigma'}. \quad (2.48)$$

Using Wigner Eckart theorem,

$$\langle N'l'\lambda'\Sigma' | r^2 Y_{20} | Nl\lambda\Sigma \rangle = \langle N'l' | r^2 | Nl \rangle \sqrt{\frac{5(2l+1)}{4\pi(2l'+1)}} \begin{pmatrix} l & 2 & l' \\ 0 & 0 & 0 \end{pmatrix} \begin{pmatrix} l & 2 & l' \\ \lambda & 0 & \lambda' \end{pmatrix} \delta_{\Sigma\Sigma'}. \quad (2.49)$$

Matrix element of r^2 :

The selection rule for l' gives $l' = l, l + 2$,

$$\langle N'l' | r^2 | Nl \rangle = \delta_{NN'} \{ \sqrt{(N-l+2)(N+l+1)} \delta_{l'l-2} + (N+3/2) \delta_{l'l} + \sqrt{(N-l)(N+l+3)} \delta_{l'l+2} \}. \quad (2.50)$$

Matrix element of $\vec{l} \cdot \vec{s}$:

$$\begin{aligned} \langle N'l'\lambda'\Sigma' | \vec{l} \cdot \vec{s} | Nl\lambda\Sigma \rangle = & \delta_{NN'} \delta_{ll'} \{ \lambda\Sigma\delta_{\lambda\lambda'}\delta_{\Sigma\Sigma'} + 1/2\sqrt{(l-\lambda)(l+\lambda+1)}\delta_{\lambda'\lambda+1}\delta_{\Sigma'\Sigma-1} \} + \\ & 1/2\sqrt{(l+\lambda)(l-\lambda+1)}\delta_{\lambda'\lambda-1}\delta_{\Sigma'\Sigma+1}. \end{aligned} \quad (2.51)$$

Matrix element of \vec{l}^2 :

$$\langle N'l'\lambda'\Sigma' | \vec{l}^2 | Nl\lambda\Sigma \rangle = l(l+1)\delta_{NN'}\delta_{ll'}\delta_{\lambda\lambda'}\delta_{\Sigma\Sigma'}. \quad (2.52)$$

The constants of C and D are given in terms of other two constants κ and μ , the relations are,

$$\kappa = \frac{C}{2\hbar\omega_0}, \quad (2.53)$$

$$\mu = \frac{2D}{C}. \quad (2.54)$$

The energy eigenvalues corresponding to the Hamiltonian can be written as

$$E_N = (N + 3/2)\eta\omega_0 + \delta\eta\omega_0(\delta)\langle U \rangle - 2\kappa\eta\omega_0\langle \vec{l} \cdot \vec{s} \rangle - \mu\kappa\eta\omega_0\langle \vec{l}^2 \rangle. \quad (2.55)$$

$$H_\delta = -\delta\hbar\omega_0(\delta) \frac{4}{3} \sqrt{\frac{\pi}{5}} r^2 Y_{20}. \quad (2.56)$$

$$H_\delta = -\delta\hbar\omega_0(\delta)U. \quad (2.57)$$

where,

$$U = -(4/3)\sqrt{\frac{\pi}{5}}r^2Y_{20}. \quad (2.58)$$

Nilsson defined new form of deformation parameter η given by

$$\eta = \frac{\delta\eta\omega_0(\delta)}{\eta\omega_0\kappa}. \quad (2.59)$$

Therefore,

$$E_N = (N + 3/2)\eta\omega_0(\delta) + \kappa\eta\omega_0(\eta\langle U \rangle - 2\langle \vec{l} \cdot \vec{s} \rangle - \mu\langle \vec{l}^2 \rangle). \quad (2.60)$$

$$E_N = (N + 3/2)\eta\omega_0(\delta) + \kappa\eta\omega_0r^{N\Omega}. \quad (2.61)$$

where,

$r^{N\Omega}$ - Eigenvalue of operators.

N – Total number of oscillator quantum number.

Ω – Quantum number corresponding to J .

Using the set of κ and μ values corresponding for principle quantum number N , the energy eigenvalues and the spin projections are generated. For our calculations, we have generated energy levels upto $N = 11$.

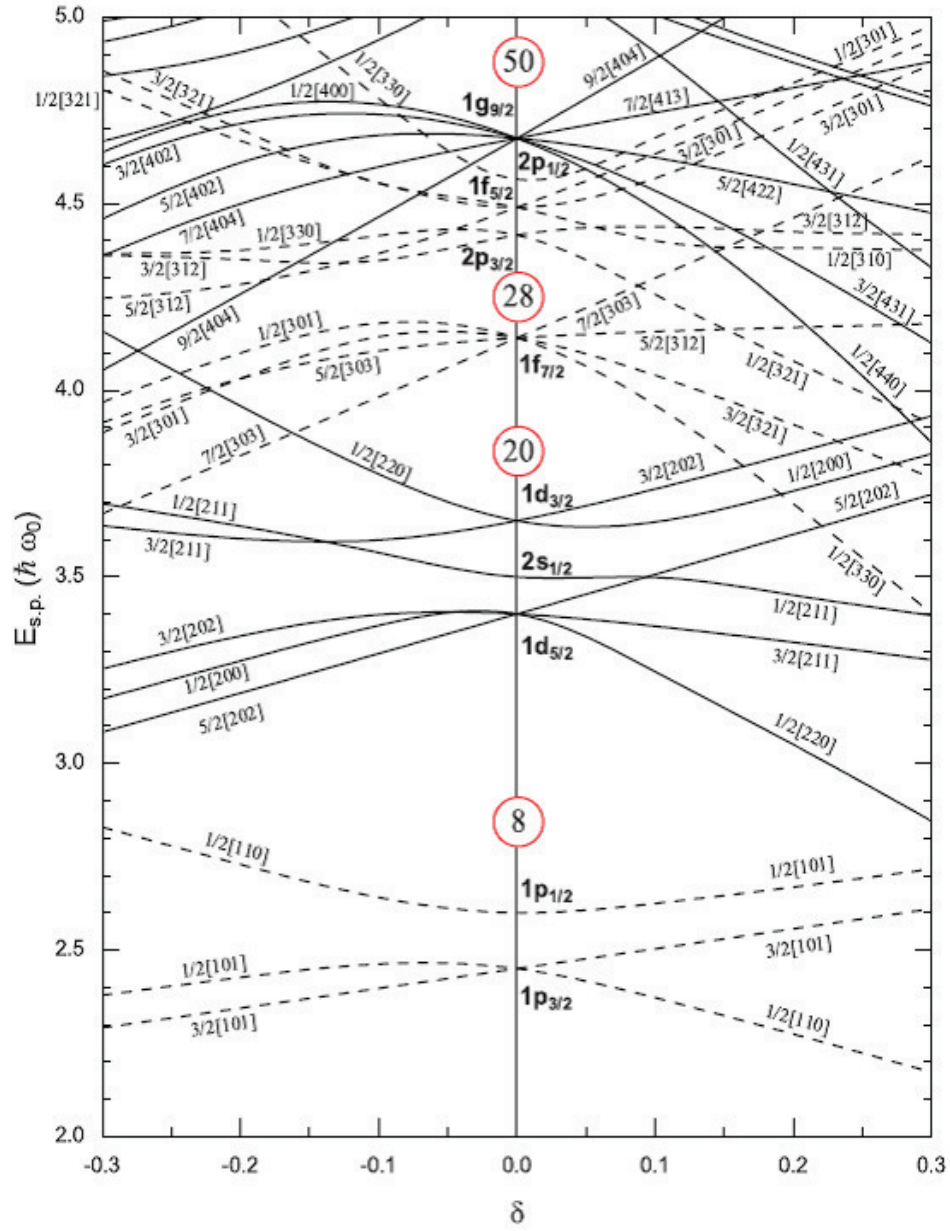


Fig. 2.1: Nilsson diagram for protons and neutrons. Single-particle energies as a function of deformation δ are shown for Z or $N \leq 50$. The even and odd parity levels are denoted by solid and dashed lines respectively. The labeling of levels are by asymptotic quantum numbers $\Omega[Nn_z m]$.

2.4.2 Triaxially deformed single particle levels

Another method for the calculation of mass parameters is the cranking model invented by [Inglis 1954]. The name reflects the idea of an external influence forcing the phenomenological single-particle potential. A simple and widely used way to describe the change of the single-particle structure with rotation is given by the cranked Nilsson model. Therefore, the deformed harmonic oscillator is assumed to be cranked and the oscillator level scheme generated by diagonalising the cranked oscillator shells which is used to investigate hot as well as hot rotating nuclei. This model gives a microscopic description of the influence of rotation on the single-particle motion. The nucleons are considered as independent particles moving in the rotating potential well with the deformation described by deformation parameter ε and shape parameter γ . The single-particle level scheme as a function of deformation parameter ε and shape parameter γ is obtained by diagonalizing the cranked Nilsson Hamiltonian in the cylindrical basis states. The single-particle Hamiltonian is given as,

$$H^\omega = H_o - \omega j_z = H_{HO} + C\bar{l} \cdot \bar{s} + D \left(\bar{l}^2 - 2 \langle \bar{l}^2 \rangle \right) - \omega j_z, \quad (2.62)$$

where, ω is the rotational frequency and H_{HO} is the triaxial Nilsson-Hamiltonian for a single particle in the non-rotating system and is given by,

$$H_{HO} = \frac{p^2}{2m} + \frac{1}{2} m \{ \omega_x^2 x^2 + \omega_y^2 y^2 + \omega_z^2 z^2 \}. \quad (2.63)$$

In the Cranking model, the nucleons move in a potential that is set to rotate with a rotational frequency ω . This is realized by the addition of the term $-\omega j_z$ to the intrinsic Hamiltonian for the cranking to be around any one of the principal axes z with the classical correspondence of both the coriolis force and the centrifugal force. It is known from earlier studies that this model accounts only for small rotational

frequencies. A more exact treatment is necessary for high rotational frequencies in a nucleus induced by heavy ion collisions.

In the Inglis model, the disturbance in the nucleons caused by the rotation is treated as a perturbation of the ground state intrinsic field whereas for high spins the coupling between the nucleons and the rotational motion is treated in a non perturbative way by [Bengtsson 1984]. At very high spins the quantum mechanical wobbling can be neglected so that the rotation is assumed to take place around a fixed axis. The Coriolis force strives to align the spin vectors of the nucleons along the rotational axis. As the rotational frequency increases, more and more nucleons become aligned. Since the aligned nucleons have a density that is symmetrical around the rotational axis, prolate nucleus rotating around an axis perpendicular to the symmetry axis will change its deformation to a triaxial form. At still higher angular momenta, such a nucleus might even get an oblate shape. It is evident that it is possible to describe the transition from prolate shapes, with the rotation axis perpendicular to the symmetry axis, to oblate shapes with the rotation around the nuclear symmetry axis. Microscopic calculations of deformation energy using a many body Hamiltonian and trial wave functions have been done in [Faessler 1976]. Based on Strutinsky shell correction method, several groups [Poloszajtak 1977, Neergard 1975, Anderson 1981, Faber 1979 and Hammamoto 1983] have performed calculations in which full cranking Hamiltonian is diagonalised for a deformed nucleus.

The three oscillator frequencies are given by

$$\omega_x = \omega_o \left[1 + \frac{1}{3} \epsilon \cos \gamma + \frac{1}{\sqrt{3}} \epsilon \sin \gamma \right], \quad (2.64)$$

$$\omega_y = \omega_o \left[1 + \frac{1}{3} \epsilon \cos \gamma - \frac{1}{\sqrt{3}} \epsilon \sin \gamma \right], \quad \text{and} \quad (2.65)$$

$$\omega_z = \omega_o \left[1 - \frac{2}{3} \varepsilon \cos \gamma \right], \quad (2.66)$$

with the constraint that the total volume remains constant, i.e.,

$$\omega_x \omega_y \omega_z = \omega_0^3. \quad (2.67)$$

The value of undeformed oscillator spacing $\hbar\omega_o = 35 \text{ MeV} / (A^{1/3} + 0.77)$ is used in our level scheme and the κ and μ values are taken from [Jinge-ye-zhang 1989 and Bengtsson 1984]. The parameter $\varepsilon = \frac{(a-b)}{R_0}$ corresponds to the elongation or flattening of the potential, while γ describes its non-axiality, where ‘a’ is the semi major axis, ‘b’ is the semi minor axis and R_0 is the radius of equivalent sphere. Calculations are carried out for the deformation parameter $\varepsilon = 0.0 - 0.6$ in steps of 0.1 and for shape parameter $\gamma = -180^\circ$ (oblate non-collective) to $\gamma = -120^\circ$ (prolate collective). The basic ingredient in the statistical theory is a single particle level scheme which is generated up to $N = 11$ shells for the finite temperature range. The significance of various regions of deformation with respect to the rotation axis is illustrated in fig. 2.2 – 2.4.

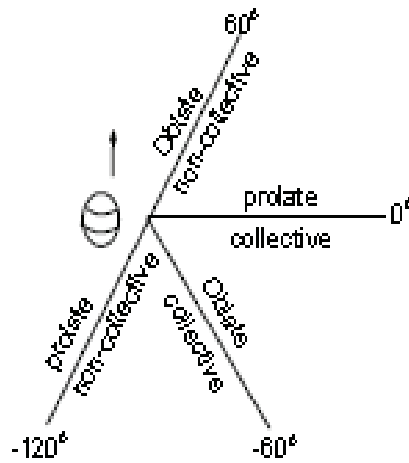


Fig. 2.2: Polar plot of nuclear deformation for rotation around x-axis.

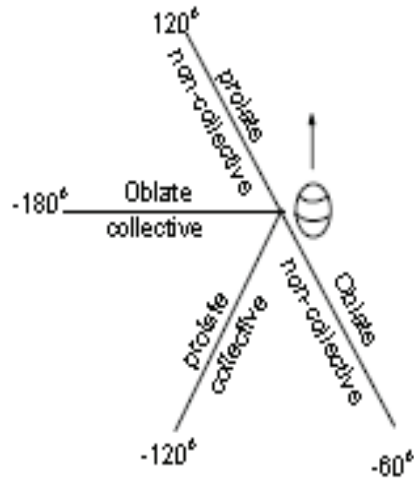


Fig. 2.3: Polar plot of nuclear deformation for rotation around y-axis.

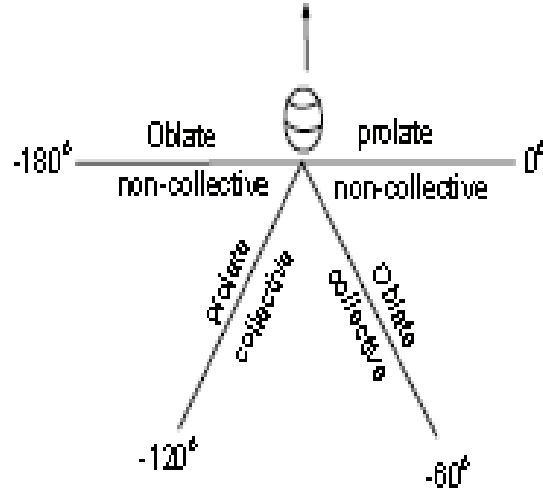


Fig. 2.4: Polar plot of nuclear deformation for rotation around z-axis.

CHAPTER – III

NUCLEAR SHAPE TRANSITIONS

3.1 Introduction

Nuclear structure studies is about probing the changes occurring in the nuclei that are hot and rotating and which have high excitation energy. The resulting effect of these two physical quantities i.e, temperature and angular momentum in the nuclei causes shape transition. Factors such as deformation parameter at different temperatures and momenta decide the shape of the nuclei. Different types of shape transitions can occur as a result of increase in temperature, such as: spherical to deformed, prolate to oblate and prolate to spherical. With increase in angular momentum, certain nuclei have the proclivity to transition from prolate to triaxial and certain other nuclei such as deformed rare earth nuclei tend to possibly transition from prolate to oblate shapes [Rajasekaran 1988 and Rajasekaran 2003]. Shell effects are the reasons for static deformations in nuclei at low temperatures and these static deformations vanish with the increase in temperature. Nevertheless, there are cases where the nuclei respond in a different way as a result of increase in temperature [Goldenfeld 1992]. Studies of theoretical and experimental nature have been done to explain the shape transition behavior, such as some given below.

[Neergard 1976 and Anderson 1976] and [Bengtsson 1975] have studied independently nuclei using Strutinsky shell correction method and their calculations have produced conforming results for the nuclei deformation behavior of nuclei with high angular momentum [Bohr 1975]. Using finite temperature Hartree – Fock – Bogolibov cranking theory, [Goodman 1989] has produced remarkable prediction of transition of prolate collective to oblate non-collective in ^{158}Yb nucleus at an angular momentum of $M = 39\hbar$. Bohr [Bohr 1975] studied nuclear behavior of the spinning

nuclei in the various regions of deformation. Castanos [Castanos 1979] investigated the transition of Sm isotopes using the interacting boson approximation model.

Werner [Werner 2000] have come up with expressions for moments up to sixth order of the ground state quadrupole operator and calculations of different shapes have been done analytically using interacting boson model (IBM). Li [Li 2010] have used the self-consistent relativistic mean field theory in the BCS calculation of quadrupole energy surfaces in Ba and Xe isotopes. [Rajasekaran 1988] have done extensive investigations in shape and phase transition in ^{154}Dy with neutron number $N = 88$. ^{154}Dy showed a shape transition from prolate collective to oblate non-collective in and around the angular momentum of 50 (\hbar) and excitation energy of 50 MeV. Other nuclei with neutron number 88 showing similar behavior have been reported by [Simpson 1988] for ^{158}Er , by [Cranmer 1987] for ^{154}Dy . Henss [Henss 1988] experimentally found shape transition from a collective prolate shape to oblate using the spin generated by single particle motion. Other experimental studies such as the Giant Dipole Resonance (GDR) built on excited states have also been done [Gaardhoje 1992, Nanal 1999 and Chakrabarty 2012]

The search for signature of transition between varieties of shapes has earned substantial attention and interest in nuclear structure physics. There are numerous experimental techniques to explore the shapes of hot rotating nuclei. The response of nuclear shape to thermal excitations has been experimentally investigated from the shapes of GDR built on excited states. The fact that the phase transition to deformed shapes causes a splitting of the giant resonance has been well known for many years and it is used to study the shape changes as a function of angular momentum or temperature by means of fine structure of the GDR.

A very simple understanding of the universal features of shape transitions in nuclei as a function of angular momentum and temperature is given by Levit [Levit 1984]. A major activity in the study of shape – phase transitions for nuclei in the ground state has been carried out with the interacting boson model (IBM) at zero temperature. The IBM naturally incorporates different symmetry limits associated with specific nuclear properties. The shell model approaches are very appropriate for describing various aspects of nuclear structure. The nuclear shell model (SM) treats the single particle and collective degrees of freedom equally and appears to be extremely successful in the calculation of the back-bending curve in light nuclei. However the drastic increase of the configuration space for medium and heavy systems makes the shell model calculations impossible. Similarly, the HFB calculation employ a model Hamiltonian in a limited model space with pairing – plus – quadrupole interaction but this may not be realistic once temperature comes into play. A self consistent mean field attained with the aid of cranked Nilsson or Saxon – Woods potentials and pairing forces has been quite competitive up to now.

3.2 Finite temperature Hartree – Fock – Bogoliubov Cranking method

In the finite temperature Hartree – Fock – Bogoliubov Cranking calculations (FTHBC), Hamiltonian H [Goodman 1983 and Tanabe 1981] is written as,

$$H = e - \mu_p N_p - \mu_n N_n - \omega J_x + \Gamma . \quad (3.1)$$

Here, e , $\mu_{p(n)}$ and ω are spherical single-nucleon energy, chemical potential and angular velocity respectively. The Hartree-Fock and pair potentials are

$$\Gamma_{ij} = \sum_{kl} \langle ik | U | jl \rangle \rho_{lk} , \quad (3.2)$$

$$\Delta_{ij} = \frac{1}{2} \sum_{kl} \langle ij | v | kl \rangle t_{kl} , \quad (3.3)$$

where, ρ_{lk} and t_{kl} are the Hartree-Fock and pairing densities.

The quasi-particle occupation probabilities in terms of temperature T and eigenvalues of FTHBC equation i.e., quasi-particle energies E_i are given by,

$$f_i = [1 + e^{\frac{E_i}{T}}]^{-1}, \quad (3.4)$$

The chemical potentials and the angular velocity are varied to satisfy the number constraints and spin constraints respectively.

$$\langle N_p \rangle = Z, \langle N_N \rangle = N, \quad (3.5)$$

$$\langle J_x \rangle = [I(I+1)]^{\frac{1}{2}}. \quad (3.6)$$

By the iteration method, the self-consistent solution to Eqs. (3.1) to (3.6) is obtained.

The free energy is

$$F = E - TS, \quad (3.7)$$

With entropy S and energy E is given by

$$S = -\sum_i [f_i \ln f_i + (1 - f_i) \ln(1 - f_i)], \quad (3.8)$$

$$E = \langle H \rangle = Tr [(e + \frac{1}{2} r) \rho + \frac{1}{2} \Delta t^+]. \quad (3.9)$$

The FTHFBC equation determines the values of the quadrupole deformation ε and γ and the values of the pairing gaps Δ_p and Δ_N . The minimization of the free energy function $F(\beta, \gamma, \Delta_p, \Delta_N; I, T)$ defines the equilibrium or most probable state of the nucleus for the given spin and temperature.

3.3 Finite temperature Strutinsky method

In this method [Ignatyuk 1969], the potential $V(r)$ is the sum of harmonic oscillator term $V_{H.O}$ and the correction term V_{corr} .

$$V(r) = V_{H.O} + V_{corr}. \quad (3.10)$$

With,

$$V_{H.O} = \frac{1}{2} \hbar \omega_o \rho^{2s} \left[1 - \frac{2}{3} \varepsilon \sqrt{\frac{4\pi}{5}} \cos \gamma Y_{20} - \varepsilon \sqrt{\frac{4\pi}{5}} \sin \gamma [Y_{23} + Y_{2-2}] \right], \quad (3.11)$$

$$V_{\text{corr}} = -k\hbar\omega_0\{2\vec{l}\cdot\vec{s} + \mu[l^2 - N(N+3)]\}. \quad (3.12)$$

The first term in Eq. (3.10) depends on the two quadrupole deformation parameters ε and γ which decide the nuclear shape. The second term is introduced to describe the inertia properties.

The expression for the routhian function of a nucleus at a temperature T rotating with the angular frequency ω is,

$$R(\varepsilon, \gamma, \omega, T) = E_{LD}(T = \omega = 0) + \sum_{i=1}^A \varepsilon_i(\varepsilon, \gamma, \omega) + \bar{n}_i(T) - \sum_{i=1}^A \left[\begin{array}{l} \varepsilon_i(\varepsilon, \gamma, \omega) = 0 \\ + \bar{n}_i(T) = 0 \end{array} \right]. \quad (3.13)$$

Here, E_{LD} is the liquid drop component of the energy, $\varepsilon_i(\varepsilon, \gamma; \omega)$ are the energies of single particle states and $\bar{n}_i(T)$ is the occupation probability of the i^{th} shell. The last term in Eq. (3.13) is the Stravinsky – smeared sum of single particle energies for $T = 0$. As this procedure is a direct consequence of the correct calculation of the nuclear moment of inertia, renormalization of the average moment of inertia is not necessary. On the basis of the relation

$$\sum_{i=1}^A \varepsilon_i(\varepsilon, \gamma, \omega) - \sum_{i=1}^A \varepsilon_i(\varepsilon, \gamma, \omega = 0) = \frac{1}{2}J_{\text{rig}}(\varepsilon, \gamma). \quad (3.14)$$

Eq. (4.13) may be rewritten as,

$$R(\varepsilon, \gamma; \omega, T) = E_{LD}(\varepsilon, \gamma, \omega = 0) - \frac{1}{2}J_{\text{rig}}(\varepsilon, \gamma) + \omega^2 - \delta S_{\text{stru}}(\varepsilon, \gamma; \omega). \quad (3.15)$$

The rigid body moment of inertia J_{rig} is valid at $T = 0$ with good accuracy.

Here, the shell correction is written as,

$$\delta S_{\text{stru}}(\varepsilon, \gamma; \omega) = \sum_{i=1}^A \varepsilon_i(\varepsilon, \gamma, \omega) - \sum_{i=1}^A \varepsilon_i(\varepsilon, \gamma, \omega). \quad (3.16)$$

Routhian function given in Eqs. (3.13) and (3.15) is used for studying the rotation in cold nuclei. The applicability of this method at $T = 0$ can be extended to nuclei at non-zero term.

3.4 Relativistic mean field theory

A classical relativistic field theory starts from a number of fields $q_j(x)$. Their dynamics is determined through a Lagrangian density, $L(q, \partial_\mu q, t)$ and the variational principle,

$$\delta \int dt L = \delta \int d^4 x L(q, \partial_\mu q, t) = 0. \quad (3.17)$$

The energy momentum tensor is given by,

$$T^{\mu\nu} = -g^{\mu\nu}L + \frac{\partial L}{\partial(\partial_\mu q_j)} \partial^\nu q_j. \quad (3.18)$$

It obeys the continuity equation,

$$\partial_\mu T^{\mu\nu} = 0. \quad (3.19)$$

In relativistic mean field theory of the nucleus the fields $q_j(x)$ are given by the wave functions of the nucleons, several meson fields and the electromagnetic potentials. The nucleons are described by Dirac spinors $\psi_i(x,s,t)$ with four components, where, $x = (t,r)$ is the space-time coordinate, s labels the four Dirac components and $t = p, n$ characterizes the isospin.

The Dirac equation for the nucleon in $\sigma - \omega - \rho$ version of Relativistic Mean Field (RMF) theory [Agarwal 2001, Jian-You Guo 2010, Bhuyan 2011 and Fu 2013] is,

$$[-i\alpha \cdot \nabla + V(r) + \beta(M + S(r))]\Psi_i = \epsilon_i \Psi_i, \quad (3.20)$$

The vector potential $V(r)$ is,

$$V(r) = g_\omega \omega_0(r) + g_\rho T_3 \rho_0(r) + e \frac{(1-r_3)}{2} A_0(r), \quad (3.21)$$

and the scalar potential $S(r)$ is,

$$S(r) = g_\sigma \sigma(r). \quad (3.22)$$

The Klein-Gordon equation for the mesons and the electromagnetic fields are

$$\{-\Delta + m_\sigma^2\} \sigma(r) = -g_\sigma \rho_s(r) - g_2 \sigma^2(r) - g_3 \sigma^3(r), \quad (3.23)$$

$$\{-\Delta + m_\omega^2\} \omega_0(r) = g_\omega \rho_v(r), \quad (3.24)$$

$$\{-\Delta + m_\rho^2\} \rho_0(r) = g_\rho \rho_3(r), \quad (3.25)$$

$$-\Delta A_0(r) = e\rho_c(r). \quad (3.26)$$

where, ρ_s , ρ_v , ρ_3 and ρ_c are the corresponding densities, neglecting the negative energy states. The occupational probability n_i at finite temperature in the constant pairing gap approximation (BCS) is,

$$n_i = \frac{1}{2} \left[1 - \frac{\epsilon_i - \lambda}{\bar{\epsilon}_i} \right] \{1 - 2f(\bar{\epsilon}_i, T)\}, \quad (3.27)$$

where, $f(\bar{\epsilon}_i, T)$ is the distribution function and ϵ_i is the single particle energy for the i^{th} state. The chemical potential λ for the protons (neutrons) is obtained from the requirement

$$\sum_i n_i = Z(N). \quad (3.28)$$

Free energy, $F = E - TS$ is minimized to find the equilibrium value of the quadrupole deformation β_2^0 and the proton (neutron) pairing gaps Δ_p (Δ_n). The total energy ,

$$E(T) = \sum_i \epsilon_i n_i + E_\sigma + E_{\sigma NL} + E_\rho + E_c + E_{pair} + E_{cm} - AM. \quad (3.29)$$

where, E_σ , $E_{\sigma NL}$, E_ω , E_ρ , E_i etc., having the usual meaning [Agarwal 2001].

3.5 Monte Carlo method

Auxiliary-field Monte Carlo (AFMC) account for correlation effects in full, it is necessary to include all fluctuations – both thermal and quantal of all the auxiliary fields σ (including large-amplitude quantal fluctuations). This requires an integration over a very large number of σ fields (at all time slices), and in practice can only be done by Monte Carlo methods. Such a quantum Monte Carlo method is generally known as the auxiliary- field Monte Carlo (AFMC) method and has been used in

strongly correlated electron systems. In the context of the configuration-interaction shell model the method is known as the shell model Monte Carlo (SMMC).

3.6 Landau theory of phase transition

This theory was developed by Landau in the 1940's , originally to describe superconductivity. Landau theory [Landau 1980] is a mean field theory, in the sense that the system is assumed to be adequately escribed by a single macroscopic state. Not only we can use Landau theory to describe and understand the nature of phase transiitons among ordered (and disordered) states, but we can use it as a starting point for understanding the behavior of ordered states.

Landau made a series of assumptions to approximate the free energy of the system in such a way that it exhibits the non – analyticity of a phase transition and turns out to capture much of the physics. Applying very basic ideas of Landau theory of phase transitions, Levit et al. [Levit 1984] expanded the free energy in terms of the deformation parameters and obtained a very simple understanding of the universal features of phase transition in nuclei as a function of angular momentum and excitation energy. By analogy, we have used a statistical theory to explore the nature of phase transition and its temperature and angular momentum dependence.

3.7 Jacobi transition

In 1961, Beringer and Knox suggested that a transition might be expected in the case of atomic nuclei, idealized with surface tension [Landau 1980]. Subsequent theoretical studies in 1974 and in 1986 confirmed this conjecture. It was also realized that the mathematical problem of a rotating, uniformly charged drop goes over smoothly into Jacobi's classic astronomical problem by making the magnitude of the repulsive electrostatic energy decrease through zero to negative values, at which point

it becomes a Newtonian attraction. Evidence for Jacobi effects must be sought in the quasi – continuous gamma spectrum emitted from states of very high angular momentum. For example, Maj et al. [Maj 2001] have presented evidence for a Jacobi transition in ^{46}Ti , based on the analysis of the gamma spectrum associated with decays of the giant – dipole resonance.

CHAPTER IV

SHAPE TRANSITIONS IN Te AND Se ISOTOPES

4.1. Introduction

Structure studies of Tellurium nuclei with two protons outside the major shell ($Z = 50$) has become essential in describing their observed energy spectrum experimentally [Saxeena 2014 and Fotaides 2014]. The present work has been extended to investigate the shape phase transition in even – even isotopes of Te for mass number 110, 114, 116, 122, 124 and 130 via the Statistical Theory of Hot Rotating Nuclei (STHRN). The thermodynamic properties such as excitation energy, level density parameter, level density, rotational energy, rotational frequency, kinematic moment of inertia, spin cut off parameter and neutron emission probability has been calculated and the impact of shape transition exhibited in these quantities has been observed. The STHRN method incorporates various degrees of freedom such as temperature, angular momentum and deformation parameters [Rajasekaran 2008, 2003]. Statistical descriptions of finite nuclear systems are generally based on grand canonical ensemble averages with good quantum numbers like angular momentum or particle number [Kandhimadhi 2011] and it is described in the formalism part.

Experimental study on ^{124}Te by [Fotiades 2014] found that the non-collective oblate states with $I^\pi = 16^+$ at excitation energy above 5.5 MeV. Several theoretical models [Vikas 2015 and Stuchbery et 2013] have been employed to investigate the structure of Te nuclei. Theoretical investigations of Te isotopes near the proton drip line were discussed by Mamta et al. [Mamta 2009] employing STHRN method. The results reveal that proton rich Te nuclei are less deformed with prolate collective or nearly prolate shapes than those near the stability valley which are well deformed with oblate non-collective shape. In our previous work [Rajasekaran 2008], the behavior of nucleons and their reactions to the collective rotation for ^{154}Dy has been

studies using the theoretical framework of STHRN. In STHRN method, the thermodynamical system of fermions is nothing but the compound nuclei formed through heavy ion fusion reaction at high excitation energy. With the increase in the excitation energy of the compound system the nuclear levels becomes 10^6 times smaller than the average single – particle spacing. Therefore the knowledge on nuclear level density becomes essential to understand the structural phenomena. Moreover, the interest in studying high spin populated state is to estimate the probability for phenomena such as fusion, fission and quasi – fission. Thus the neutron emission probability is also an important factor to determine the probable nuclear reaction.

Statistical approach is the most prominent one to describe the average behavior of the compound nucleus [Gupta 2008] using the grand partition function of the system. The main assumption of the statistical theory is the microscopic equilibrium, which means that all states with same excitation energy are equally populated. The intrinsic properties of these nuclei may be described as a function of temperature, spin and deformation. Also the statistical theory of the nucleus incorporating the deformation degrees of freedom, pairing correlation and collective rotation of the system to obtain the separation energy of nucleons [Moretto 1973]. The statistical theory of hot rotating nuclei is used to predict the nuclear properties which are related with the shape transition. The statistical calculation involves the determination of the grand partition function of the system with the condition that it conserves energy, the particle number, and the total angular momentum of the system. The statistical theory which incorporates different degrees of freedom like deformation parameter, angular momentum, and temperature is used to study some of the structural properties of nuclei. The following parameters can be studied on the

basis of statistical theory: Nuclear level density parameter, Entropy, Rotational energy, Excitation energy, Moment of inertia, Level density, Single nucleon separation energy. Also, the shape changes of nuclei from prolate shape to oblate is investigated by statistical theory, adopted by Moretto [Moretto 1972]. In this present work, the above mentioned thermal and rotational properties were studied for the isotopes of ^{110}Te , ^{114}Te , ^{116}Te , ^{122}Te , ^{124}Te and ^{130}Te .

Also, calculations of excitation energy based on the statistical theory of hot rotating nuclei in the most neutron deficient Se isotopes such as ^{68}Se , ^{70}Se , ^{72}Se , ^{74}Se for an angular momentum range of $0\hbar$ - $14\hbar$ and a temperature range of 0.4 MeV – 1.0 MeV in steps of 0.1 MeV show a comparable results with the experimental data. A shape transition was found which is reflected in other thermodynamical parameters such as spin cut off parameter and rotational frequency with respect to angular momentum. A comparison of excitation energy of ^{74}Se based on the statistical model with its experimental counterpart was also done in the form of an energy level diagram and a closeness of the theoretical and the experimental values for the same momenta was found.

4.2 Determination of structural properties

Shape transition are investigated for high spin hot rotating nuclei ^{110}Te , ^{114}Te , ^{116}Te , ^{122}Te , ^{124}Te & ^{130}Te and for ^{68}Se , ^{70}Se , ^{72}Se & ^{74}Se using statistical theory of hot rotating nuclei by the following structural properties of nuclei. The statistical theory of hot rotating nuclei is employed to study the structure of the nucleus at high spin states. The single particle energy levels are engendered from triaxially deformed harmonic oscillator explained in Chapter II. The shape transition is investigated by obtaining the following structural properties of nuclei:

- (i) Excitation energy

- (ii) Level density parameter
- (iii) Spin cut off parameter
- (iv) Rotational energy
- (v) Kinematical moment of inertia
- (vi) Neutron emission probability
- (vii) Single nucleon separation energy

4.2.1 Excitation energy

Excitation energy is the amount of energy required to excite the nucleons from the ground state to an excited state by means of temperature (T) at a given angular momentum (M). The excitation energy $E^*(M, T)$ is obtained by taking the difference between the ground state energy $E(0, 0)$ and the excited state $E(M, T)$ which is derived from the grand partition function given in eq.2.9. Therefore, $E^*(M, T)$ is expressed as,

$$E^*(M, T) = E(M, T) - E(0, 0). \quad (4.1)$$

where, $E(0, 0)$ is the ground state energy of the nucleus and is given by,

$$E(0, 0) = \sum_{i=1}^N \varepsilon_i^N + \sum_{i=1}^Z \varepsilon_i^Z. \quad (4.2)$$

4.2.2 Level density parameter

The single particle level density parameter ‘ a ’ as function of angular momentum M, temperature T, deformation parameter ε and shape parameter γ is extracted using the expression,

$$a(M, T) = S^2(M, T, \varepsilon, \gamma) / 4E^*(M, T, \varepsilon, \gamma). \quad (4.3)$$

where, S is entropy and E^* is excitation energy.

4.2.3 Spin cut off parameter

The spin cut-off parameter is a free parameter and it is related to an effective moment of inertia. The spin cut-off parameter σ^2 as a function temperature T and angular momentum M is given as,

$$\sigma^2(M, T) = \sum_i n_i^N (1 - n_i^N) m_i^{N^2} + \sum_i n_i^Z (1 - n_i^Z) m_i^{Z^2}. \quad (4.4)$$

4.2.4 Rotational energy

The rotational energy E_{rot} is expressed as,

$$E_{rot} = E(M, T) - E(0, T). \quad (4.5)$$

4.2.5 Kinematical moment of inertia

The kinematical $j^{(1)}$ and moment of inertia are given by,

$$j^{(1)} = \hbar^2 I \left(\frac{\partial E_{rot}}{\partial I} \right)^{-1}. \quad (4.6)$$

4.2.6 Neutron emission probability

The number of neutrons emitted with an energy interval E_n and $(E_n + dE_n)$ is evaluated as ,

$$\varphi(E_n) = \frac{dN(E_n)}{dE_n} = C E_n \rho(U), \quad (4.7)$$

where, $U = E^* - E_{rot} - S_N - E_n$ and E_n is the outgoing neutron energy and the level density $\rho(U)$ at an excitation U is obtained using the formula.

$$\rho(E^*) = \frac{\left(\frac{\hbar^2}{2\theta}\right)^{\frac{3}{2}} (2M+1)\sqrt{a} e^{2\sqrt{aE^*}}}{12(E^*+T)^2}. \quad (4.8)$$

4.2.7 Single nucleon separation energy

The nucleon separation energy as a function of angular momentum M , temperature T and the deformation parameters ε and γ is calculated using the expressions,

$$S_n(M, T) = TN / [\sum_i(1 - n_i^N)n_i^N] \text{ and} \quad (4.9)$$

$$S_z(M, T) = TZ / [\sum_i(1 - n_i^Z)n_i^Z]. \quad (4.10)$$

4.3 Results and discussions

Figures 4.1(a-f) illustrate the hodograph of the deepest energy minima of the nuclei as a function of the deformation parameters ε , γ and angular momentum M obtained for temperatures $T = 0.5$ MeV. The equilibrium shape of the system is determined by minimizing the free energy with respect to the deformation parameters ε , γ at finite angular momentum M and temperature T and it is denoted by a dot in these figures. It is observed from fig.4.1(a) that the nucleus ^{110}Te is found to be spherical ($\varepsilon = 0.0$) for the angular-momentum range $M = 0 - 9\hbar$ and finally reaches the highly deformed non-collective oblate shape ($\varepsilon = 0.1$ and $\gamma = -180^\circ$) for $M = 10 - 25\hbar$. Figure 4.1(a) shows that the nucleus ^{114}Te remains at spherical shape with $\varepsilon = 0.0$ for the angular momentum range $M = 0 - 7\hbar$ and becomes oblate shape ($\varepsilon = 0.1$ and $\gamma = -180^\circ$) for $M = 8 - 25\hbar$ in fig. 4.1(b). A similar behavior is exhibited in figs. 4.1(c), 1(d), 1(e) and 1(f) for four other nuclei ^{116}Te , ^{122}Te , ^{124}Te and ^{130}Te .

Figure 4.2 gives a comparative analysis of excitation energy calculated from STHRN method for ^{124}Te and ^{126}Te for different angular momenta with the available experimental data and other theoretical models such as shell model. It is quite obvious that the shell model closely matches with experimental data for the states of the lower angular momenta but at higher angular momenta the results seems to

deviate from the experimental data. From the excitation energy diagram it is observed that the STHR method produces the results more accurately for the states of the higher angular momenta.

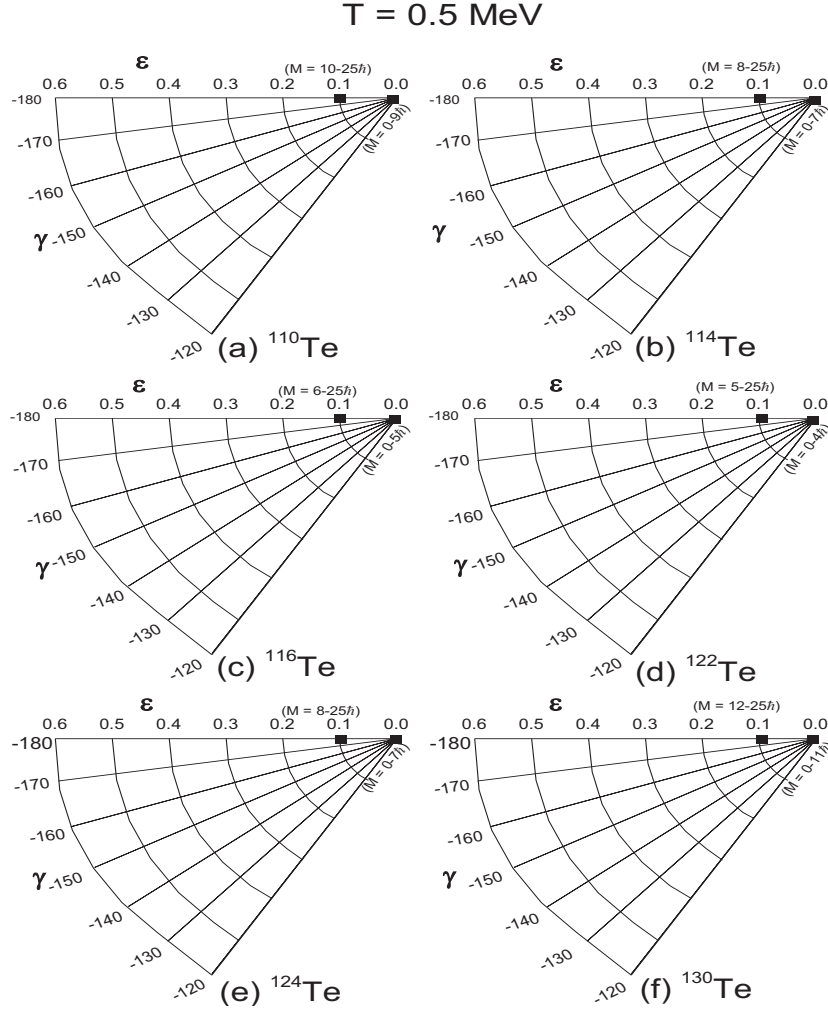


Fig. 4.1 (a-f): The shape evolution of ^{110}Te , ^{114}Te , ^{116}Te , ^{122}Te , ^{124}Te and ^{130}Te as a function of the angular momentum $M(\hbar)$ at the temperature $T = 0.5 \text{ MeV}$. The dot refers to the free energy minimized with respect to deformation parameters ϵ and γ for a particular range of angular momentum M .

It is seen that the calculated parameters as a function of angular momentum, temperature and deformation parameter ϵ and γ showed an abrupt change for these heavier nuclei beyond the angular momentum $M = 12\hbar$. This abrupt fall causes a

minimum in the parameter values and it corresponds to a shape transition from spherical to non collective oblate.

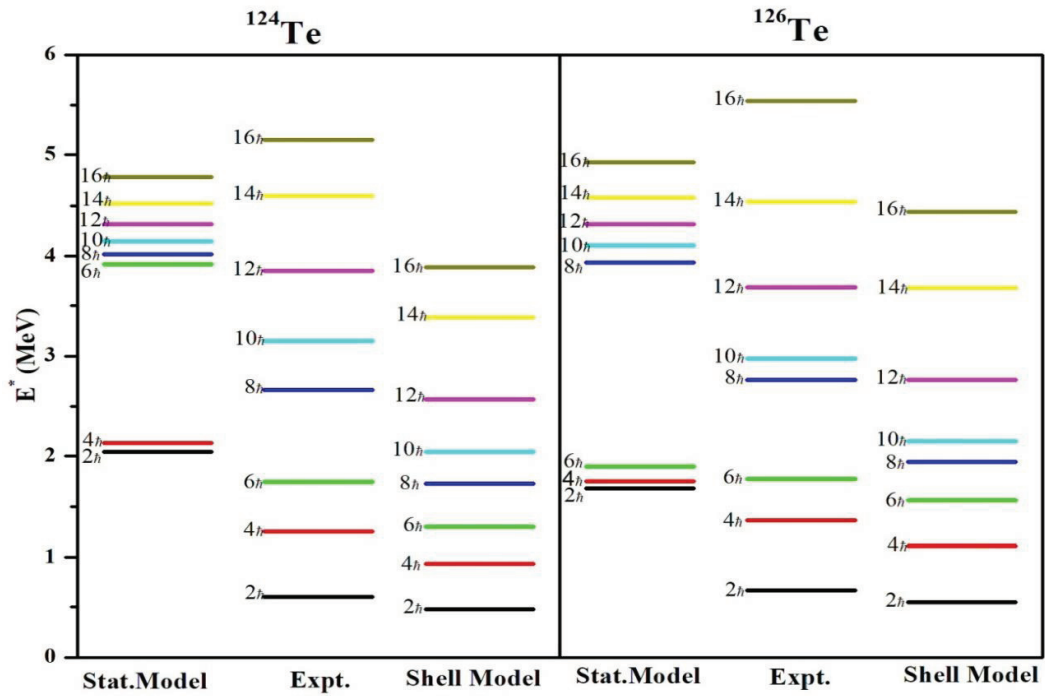


Fig.4.2: Excitation energy E^* (MeV) for ^{124}Te and ^{126}Te as a function of the angular momentum M (\hbar) at the temperature $T = 0.5$ MeV. Results are compared with available experimental data and with shell model.

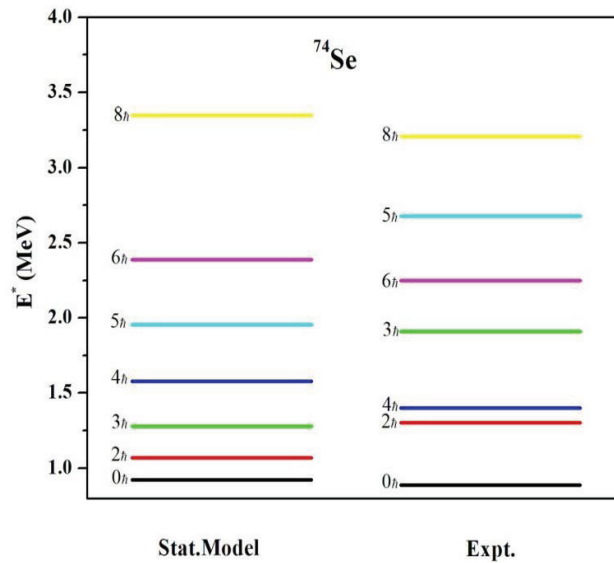


Fig. 4.3: Comparison of calculated and experimental excitation energy E^* (MeV) for ^{74}Se .

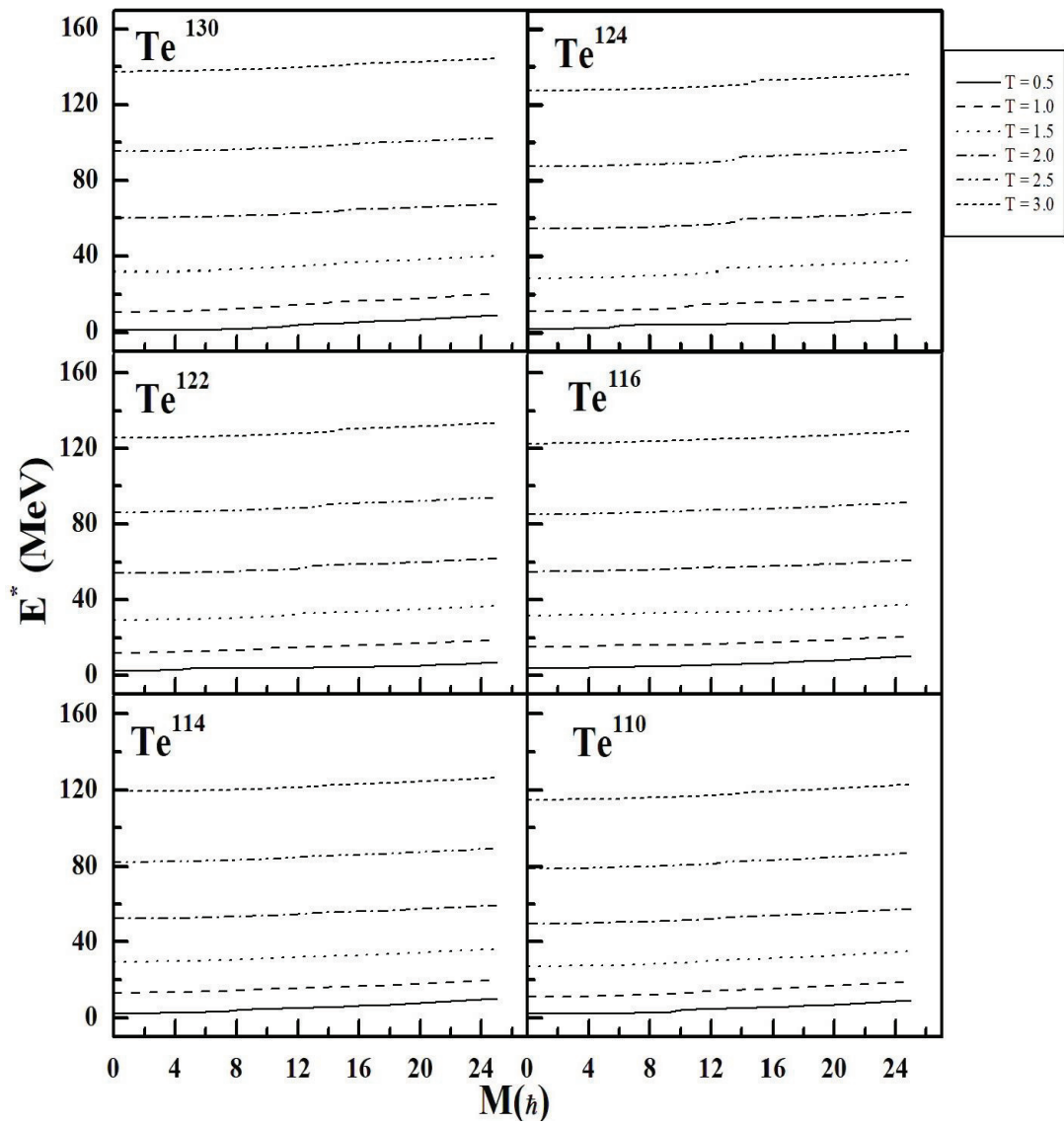


Fig.4.4: Excitation energy E^* (MeV) as a function of angular momentum $M(\hbar)$ for various temperatures T (MeV) for Te isotopes.

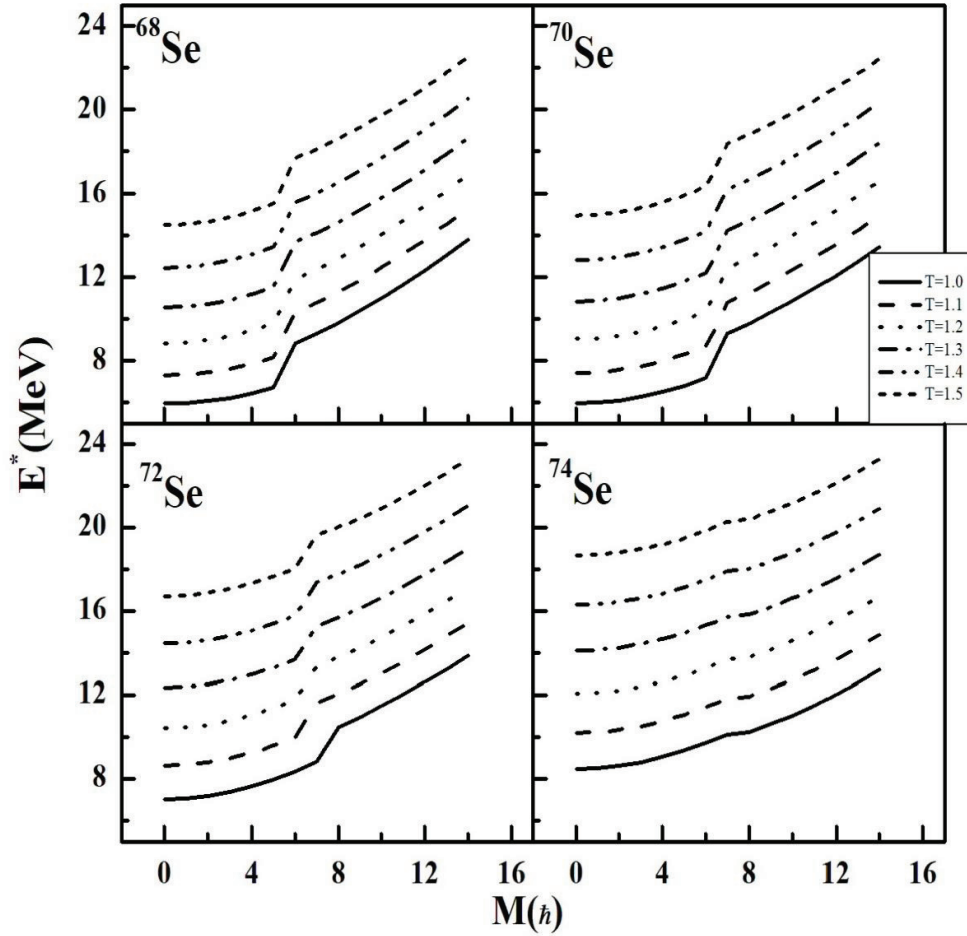


Fig.4.5: Excitation energy E^* (MeV) as a function of angular momentum M (\hbar) for various temperatures for Se isotopes.

From fig.4.2 it is illustrated that the excitation energies that correspond to $2\hbar$ and $4\hbar$ are higher than those that correspond to the same states of the experimental data. This might be due to the temperature dependence (0.5 MeV), as STHR method takes into account the effect of temperature. As the angular momentum increases to higher values, one can observe the tendency of the excitation energies getting close to the experimental data. Especially, the levels that corresponds to $14\hbar$ and $16\hbar$ exhibit remarkable proximity to the corresponding experimental data [<https://www.nndc.bnl.gov/>].

Figure 4.3 illustrates the excitation energies obtained using the statistical model at 0h - 8h for the ^{74}Se were compared with the experimental values [Nomura 2017, <https://www.nndc.bnl.gov/>] corresponding to the same angular momenta. The comparison showed greater agreement between the two for certain angular momenta. Figure 4.4 shows the excitation energy for the Te isotopes which shows an abrupt change in the angular momentum showing shape transition from spherical to non-collective oblate. From fig.4.5, it is observed that excitation energy as a function of angular momentum for the isotopes of Se reveals that at a certain angular momentum a sudden change in the angular momentum results in shape transition of the nuclei from spherical to non-collective oblate. Moreover the excitation energy for all the nuclei ^{68}Se , ^{70}Se and ^{72}Se shows that the free energy minimized excitation energy increases after the critical angular momentum whereas for ^{74}Se it decreases.

Level density parameter as a function of temperature and angular momentum for the nuclei ^{110}Te , ^{114}Te , ^{116}Te , ^{122}Te , ^{124}Te and ^{130}Te are presented in fig. 4.6. At zero angular momentum, the level density parameter a remains almost constant without any fluctuations. For a given temperature, level density parameter is found to decrease with increasing angular momentum. The variations in the level density parameter are different for different angular momentum states at low temperatures because shell structure plays a major role at these temperatures. Another significant change in the level density parameter occurs when the temperature $T > 1.0$ MeV. At these temperatures the occupancies n_i within the active shells near the Fermi level becomes comparable. A change in T to higher values would correspond to an appreciable contribution from higher shells. For temperature $T > 1.0$ MeV the level density parameter shows a linear behavior for all the angular momentum considered.

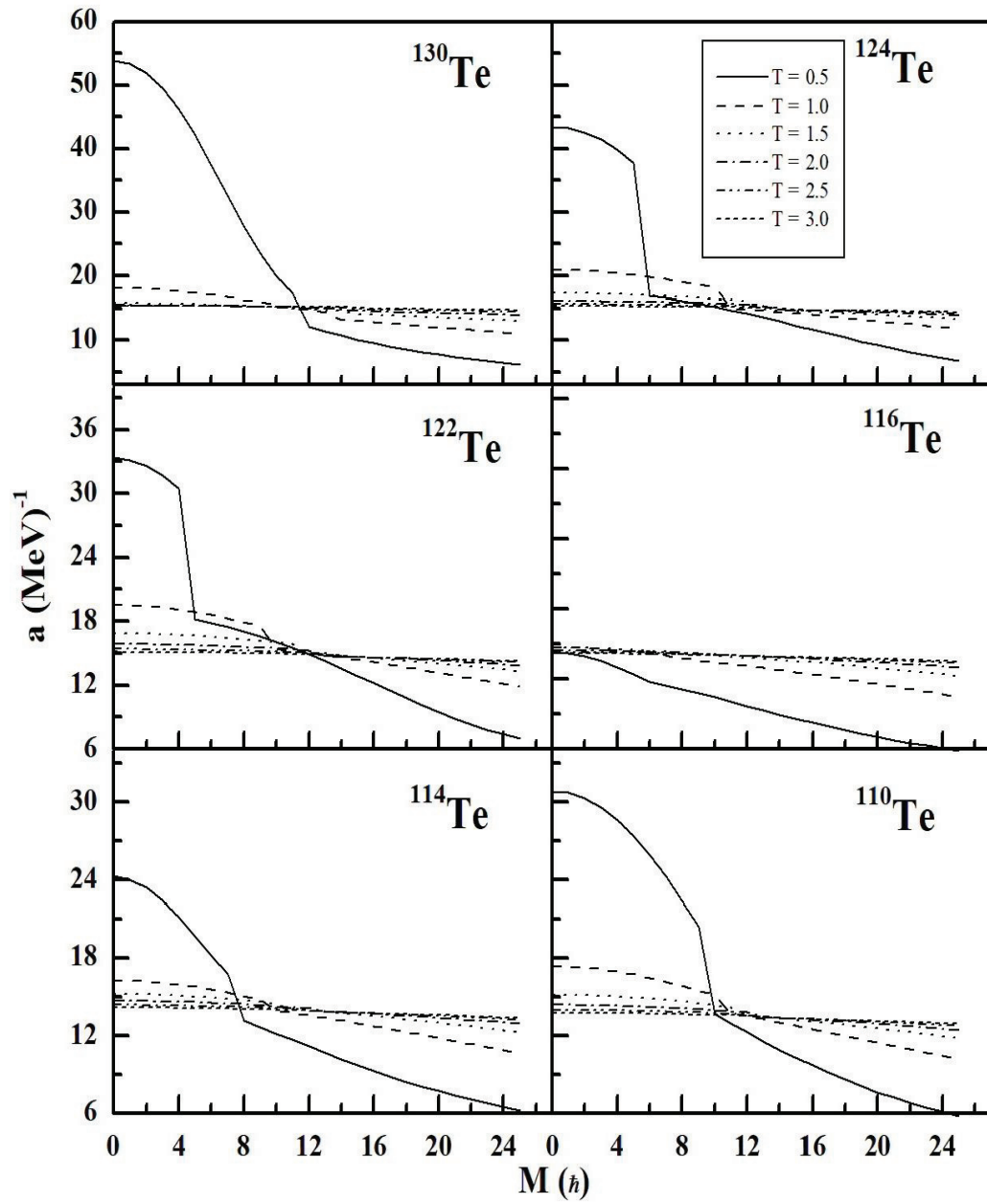


Fig. 4.6: The level density parameter a (MeV^{-1}) as a function of angular momentum M (\hbar) with various temperatures T (MeV) for Te nuclei.

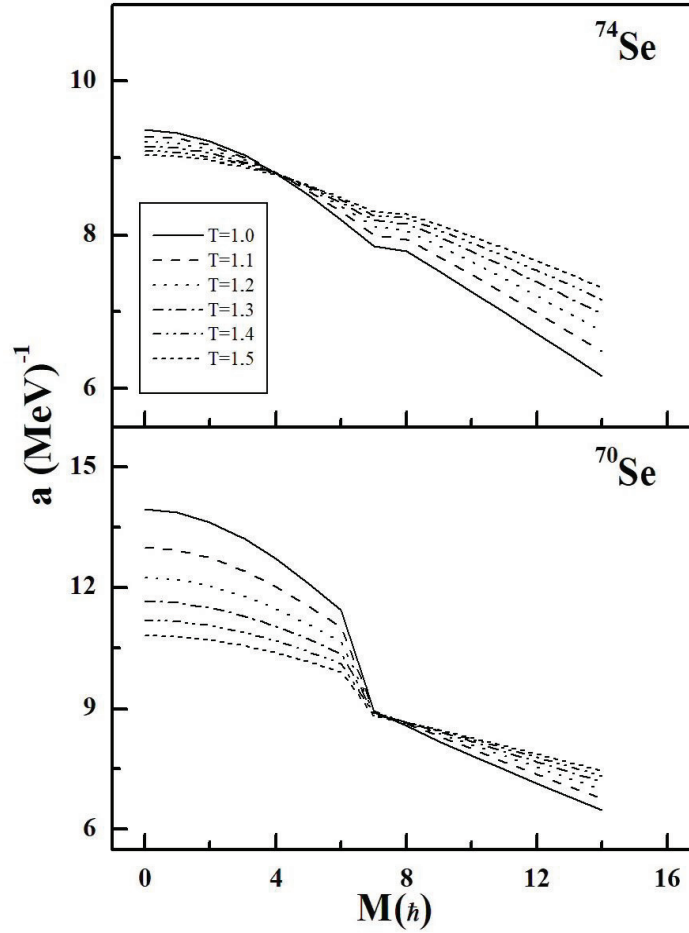


Fig. 4.7: Level density parameter a (MeV^{-1}) as a function of angular momentum $M(\hbar)$ for various temperatures T (MeV) for Se nuclei.

The level density parameter as a function of angular momenta for various temperatures are shown in fig.4.7 for the nuclei ^{70}Se and ^{74}Se . These curves for different temperatures exhibit a sharp decrease at specific angular momenta indicating shape transition from spherical ($\varepsilon = 0.0$) to non-collective oblate ($\varepsilon = 0.1, \gamma = -180^\circ$). Table 4.1 clearly indicates shape transition occurring in terms of behavior of level density parameter sharply decreasing at specific angular momenta values at both the temperatures.

Table:- 4.1 Comparison of Level density parameter as function of angular momentum for the isotopes ^{110}Te , ^{114}Te , ^{116}Te , ^{122}Te , ^{124}Te and ^{130}Te for temperatures $T=1$ and $T=3$ MeV.

Sl.No	M (\hbar)	Level density Parameter ($a(\text{MeV}^{-1})$)											
		^{110}Te		^{114}Te		^{116}Te		^{122}Te		^{124}Te		^{130}Te	
		T=1	T=3	T=1	T=3	T=1	T=3	T=1	T=3	T=1	T=3	T=1	T=3
1.	0	17.371	13.764	16.286	14.164	14.727	14.198	19.557	15.129	20.982	15.333	18.125	15.389
2.	1	17.341	13.763	16.263	14.162	14.715	14.197	19.530	15.126	20.949	15.332	18.087	15.387
3.	2	17.261	13.757	16.200	14.157	14.665	14.192	19.446	15.121	20.849	15.328	17.984	15.384
4.	3	17.132	13.749	16.099	14.148	14.588	14.184	19.309	15.113	20.682	15.321	17.821	15.377
5.	4	16.950	13.736	15.959	14.137	14.480	14.173	19.117	15.103	20.460	15.311	17.606	15.369
6.	5	16.730	13.721	15.785	14.122	14.343	14.159	18.882	15.088	20.177	15.298	17.338	15.356
7.	6	16.464	13.701	15.580	14.104	14.182	14.141	18.601	15.072	19.846	15.280	17.031	15.342
8.	7	16.164	13.679	15.343	14.082	14.001	14.121	18.283	15.052	19.474	15.261	16.696	15.325
9.	8	15.837	13.653	15.083	14.058	13.798	14.098	17.931	15.029	19.064	15.238	16.332	15.307
10.	9	15.483	13.625	14.804	14.030	13.570	14.071	17.560	15.003	18.626	15.213	15.954	15.285
11.	10	15.108	13.592	13.921	13.999	13.431	14.042	15.404	14.975	18.167	15.185	15.566	15.261
12.	11	13.730	13.557	13.750	13.965	13.281	14.009	15.226	14.942	15.001	15.154	15.172	15.234
13.	12	13.502	13.518	13.563	13.928	13.120	13.974	15.034	14.908	14.814	15.120	14.772	15.206
14.	13	13.266	13.476	13.367	13.889	12.951	13.936	14.834	14.871	14.614	15.084	14.380	15.175
15.	14	13.020	13.331	13.164	13.776	12.770	13.907	14.623	14.832	14.407	15.045	13.218	15.142
16.	15	12.771	13.301	12.953	13.747	12.585	13.879	14.399	14.609	14.188	14.724	13.020	15.106
17.	16	12.515	13.269	12.734	13.716	12.391	13.850	14.167	14.582	13.961	14.698	12.818	14.966
18.	17	12.255	13.234	12.510	13.684	12.193	13.819	13.928	14.552	13.729	14.670	12.614	14.941
19.	18	11.994	13.199	12.282	13.650	11.986	13.786	13.684	14.522	13.490	14.640	12.408	14.915
20.	19	11.731	13.160	12.050	13.615	11.778	13.752	13.433	14.490	13.248	14.609	12.202	14.887
21.	20	11.466	13.121	11.816	13.577	11.565	13.716	13.177	14.456	13.002	14.577	11.995	14.859
22.	21	11.202	13.079	11.578	13.538	11.352	13.678	12.920	14.421	12.752	14.543	11.789	14.828
23.	22	10.940	13.036	11.340	13.497	11.135	13.639	12.661	14.384	12.501	14.507	11.581	14.798
24.	23	10.678	12.991	11.102	13.454	10.916	13.598	12.400	14.346	12.251	14.471	11.374	14.765
25.	24	10.420	12.946	10.863	13.411	10.698	13.556	12.140	14.306	12.000	14.432	11.170	14.730
26.	25	10.164	12.897	10.625	13.365	10.479	13.512	11.882	14.264	10.620	14.410	10.970	14.696

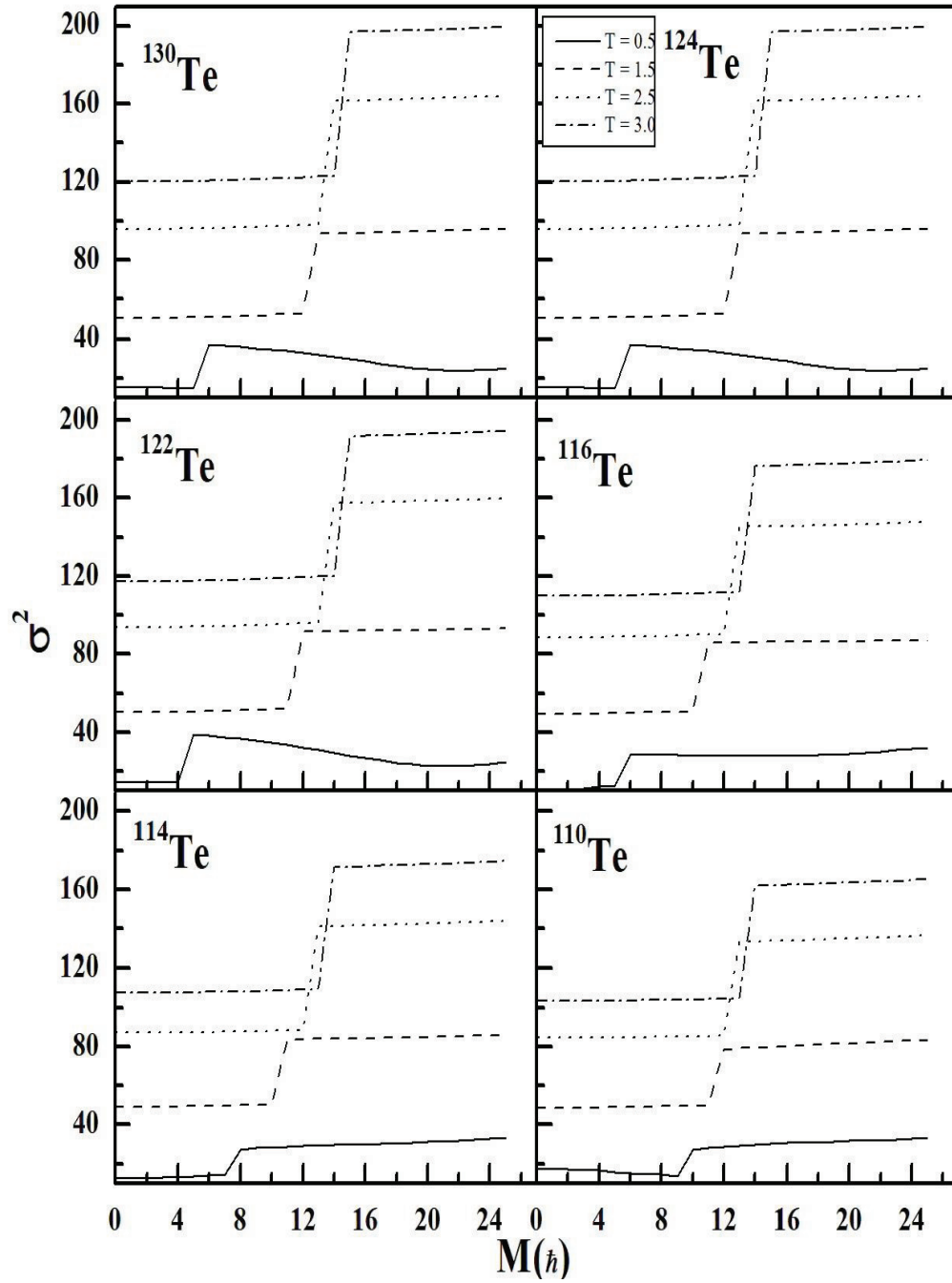


Fig. 4.8: Spin cut-off factor (σ^2) as a function of angular momentum M (\hbar) at various temperatures T (MeV) for ^{110}Te , ^{114}Te , ^{116}Te , ^{122}Te , ^{124}Te and ^{130}Te nuclei.

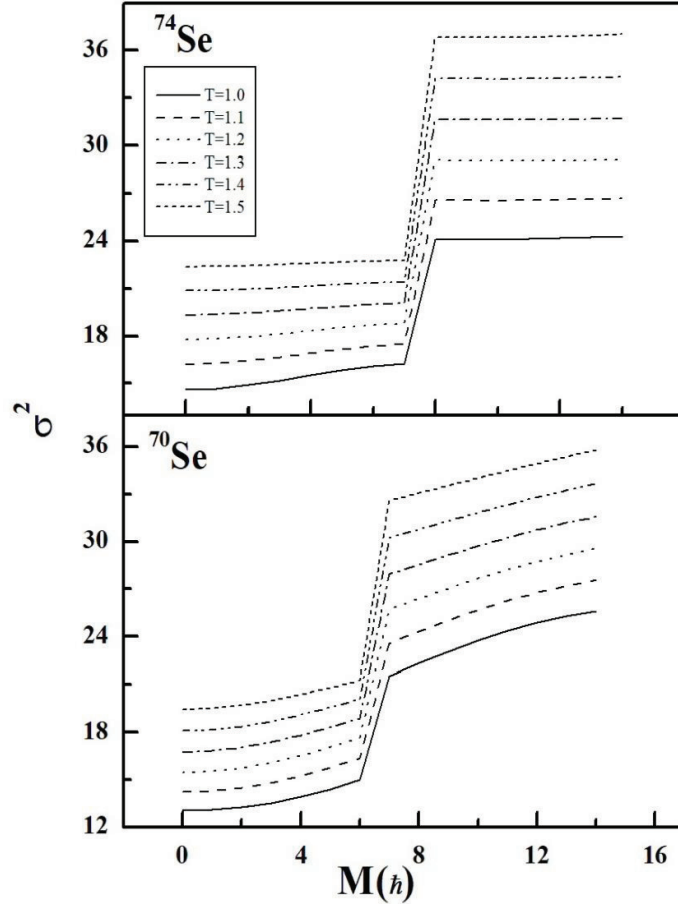


Fig. 4.9: Spin cut-off parameter (σ^2) as a function of angular momentum $M(\hbar)$ for various temperatures T (MeV) for Se nuclei.

In fig. 4.7 results of the level density parameter as a function of angular momentum for various temperatures are shown. These curves for various temperatures show minima at specific angular momentum values indicating a rearrangement of particle distribution near the Fermi level at the excitation energy considered. These minimum are associated with shape transition of the nucleus. The appearance of prominent minima for an angular momentum $M = 12\hbar$ are interpreted as the signature for a shape transition from spherical to oblate non-collective. The

variations in the value of a indicate a greater stability of the system at high spin states on the basis of shell corrections.

Figure 4.8 illustrates the spin cut-off parameter as a function of temperature T and angular momentum M for the system ^{110}Te , ^{114}Te , ^{116}Te , ^{122}Te , ^{124}Te and ^{130}Te . It is observed that the parameter values increase with rise in temperature. It is also obvious that the spin cut-off parameter values vary smoothly with angular momentum but a sudden change in parameter value is observed at particular angular momentum values. This change occurs at $M = 15\hbar$ for ^{116}Te , ^{122}Te , ^{124}Te and ^{130}Te , $M = 12\hbar$ for ^{110}Te and ^{114}Te due to shape transition. The shape of the nuclei ^{110}Te , ^{114}Te , ^{116}Te , ^{122}Te , ^{124}Te and ^{130}Te change from spherical to oblate non-collective. The spin cut off parameter for ^{110}Te , ^{114}Te , ^{116}Te , ^{122}Te , ^{124}Te and ^{130}Te isotopes for temperature 1.0 and 3.0 MeV has been tabulated in Table.4.2.

The spin cut-off parameter as a function of angular momenta for various temperatures is shown in fig.4.9 for the nuclei ^{70}Se and ^{74}Se . From this figure, the spin cut-off parameter values are found to increase sharply at $6\hbar$ and $8\hbar$ respectively for ^{70}Se and ^{74}Se which shows the shape transition from spherical ($\epsilon = 0.0$) to non-collective oblate ($\epsilon = 0.1$, $\gamma = -180^\circ$).

Table: 4.2 Comparison of spin cut off parameter σ^2 as a function of angular momentum and temperature for the Te isotopes

Sl.No	M (h)	Spin cutoff parameter (σ^2)																	
		^{110}Te			^{114}Te			^{116}Te			^{122}Te			^{124}Te			^{130}Te		
		T = 1	T = 3		T = 1	T = 3		T = 1	T = 3		T = 1	T = 3		T = 1	T = 3		T = 1	T = 3	
1.	0	30.594	103.313	30.565	107.520	30.322	104.798	30.206	117.284	30.085	120.139	30.085	120.139	30.085	120.139	30.085	120.139	30.085	120.139
2.	1	30.610	103.322	30.592	107.555	30.355	104.467	30.235	117.299	30.112	120.154	30.112	120.154	30.112	120.154	30.112	120.154	30.112	120.154
3.	2	30.658	103.349	30.671	107.613	30.453	104.142	30.323	117.345	30.195	120.200	30.195	120.200	30.195	120.200	30.195	120.200	30.195	120.200
4.	3	30.739	103.393	30.801	107.695	30.614	103.826	30.467	117.420	30.331	120.278	30.331	120.278	30.331	120.278	30.331	120.278	30.331	120.278
5.	4	30.855	103.455	30.980	107.800	30.834	103.525	30.667	117.526	30.521	120.386	30.521	120.386	30.521	120.386	30.521	120.386	30.521	120.386
6.	5	31.006	103.535	31.204	107.929	31.107	103.244	30.918	117.662	30.763	120.525	30.763	120.525	30.763	120.525	30.763	120.525	30.763	120.525
7.	6	31.194	103.632	31.470	108.080	31.427	101.028	31.218	117.828	31.054	120.695	31.054	120.695	31.054	120.695	31.054	120.695	31.054	120.695
8.	7	31.421	103.748	31.774	108.256	31.787	100.950	31.562	118.024	31.395	120.895	31.395	120.895	31.395	120.895	31.395	120.895	31.395	120.895
9.	8	31.688	103.882	32.111	108.454	32.180	100.909	31.947	118.250	31.781	121.127	31.781	121.127	31.781	121.127	31.781	121.127	31.781	121.127
10.	9	31.995	104.034	32.477	108.677	32.441	102.559	32.368	118.506	32.210	121.388	32.210	121.388	32.210	121.388	32.210	121.388	32.210	121.388
11.	10	32.341	104.205	55.636	108.922	57.406	102.554	60.842	118.791	32.680	121.681	32.680	121.681	32.680	121.681	32.680	121.681	32.680	121.681
12.	11	52.073	104.395	55.841	109.192	57.380	111.924	60.582	119.106	60.751	122.002	60.751	122.002	60.751	122.002	60.751	122.002	60.751	122.002
13.	12	52.680	104.604	56.058	109.485	57.365	111.911	60.326	119.450	60.681	122.354	60.681	122.354	60.681	122.354	60.681	122.354	60.681	122.354
14.	13	53.296	104.832	56.285	171.547	57.364	169.203	60.079	119.824	60.624	122.736	60.624	122.736	60.624	122.736	60.624	122.736	60.624	122.736
15.	14	53.917	161.945	56.520	171.751	57.380	169.034	59.848	120.227	60.584	123.147	60.584	123.147	60.584	123.147	60.584	123.147	60.584	123.147
16.	15	54.535	162.165	56.762	171.968	57.414	168.873	59.639	191.682	60.565	196.850	60.565	196.850	60.565	196.850	60.565	196.850	60.565	196.850
17.	16	55.147	162.401	57.010	172.200	57.466	168.717	59.458	191.883	60.571	197.050	60.571	197.050	60.571	197.050	60.571	197.050	60.571	197.050
18.	17	55.746	162.650	57.261	172.445	57.538	168.567	59.312	192.097	60.606	197.262	60.606	197.262	60.606	197.262	60.606	197.262	60.606	197.262
19.	18	56.329	162.915	57.515	172.705	57.630	168.423	59.204	192.324	60.673	197.488	60.673	197.488	60.673	197.488	60.673	197.488	60.673	197.488
20.	19	56.893	163.193	57.769	172.979	57.742	168.284	59.139	192.564	60.773	197.727	60.773	197.727	60.773	197.727	60.773	197.727	60.773	197.727
21.	20	57.433	163.487	58.022	173.266	57.872	168.152	59.120	192.817	60.911	197.978	60.911	197.978	60.911	197.978	60.911	197.978	60.911	197.978
22.	21	57.948	163.795	58.272	173.569	58.020	168.026	59.149	193.083	61.086	198.242	61.086	198.242	61.086	198.242	61.086	198.242	61.086	198.242
23.	22	58.433	164.117	58.518	173.885	58.183	167.908	59.229	193.362	61.299	198.518	61.299	198.518	61.299	198.518	61.299	198.518	61.299	198.518
24.	23	58.888	164.453	58.756	174.215	58.359	167.800	59.359	193.654	61.552	198.807	61.552	198.807	61.552	198.807	61.552	198.807	61.552	198.807
25.	24	59.309	164.803	58.985	174.559	58.546	167.702	59.538	193.959	61.842	199.109	61.842	199.109	61.842	199.109	61.842	199.109	61.842	199.109
26.	25	59.695	165.168	59.204	188.941	58.740	167.618	59.765	194.277	62.169	199.423	62.169	199.423	62.169	199.423	62.169	199.423	62.169	199.423

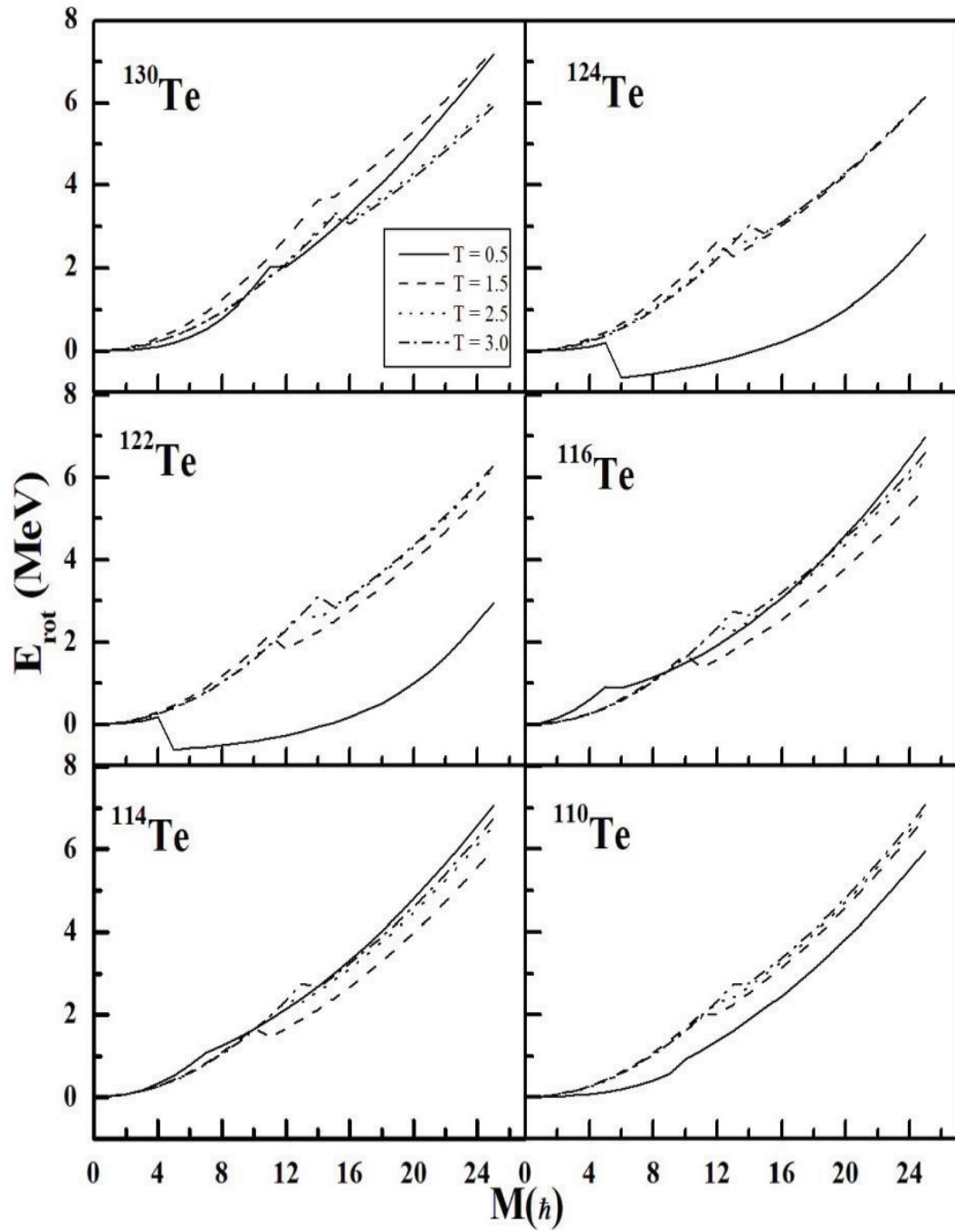


Fig. 4.10: Rotational energy E_{rot} (MeV) as a function of angular momentum M (\hbar) for ^{110}Te , ^{114}Te , ^{116}Te , ^{122}Te , ^{124}Te and ^{130}Te .

Table:-4.3 Comparison of rotational energy (MeV) as a function of angular momentum and temperature for the Te isotopes.

Sl.No	M (h)	Rotational Energy [E _{rot} (MeV)]																	
		¹¹⁰ Te			¹¹⁴ Te			¹¹⁶ Te			¹²² Te			¹²⁴ Te			¹³⁰ Te		
		T=1	T=3	T=1	T=3	T=1	T=3	T=1	T=3	T=1	T=3	T=1	T=3	T=1	T=3	T=1	T=3	T=1	T=3
1.	0	0.000	0.000	0.000	0.000	0.000	0.000	0.000	0.000	0.000	0.000	0.000	0.000	0.000	0.000	0.000	0.000	0.000	0.000
2.	1	0.021	0.015	0.022	0.017	0.019	0.018	0.020	0.023	0.021	0.023	0.021	0.023	0.021	0.023	0.021	0.023	0.021	0.023
3.	2	0.078	0.065	0.085	0.072	0.085	0.068	0.083	0.074	0.084	0.068	0.083	0.074	0.084	0.068	0.083	0.074	0.084	0.068
4.	3	0.171	0.145	0.188	0.152	0.193	0.146	0.187	0.156	0.190	0.146	0.187	0.156	0.190	0.146	0.187	0.156	0.190	0.146
5.	4	0.305	0.261	0.331	0.267	0.343	0.263	0.334	0.261	0.334	0.263	0.334	0.261	0.334	0.263	0.334	0.261	0.334	0.263
6.	5	0.471	0.408	0.512	0.411	0.536	0.410	0.520	0.412	0.523	0.410	0.520	0.412	0.523	0.410	0.520	0.412	0.523	0.410
7.	6	0.679	0.589	0.732	0.592	0.767	0.590	0.748	0.582	0.752	0.590	0.748	0.582	0.752	0.590	0.748	0.582	0.752	0.590
8.	7	0.922	0.798	0.992	0.804	1.033	0.799	1.014	0.784	1.020	0.799	1.014	0.784	1.020	0.799	1.014	0.784	1.020	0.799
9.	8	1.200	1.044	1.287	1.050	1.337	1.043	1.320	1.025	1.328	1.043	1.320	1.025	1.328	1.043	1.320	1.025	1.328	1.043
10.	9	1.514	1.318	1.615	1.328	0.917	1.321	1.657	1.294	1.673	1.321	1.657	1.294	1.673	1.321	1.657	1.294	1.673	1.321
11.	10	1.865	1.630	1.247	1.638	1.083	1.632	0.947	1.591	2.055	1.632	0.947	1.591	2.055	1.632	0.947	1.591	2.055	1.632
12.	11	1.817	1.970	1.448	1.979	1.267	1.973	1.103	1.931	1.345	1.973	1.103	1.931	1.345	1.973	1.103	1.931	1.345	1.973
13.	12	2.079	2.344	1.673	2.355	1.470	2.344	1.275	2.291	1.527	2.344	1.275	2.291	1.527	2.344	1.275	2.291	1.527	2.344
14.	13	2.358	2.749	1.915	2.757	1.690	2.751	1.461	2.68	1.729	2.751	1.461	2.68	1.729	2.751	1.461	2.68	1.729	2.751
15.	14	2.657	2.772	2.173	2.674	1.931	2.647	1.666	3.101	1.945	2.647	1.666	3.101	1.945	2.647	1.666	3.101	1.945	2.647
16.	15	2.972	3.063	2.448	2.952	2.187	2.914	1.890	2.866	2.182	2.914	1.890	2.866	2.182	2.914	1.890	2.866	2.182	2.914
17.	16	3.305	3.377	2.744	3.251	2.463	3.197	2.134	3.128	2.437	3.197	2.134	3.128	2.437	3.197	2.134	3.128	2.437	3.197
18.	17	3.657	3.709	3.056	3.564	2.755	3.503	2.394	3.414	2.710	3.503	2.394	3.414	2.710	3.503	2.394	3.414	2.710	3.503
19.	18	4.022	4.060	3.385	3.897	3.070	3.828	2.674	3.709	3.003	3.828	2.674	3.709	3.003	3.828	2.674	3.709	3.003	3.828
20.	19	4.406	4.434	3.729	4.244	3.399	4.169	2.974	4.026	3.313	4.169	2.974	4.026	3.313	4.169	2.974	4.026	3.313	4.169
21.	20	4.806	4.824	4.091	4.615	3.748	4.530	3.296	4.358	3.643	4.530	3.296	4.358	3.643	4.530	3.296	4.358	3.643	4.530
22.	21	5.221	5.240	4.471	5.003	4.112	4.905	3.636	4.710	3.994	4.905	3.636	4.710	3.994	4.905	3.636	4.710	3.994	4.905
23.	22	5.649	5.670	4.864	5.411	4.495	5.301	3.996	5.078	4.364	5.301	3.996	5.078	4.364	5.301	3.996	5.078	4.364	5.301
24.	23	6.095	6.124	5.274	5.840	4.896	5.718	4.377	5.462	4.750	5.718	4.377	5.462	4.750	5.718	4.377	5.462	4.750	5.718
25.	24	6.554	6.591	5.699	6.284	5.314	6.149	4.777	5.86	5.158	6.149	4.777	5.86	5.158	6.149	4.777	5.86	5.158	6.149
26.	25	7.028	7.085	6.140	6.747	5.747	6.604	5.196	6.284	5.583	6.604	5.196	6.284	5.583	6.604	5.196	6.284	5.583	6.604

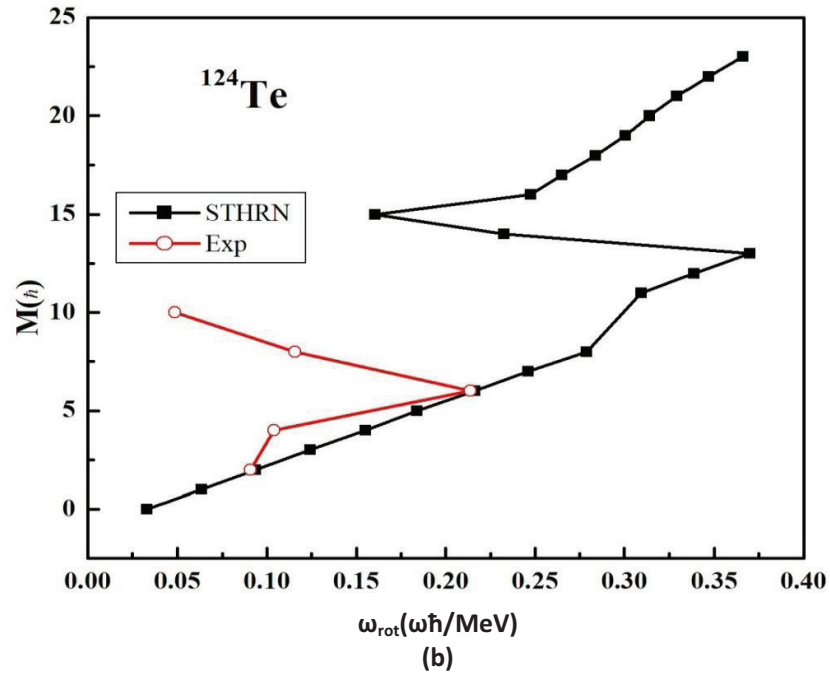
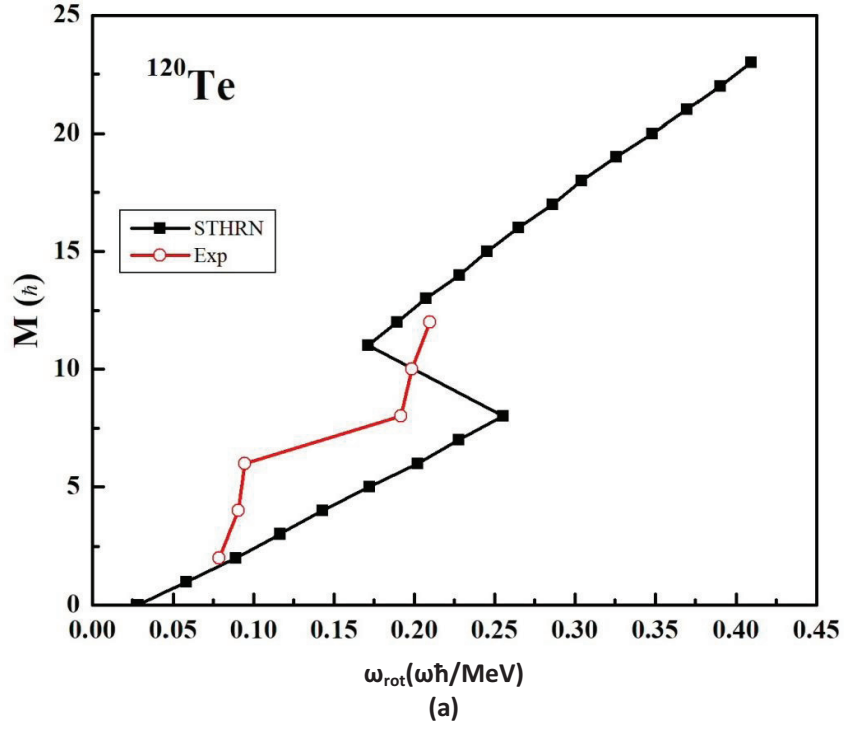


Fig.4.11: Angular momentum $M(\hbar)$ as a function of rotational frequency ($\omega\hbar/\text{MeV}$) for (a) ^{120}Te at $T = 1.0$ MeV and (b) ^{124}Te at $T = 2.5$ MeV. The open circles represent the experimental value [Hossain 2015].

In fig.4.10, the rotational energies are shown as a function of angular momentum for ^{110}Te , ^{114}Te , ^{116}Te , ^{122}Te , ^{124}Te and ^{130}Te . The rotational energy is lowered by the shape transitions and the angular momentum states beyond these transition points correspond to the different shapes brought about by the minimization of energy. It is referred to as the band crossing. For ^{110}Te , ^{114}Te , ^{116}Te , ^{122}Te , ^{124}Te and ^{130}Te a single band crossing, around $M \approx 12\hbar$ is observed. Significant deviation of rotational levels at a particular angular momentum is a case of both the single particle alignment and collective rotation contributing to the structural change. The rotational energy E_{rot} of the residual nucleus is used in the calculation of neutron emission probability.

In fig.4.11 (a and b) the angular momentum as a function of rotational frequency is plotted for ^{120}Te & ^{124}Te and the results are compared with available experimental values [Hossain 2015]. The rotational frequency calculated from STHRN method gives very good comparison with the experimental data. As discussed earlier in the introduction part, the Interacting Boson Model (IBM-1) has been applied for the study of rotational behavior in Te isotopes [Hossain 2015]. Although this model was able to reproduce the energy levels for higher angular momenta comparable with the experimental data but the moment of inertia plot seems to increase linearly with increasing angular momentum which shows a deviation from the experimental value. This discrepancy has been overcome in STHRN method since the values calculated via STHRN method was able to show very good comparison with the numerical and follows almost the same pattern as that of the experimental data. This similar behavior has been observed in the moment of inertia plot shown in fig.4.12. The deviation in rotational frequency for certain angular momentum states correspond to the different shapes brought about by the

minimization of free energy. It is referred to as the band crossing. For ^{120}Te and ^{124}Te a single band crossing, around $M \approx 10\hbar$ and $12\hbar$ is observed respectively. Significant deviation of rotational levels at a particular angular momentum is a case of both the single particle alignment and collective rotation contributing to the structural change.

In fig.4.12, the kinematic moment of inertia as a function of angular momentum is shown for ^{120}Te and ^{124}Te . In figure, the open circles correspond to the experimental values while the solid symbols correspond to the MOI calculated from STHR method. At low and high angular momentum, the calculated moment of inertia is compared with the experimental values. The kinematical moment of inertia changes sharply at $M = 10\hbar$ for ^{120}Te and at $M = 14\hbar$ for ^{124}Te . It corresponds to shape changes due to band crossing and these are compared with experimental data.

The rotational frequency and kinematic moment of inertia as a function of angular momentum has been calculated by STHR method for ^{120}Te , ^{122}Te and ^{124}Te and compared with the experimental and other theoretical model such as IBM-1 [Hossain 2015] are tabulated in Table.4.4 and Table.4.5 respectively. The results show very good agreement with the available experimental data and STHR method follows the same pattern as that of experimental value instead of a linear pattern obtained in IBM – 1 model. It is also seen that the values of rotational frequency and kinematic moment of inertia show very good agreement with the available experimental data.

Table 4.4. Comparison of rotational frequency as a function of angular momentum and temperatures calculated from STHRN method with the available IBM – 1 model and experimental data [Hossain 2015] for the Te isotopes.

M (\hbar)	Rotational frequency ($\omega\hbar/\text{MeV}$)												
	^{120}Te				^{122}Te				^{124}Te				
	STHRN	EXP	IBM-I		STHRN	EXP	IBM – 1		STHRN	EXP	STHRN	EXP	IBM-I
2	0.05798	0.0784	0.0784		0.0946	0.0795	0.0784		0.09351	0.0906			0.0908
4	0.11658	0.0903	0.0951		0.1589	0.0952	0.0946		0.15503	0.1040			0.0951
6	0.17200	0.0946	0.1132		0.2277	0.0812	0.1083		0.21619	0.2139			0.0995
8	0.22778	0.1918	0.1329		0.2865	0.2100	0.1243		0.27893	0.1156			0.1039
10	0.17139	0.1984	0.1542		0.3477	0.0964	0.1414		0.30933	0.0484			0.1086
12	0.20715	0.2097	0.1777		0.1905	0.1243	0.1599		0.33862	-			0.1133

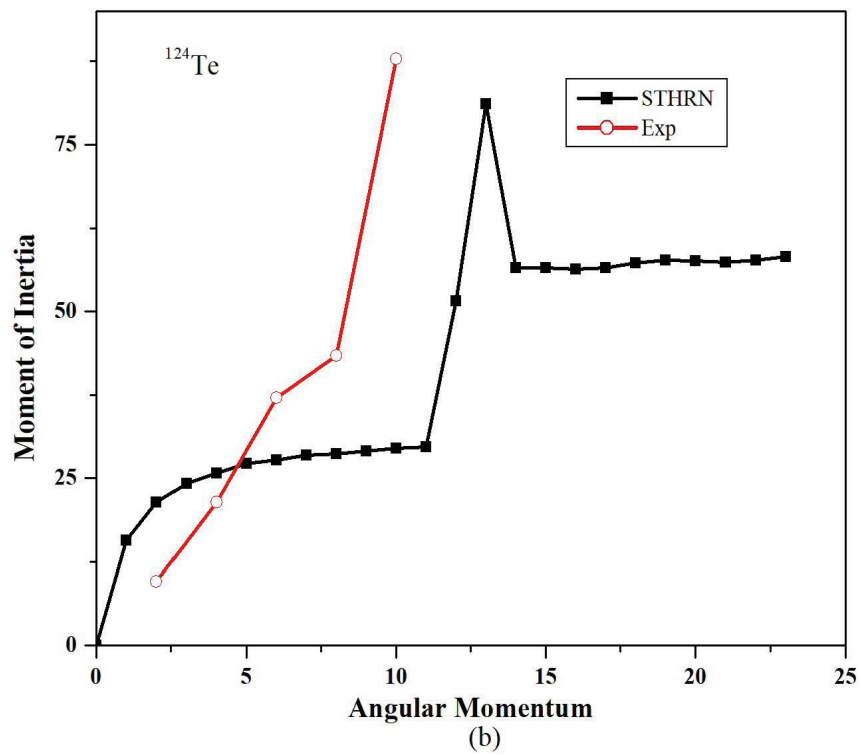
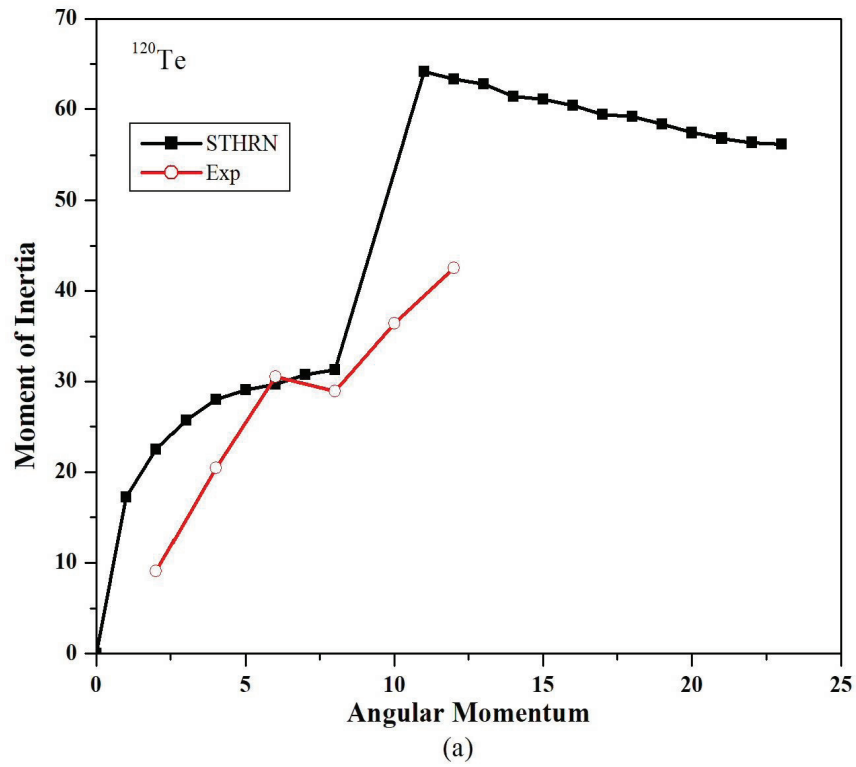


Fig. 4.12: Moment of inertia (\hbar^2/MeV) as a function of angular momentum M (\hbar) for (a) ^{120}Te and (b) ^{124}Te with same description as in fig.5.

Table 4.5. Comparison of moment of inertia as a function of angular momentum and temperatures calculated from STHRN method with the available IBM – 1 model and experimental data [Hossain 2015] for the isotopes ^{120}Te , ^{122}Te and ^{124}Te .

Moment of inertia (\hbar^2/MeV)									
M (\hbar)	^{120}Te			^{122}Te			^{124}Te		
	STHRN	EXP	IBM-I	STHRN	EXP	IBM – 1	STHRN	EXP	IBM-I
2	22.5055	9.04	10.707	21.1406	10.639	10.713	21.3890	9.538	9.956
4	28.0308	20.4	22.701	25.1674	22.690	22.760	25.8015	21.36	22.698
6	29.6990	30.5	32.699	26.9326	38.596	33.424	27.7538	37.08	34.871
8	31.3119	28.9	41.147	27.9233	41.394	42.541	28.6809	43.37	46.529
10	64.1823	36.4	48.392	28.7539	61.191	50.518	29.5313	87.76	57.654
12	63.3402	42.5	54.658	62.9750	65.248	57.522	81.1089	-	68.341

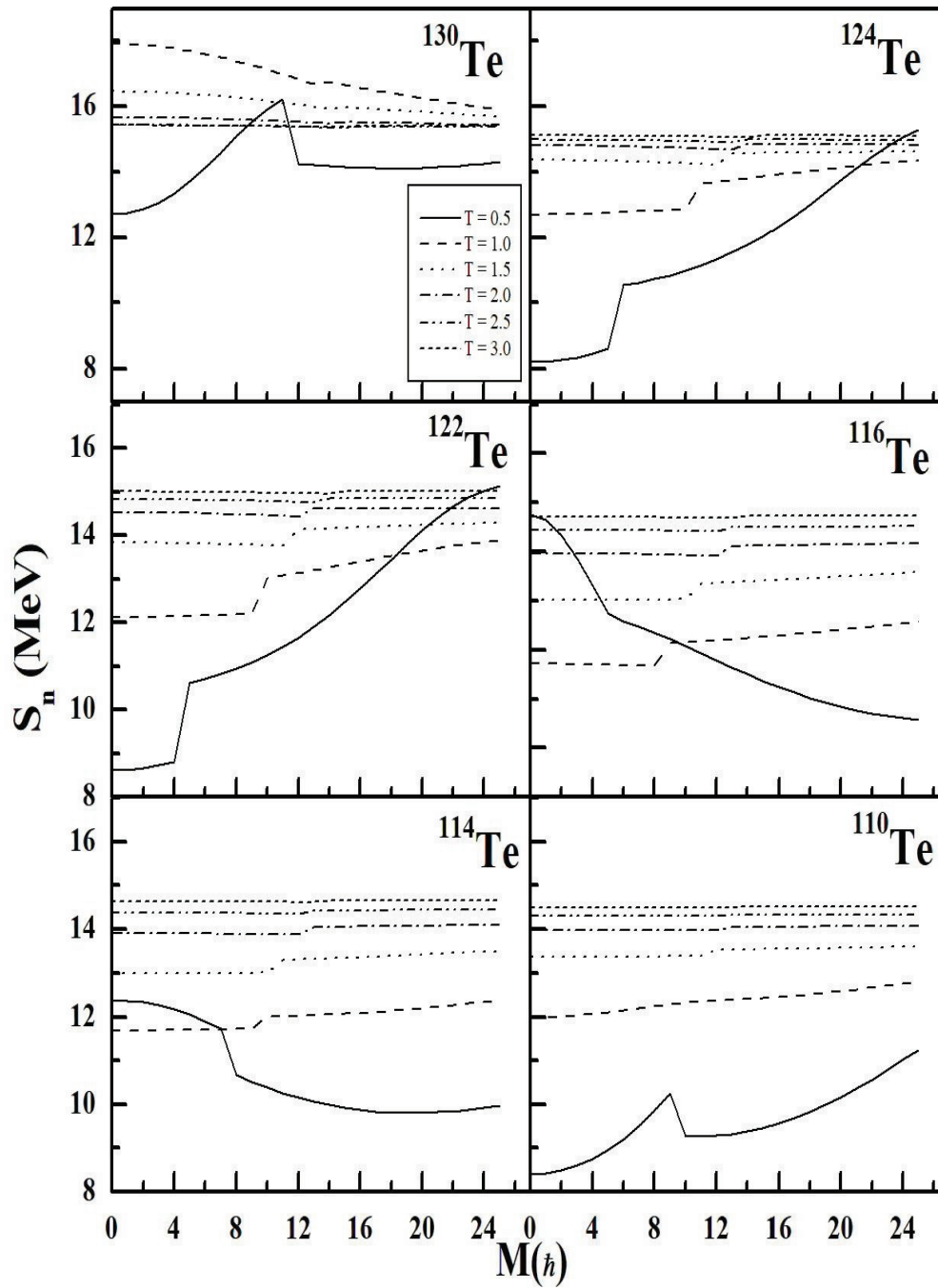


Fig. 4.13: The neutron separation energy (MeV) as a function of angular momentum M (\hbar) with various temperatures (MeV).

Table:- 4.6 Comparison of neutron separation energy (MeV) as a function of angular momentum and temperatures for the Te isotopes.

Sl.No	M(h)	Neutron separation energy [S_n (MeV)]																	
		^{110}Te			^{114}Te			^{116}Te			^{122}Te			^{124}Te			^{130}Te		
		T=1	T=3	T=1	T=3	T=1	T=3	T=1	T=3	T=1	T=3	T=1	T=3	T=1	T=3	T=1	T=3	T=1	T=3
1.	0	12.000	14.498	11.693	14.632	11.719	14.714	12.125	15.010	12.694	15.118	17.911	15.428						
2.	1	12.004	14.498	11.694	14.632	11.718	14.714	12.126	15.010	12.697	15.117	17.903	15.428						
3.	2	12.018	14.498	11.696	14.632	11.715	14.713	12.130	15.009	12.704	15.116	17.877	15.427						
4.	3	12.040	14.498	11.699	14.631	11.710	14.712	12.136	15.007	12.715	15.115	17.834	15.425						
5.	4	12.070	14.498	11.703	14.630	11.703	14.711	12.144	15.005	12.730	15.113	17.775	15.423						
6.	5	12.107	14.498	11.708	14.629	11.696	14.710	12.154	15.003	12.749	15.110	17.701	15.421						
7.	6	12.149	14.498	11.714	14.628	11.688	14.708	12.165	15.000	12.770	15.107	17.612	15.418						
8.	7	12.197	14.498	11.722	14.626	11.680	14.705	12.178	14.996	12.792	15.103	17.509	15.414						
9.	8	12.247	14.498	11.731	14.624	11.673	14.703	12.192	14.992	12.815	15.099	17.395	15.410						
10.	9	12.299	14.498	11.742	14.622	12.130	14.700	12.207	14.987	12.838	15.094	17.270	15.405						
11.	10	12.351	14.499	12.012	14.620	12.149	14.696	13.027	14.982	12.860	15.088	17.135	15.400						
12.	11	12.366	14.499	12.021	14.617	12.171	14.693	13.083	14.976	13.638	15.082	16.994	15.394						
13.	12	12.378	14.499	12.033	14.614	12.193	14.689	13.143	14.970	13.691	15.076	16.846	15.388						
14.	13	12.394	14.499	12.047	14.611	12.217	14.685	13.205	14.963	13.746	15.069	16.695	15.381						
15.	14	12.413	14.514	12.062	14.656	12.242	14.738	13.269	14.956	13.803	15.061	16.750	15.374						
16.	15	12.435	14.514	12.081	14.655	12.268	14.737	13.335	15.020	13.861	15.121	16.664	15.366						
17.	16	12.461	14.513	12.101	14.655	12.295	14.737	13.400	15.019	13.919	15.120	16.578	15.413						
18.	17	12.490	14.512	12.124	14.655	12.324	14.736	13.466	15.018	13.978	15.119	16.493	15.411						
19.	18	12.522	14.512	12.150	14.654	12.352	14.736	13.530	15.017	14.035	15.117	16.411	15.410						
20.	19	12.557	14.511	12.178	14.653	12.382	14.735	13.592	15.016	14.090	15.116	16.330	15.408						
21.	20	12.595	14.510	12.208	14.653	12.412	14.735	13.651	15.015	14.143	15.115	16.251	15.407						
22.	21	12.636	14.510	12.241	14.652	12.443	14.734	13.707	15.014	14.193	15.113	16.176	15.405						
23.	22	12.678	14.509	12.276	14.652	12.474	14.733	13.759	15.012	14.239	15.112	16.103	15.403						
24.	23	12.723	14.508	12.312	14.651	12.505	14.732	13.806	15.011	14.281	15.110	16.033	15.401						
25.	24	12.769	14.507	12.351	14.650	12.536	14.731	13.847	15.010	14.317	15.109	15.967	15.400						
26.	25	12.816	14.507	12.391	14.649	12.568	14.731	13.883	15.008	14.349	15.107	15.904	15.398						

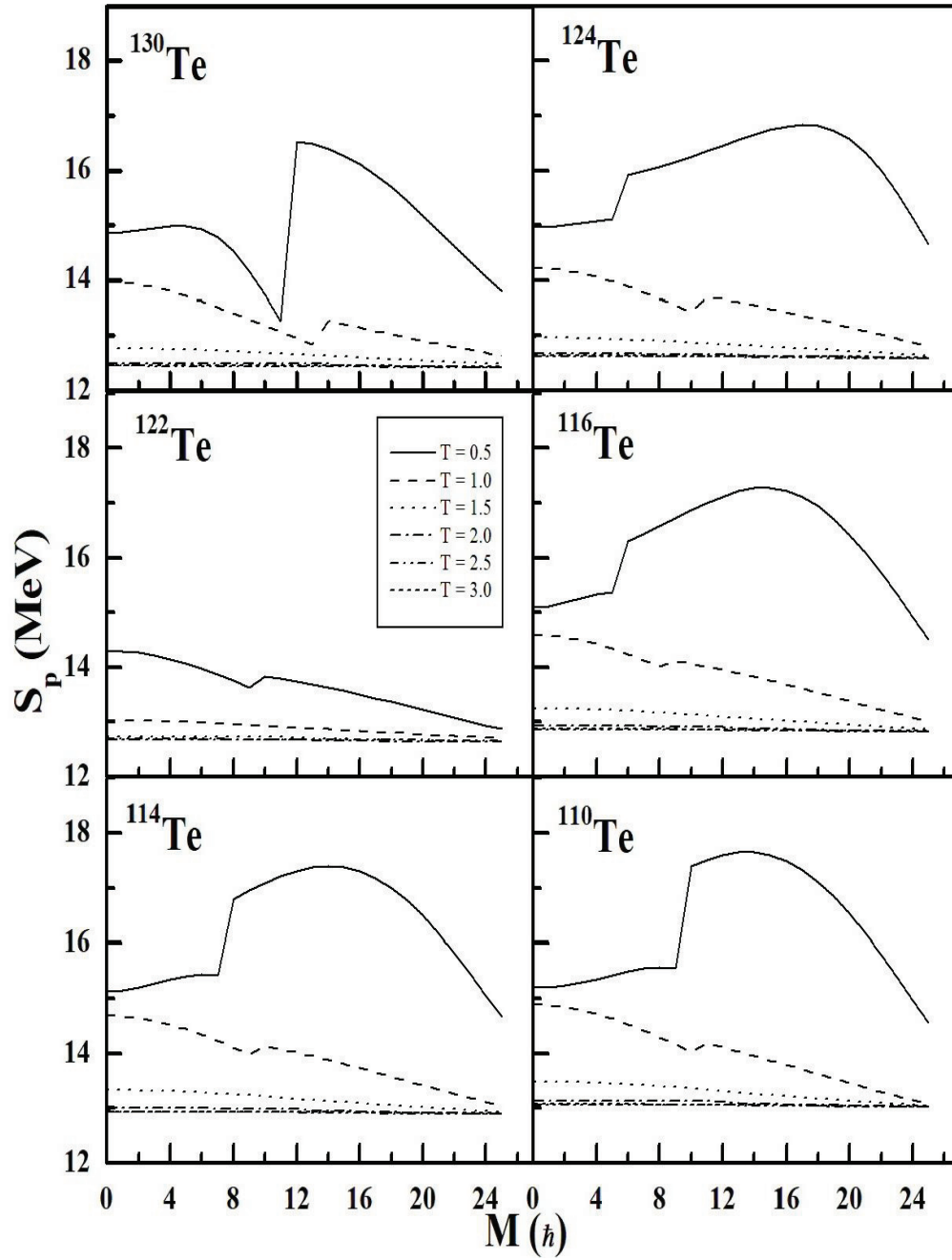


Fig. 4.14: The proton separation energy S_p (MeV) as a function of angular momentum M (\hbar) with various temperatures T (MeV).

Table:- 4.7 Comparison of proton separation energy (MeV) as a function of angular momentum M (h) and temperature for the Te isotopes.

Sl.No	M(h)	Proton separation energy [(S _p (MeV))]																	
		¹¹⁰ Te			¹¹⁴ Te			¹¹⁶ Te			¹²² Te			¹²⁴ Te			¹³⁰ Te		
		T=1	T=3	T=1	T=3	T=1	T=3	T=1	T=3	T=1	T=3	T=1	T=3	T=1	T=3	T=1	T=3	T=1	T=3
1.	0	14.890	13.072	14.688	12.941	14.590	12.877	14.311	12.693	14.222	12.635	14.222	12.635	14.222	12.635	14.222	12.635	14.222	12.635
2.	1	14.880	13.072	14.677	12.940	14.579	12.877	14.300	12.693	14.211	12.635	14.211	12.635	14.211	12.635	14.211	12.635	14.211	12.635
3.	2	14.847	13.072	14.646	12.940	14.548	12.876	14.270	12.693	14.181	12.635	14.181	12.635	14.181	12.635	14.181	12.635	14.181	12.635
4.	3	14.795	13.072	14.595	12.940	14.497	12.876	14.220	12.693	14.132	12.634	14.132	12.634	14.132	12.634	14.132	12.634	14.132	12.634
5.	4	14.724	13.071	14.525	12.939	14.427	12.876	14.153	12.692	14.064	12.634	14.064	12.634	14.064	12.634	14.064	12.634	14.064	12.634
6.	5	14.635	13.071	14.439	12.939	14.342	12.875	14.070	12.692	13.982	12.633	13.982	12.633	13.982	12.633	13.982	12.633	13.982	12.633
7.	6	14.532	13.070	14.340	12.938	14.243	12.874	13.973	12.691	13.886	12.633	13.886	12.633	13.886	12.633	13.886	12.633	13.886	12.633
8.	7	14.416	13.069	14.228	12.937	14.133	12.874	13.866	12.691	13.780	12.632	13.780	12.632	13.780	12.632	13.780	12.632	13.780	12.632
9.	8	14.291	13.068	14.108	12.936	14.014	12.873	13.752	12.690	13.665	12.631	13.665	12.631	13.665	12.631	13.665	12.631	13.665	12.631
10.	9	14.159	13.067	13.982	12.935	14.118	12.872	13.631	12.689	13.546	12.630	13.546	12.630	13.546	12.630	13.546	12.630	13.546	12.630
11.	10	14.022	13.066	14.134	12.934	14.069	12.870	13.843	12.688	13.424	12.629	13.424	12.629	13.424	12.629	13.424	12.629	13.424	12.629
12.	11	14.185	13.064	14.077	12.933	14.016	12.869	13.796	12.686	13.708	12.628	13.708	12.628	13.708	12.628	13.708	12.628	13.708	12.628
13.	12	14.112	13.062	14.014	12.931	13.958	12.867	13.746	12.685	13.658	12.627	13.658	12.627	13.658	12.627	13.658	12.627	13.658	12.627
14.	13	14.035	13.061	13.948	12.929	13.896	12.866	13.691	12.683	13.604	12.625	13.604	12.625	13.604	12.625	13.604	12.625	13.604	12.625
15.	14	13.955	13.056	13.879	12.925	13.830	12.862	13.633	12.682	13.547	12.624	13.547	12.624	13.547	12.624	13.547	12.624	13.547	12.624
16.	15	13.874	13.054	13.806	12.924	13.761	12.860	13.572	12.679	13.486	12.621	13.486	12.621	13.486	12.621	13.486	12.621	13.486	12.621
17.	16	13.790	13.052	13.731	12.922	13.690	12.859	13.508	12.678	13.423	12.620	13.423	12.620	13.423	12.620	13.423	12.620	13.423	12.620
18.	17	13.706	13.050	13.655	12.920	13.616	12.857	13.441	12.676	13.358	12.618	13.358	12.618	13.358	12.618	13.358	12.618	13.358	12.618
19.	18	13.621	13.048	13.576	12.918	13.540	12.855	13.372	12.675	13.291	12.617	13.291	12.617	13.291	12.617	13.291	12.617	13.291	12.617
20.	19	13.537	13.046	13.498	12.916	13.463	12.854	13.301	12.673	13.223	12.615	13.223	12.615	13.223	12.615	13.223	12.615	13.223	12.615
21.	20	13.455	13.044	13.419	12.914	13.385	12.852	13.229	12.672	13.154	12.614	13.154	12.614	13.154	12.614	13.154	12.614	13.154	12.614
22.	21	13.374	13.041	13.340	12.912	13.307	12.850	13.157	12.670	13.085	12.612	13.085	12.612	13.085	12.612	13.085	12.612	13.085	12.612
23.	22	13.296	13.039	13.263	12.910	13.230	12.848	13.084	12.668	13.016	12.610	13.016	12.610	13.016	12.610	13.016	12.610	13.016	12.610
24.	23	13.220	13.036	13.187	12.908	13.155	12.845	13.013	12.666	12.948	12.609	12.948	12.609	12.948	12.609	12.948	12.609	12.948	12.609
25.	24	13.149	13.034	13.114	12.905	13.081	12.843	12.942	12.664	12.881	12.607	12.881	12.607	12.881	12.607	12.881	12.607	12.881	12.607
26.	25	13.082	13.031	13.044	12.903	13.011	12.841	12.874	12.662	12.816	12.605	12.816	12.605	12.816	12.605	12.816	12.605	12.816	12.605

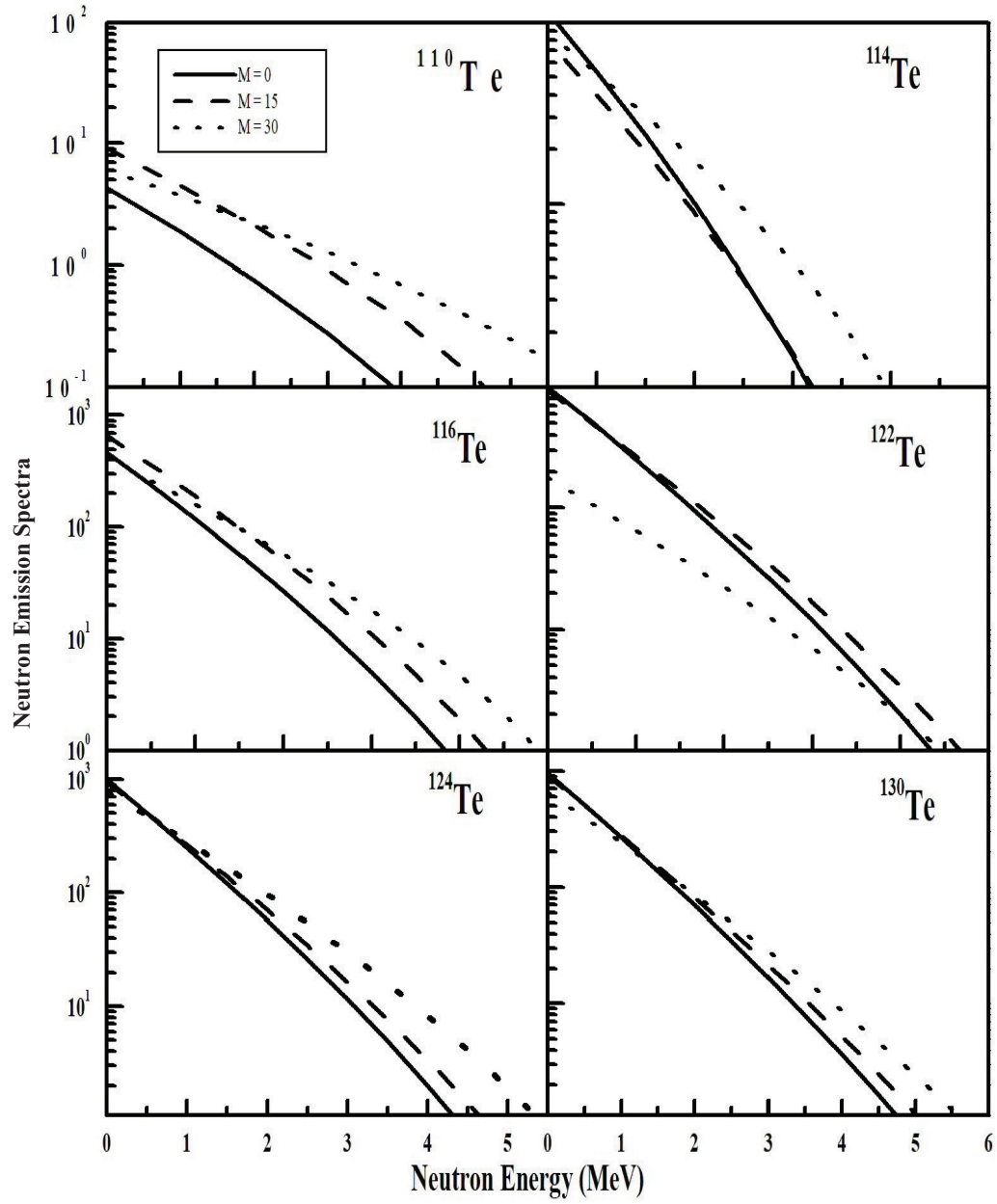


Fig. 4.15: Neutron emission spectrum for various angular momenta M (\hbar) as a function of neutron kinetic energy (MeV) for ^{110}Te , ^{114}Te , ^{116}Te , ^{122}Te , ^{124}Te and ^{130}Te nuclei.

The single neutron and proton separation energy as a function of angular momentum for various temperatures are shown in figs. 4.13 and 4.14 for the nuclei. From these figures, the separation energy values are observed to decrease sharply for the angular momentum $M = 10\hbar$ and this sudden drop corresponds to a shape transition from spherical to oblate non-collective for all the systems. It is found that in a rotating prolate system the Coriolis and centrifugal forces favor the alignment of the individual nucleons with the rotation axis. With increasing angular momentum, the aligning nucleons polarize the nuclear potential resulting in axial symmetry about the rotational axis. The result is that the nucleus undergoes a shape transition from spherical to oblate non-collective. It is also observed that single neutron separation energy values S_N increase rapidly with angular momentum at very low temperatures. This behavior is due to the presence of shell effects at low temperatures. Beyond $12\hbar$ the variations in the separation energy values disappear since the shell effects get washed out for $T = 2, 2.5$ and 3 MeV.

In figs. 4.16 and 4.17, the variation of nucleon separation energy as a function of temperature is presented for various angular momentum. The effects of rotation affect the separation energy values at low temperatures where shell effects play a very important role. At higher temperatures for $T > 0.8$ MeV, these fluctuations disappear and the energy values become almost constant due to the absence of shell effects ($M > 2\hbar$).

In fig. 4.15 neutron emission spectra for various angular momentum is shown for the nuclei ^{110}Te , ^{114}Te , ^{116}Te , ^{122}Te , ^{124}Te and ^{130}Te . The curves are all normalized to 2000. There is a general tendency that the neutron emission probability decreases with increasing neutron energy, but the emission probability for large E_n values are slightly higher compared to the emission probability of the spinless system.

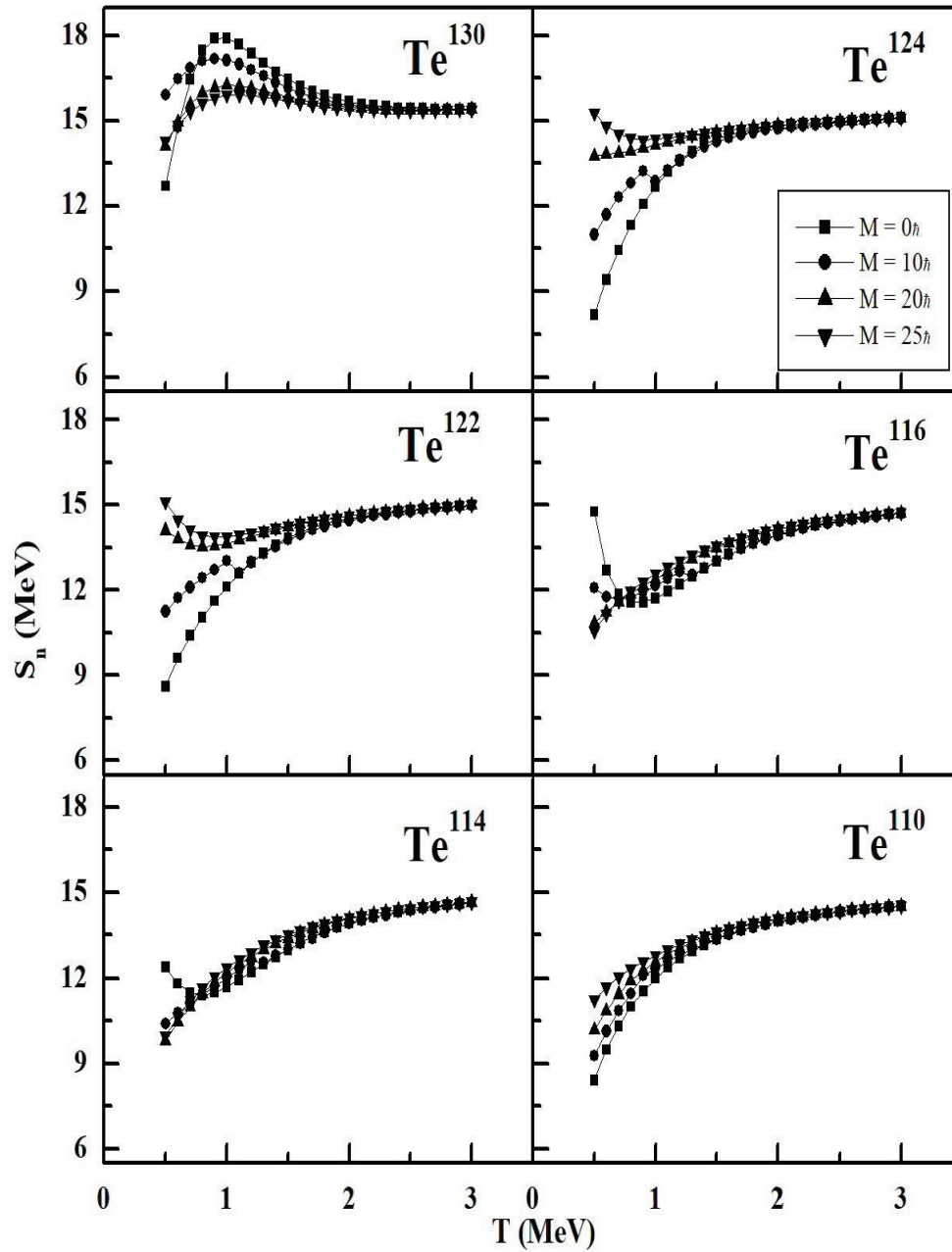


Fig. 4.16: The neutron separation energy (MeV) as a function of temperature T (MeV) with various angular momenta M (\hbar) for ^{110}Te , ^{114}Te , ^{116}Te , ^{122}Te , ^{124}Te and ^{130}Te nuclei.

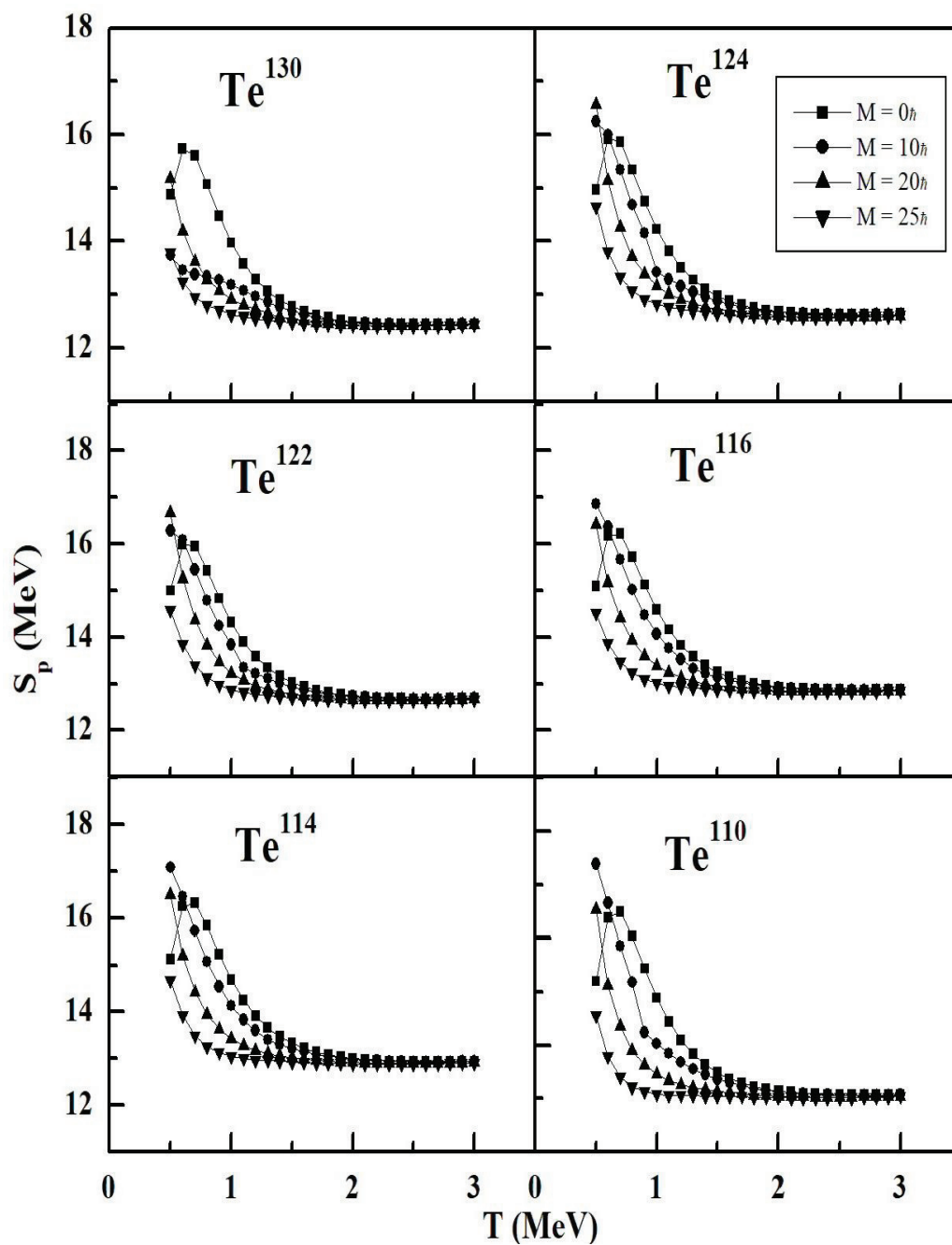


Fig. 4.17: The proton separation energy (MeV) as a function of temperature T (MeV) with various angular momenta M (\hbar) for ^{110}Te , ^{114}Te , ^{116}Te , ^{122}Te , ^{124}Te and ^{130}Te nuclei.

4.4 Conclusion

Depending upon the thermodynamic parameters such as excitation energy, separation energy for protons and neutrons, rotational frequency, kinematic moment of inertia and spin-cut off parameter shape transition behavior has been studied for Tellurium isotopes. The equilibrium shape at non-zero temperature is found by minimizing free energy function rather than the energy function. From the thermodynamical parameters, it is observed that, the nucleus ^{110}Te is found to be spherical for $\varepsilon = 0.0$ at the angular momentum range $M = 0 - 9\hbar$ and finally reaches the highly deformed non-collective oblate shape for $\varepsilon = 0.1$ and $\gamma = -180^\circ$ at $M = 10 - 25\hbar$. And the nucleus ^{130}Te remains at spherical shape with $\varepsilon = 0.0$ for the angular momentum range $M = 0 - 14\hbar$ and becomes oblate shape with $\varepsilon = 0.1$ and $\gamma = -180^\circ$ at $M = 15 - 25\hbar$. A similar behavior is exhibited for four other nuclei ^{116}Te , ^{120}Te , ^{122}Te , ^{124}Te , ^{126}Te and ^{130}Te around $M = 12\hbar$. The observed deformation at $\varepsilon = 0.1$ is found to be comparable with the experimentally obtained deformation $\varepsilon = 0.15$ which is found to be more accurate.

A sudden change arises in the spin-cut off parameter and separation energy of neutron and proton at the angular momentum $M = 12\hbar$ for the Tellurium isotopes which confirms the shape transition behavior indicates an effect in all the thermodynamical parameters. The excitation energy or the energy level diagram compared with shell model and experimental data in fig.1 reveals that STHRN method was strong enough to generate energy levels at high angular momentum particularly at 14^+ and 16^+ . The moment of inertia and rotational frequency describes the spin distribution of nuclear levels. The calculated results are in very good agreement with the experimental data and it overcomes the linear pattern obtained by IBM-1 model. Thus, using cranked Nilsson shell model the shape transition for the

eight isotopes of Te is discussed. From the results obtained, STHRN method is found to be the most suitable method to study the even – even isotopes of Tellurium nucleus at high spin states compared to Shell model and IBM – 1 model. However, the deviations in excitation energy observed at low spin can be overthrown by the inclusion of pairing interactions in STHRN method.

CHAPTER V

PHASE TRANSITION IN HOT ROTATING NUCLEI

5.1 Introduction

In thermodynamics, a phase transition is the transformation of a thermodynamic system from one phase to another. At phase transition point, physical properties may undergo abrupt change for instance, volume of the two phases may be vastly different. Paul Ehrenfest came up with a classification scheme for phase transitions, based on the thermodynamic properties of substances but it is an inaccurate method of classifying phase transitions, for it does not take into account the case where a derivative of free energy diverges.

In the modern classification scheme, phase transitions are divided into two broad categories, named similarly to the Ehrenfest classes. The first-order phase transitions are those that involve a latent heat. During such a transition, a system either absorbs or releases a fixed amount of energy and many important phase transitions fall in this category, including the solid/ liquid/gas transitions. The second class of phase transitions are the continuous phase transitions, also called second – order phase transitions. Examples superfluid transition. Lev Landau [Alhassid 1994] gave a phenomenological theory of second order phase transitions and can be applied to nuclear systems.

Examples of nuclear phase transitions are given below:

- (i) The emergence of superfluidity in nuclei when temperature or angular momentum reaches a critical value.
- (ii) The breaking of axial symmetries in the ground state as regards the deformed to spherical transition.

Recently [Kargar 2013, Dhivya 2016, Sofia 2017 and Danilo 2013] a lot of effort has been made to describe the behavior of paired small systems such as atomic nuclei. The investigation on specific heat is important since it plays a significant role within the determination of the phase transition in finite nuclei. Several authors [Algin 2008, Alhassid 2000, Dukelsky 1991, Rossingoli 1998, Ngyen 1990 and Bhaduri 1988] have investigated the existence of phase transition in finite nuclei. The change in the nuclear shape induced by thermal excitation is related to this phase transition. Danilo [Danilo 2013] have discussed the pairing phase transition from specific heat capacity (C_V) in hot nuclei by finite – temperature variation after projection BCS approach (FT – VAP). The pairing correlations existing in nuclei are counteracted by interactions induced in nuclear rotation. Indeed a short range monopole pairing force i.e., an attractive two body nucleon – nucleon force tends to couple nucleons in pairs resulting in zero angular momentum. On the other hand the Coriolis force exhibits an immediate tendency to align the angular momentum of the nucleons with rotation axis. It has been expected that with increasing angular momentum the pairing correlations will gradually collapse. This has been explained by Bardeen – Cooper – Schrieffer (BCS) formalism to investigate the theory of superconductors and modified to finite nuclear system by Bohr, Mottelson and Pines. The overall pairing collapse takes place in nuclei at high spins due to the breaking of individual pairs by Coriolis force and by high temperature. In BCS theory, this results in the prediction of some unreal singularities within the heat capacity by ignoring the impact of fluctuations. The gradual decreasing of gap parameter with respect to temperature, followed by a sudden decrease is interpreted as a rapid breaking of nucleon Cooper pairs and also the suppression of pairing correlation. This is often related with the S shape heat capacity.

The heat capacity exhibiting S shape as a function of temperature is interpreted as a fingerprint of a phase transition from a strongly correlated to an uncorrelated phase system. The existence of the bump in the specific heat is better explained by the finite size of the configuration space. The low temperature bump in the specific heat is just a remnant of the two level like structure, which is adding gradually more states to the partition function [Civitaresse 1989]. The theoretical investigations extended to $^{93} - ^{98}\text{Mo}$ [Kargar 2011] determined a S – shape heat capacity curve around the critical temperature which is correlated with the suppression of pairing correlations and corresponds to the transition from superfluid to normal phase. Recent study on heat capacities of Fe isotopes within interacting shell model [Liu 2001] reveals that pairing leads to an odd – even staggering effect within the mass dependence where the heat capacity of an odd – mass nucleus is significantly lower than that of the adjacent even – mass nuclei. Microscopic calculations on quantum phase transition have been carried out for Nd, Sm and Gd isotopes [Li 2009] employing cranked Nilsson hamiltonian for high spin states.

Moretto [Moretto 1974, 1973 and 1972] has given an expression for the thermodynamical potential of rotating nuclei at a finite temperature. The angular momentum is generated by the lagrangian multiplier which conserves the total angular momentum of the system. In this work we tend to extend the analysis of phase transitions from heat capacity plot in $^{141}, ^{142}\text{Ce}$, $^{145}, ^{146}\text{Nd}$ and $^{150}, ^{151}\text{Sm}$. The results obtained from our calculations show the presence of bump at T of the order 0.5 to 1.0 MeV for all the heavy nuclei. The occurrence of a bump in the specific heat might be due to a nuclear structure effect leading to a phase transition rather than finite size effect. Therefore, it is found that pairing has significant effects on the specific heat. Since within the superfluid state, the nucleon occupation probability

near the Fermi surface is seared out as a result of pairing correlations even at $T = 0$, C_v is significantly increased. And the difference in C_v between even and odd neutron system as a function of temperature for varying angular momentum is plotted and the results are discussed. In this work we assume neutrons and protons as two distinct non – interacting thermodynamic systems. Statistical description of finite nuclear systems is generally based on grand canonical ensemble averages.

The statistical theory with single particle level structure as the input can be used to extract information about the complex phenomena such as phase transitions and shape transitions. The energy levels and the intrinsic spin for proton and neutron systems were generated by diagonalising the axially symmetric Nilsson Hamiltonian [Nilsson 2005] for the deformation parameter (ϵ) -0.6 to 0.6 insteps of 0.1. The specific heat is recognized as a quantity which indicates the occurrence of phase transition. The nuclear specific heat can be estimated from a fused compound system formed in heavy ion collision if the excited states spectrum is well – known. The behavior of nuclear specific heat at high temperature directly yields the information about the relevant degrees of freedom in the spectrum of Dulong and Petti’s law. The motivating feature of specific heat is the peak structure which endorses the existence of phase transition. The appearance of peaks in the specific heat at temperatures $T = 1.7$ MeV and 3.1 MeV for the nuclei ^{24}Mg corresponding to average change in shape of the nucleus from ellipsoidal to axially symmetric and from axially symmetric to spherically symmetric shapes, emerges as a signal for phase transitions [Miller 1989].

5.2 Significance of phase transition

Since the pioneering work of Newton and his coworkers much efforts have gone into the investigation of phase transitions in hot rotating nuclei. Of late, investigations on phase transition in finite nuclei have created new attention among physicists, but many questions remain still open. One of the pertinent questions which arise in the finite temperature description of the nuclei is whether phase transition really occurs. Till date, there are many unresolved problems concerning the meaning of phases and phase transitions in finite nuclei.

At the outset, Thouless proposed to differentiate the types of phase transition. Later, the Landau theory has forecasted a sharp first order liquid – gas phase transition in nuclei for temperatures below the critical temperature (T_c). A phase transition from the superfluid to normal fluid has also been investigated based on the finite temperature (Ft) mean field theories such as Bardeen – Cooper – Schrieffer (BCS), Hartree – Fock (HF) and Hartree – Fock – Bogoliubov (HFB). For instance, the FTHFB theory predicts the occurrence of sharp second order phase transition from superfluid nucleus to the normal nuclear matter.

The accomplishment of mean field theories is based to certain degree, on the breaking of symmetries which permits a considerable enlargement of the variational Hilbert space so as to include the appropriate correlations. The breaking of particle number symmetry in the BCS theory and of the rotational invariant in deformed nuclei are two renowned examples. The symmetry breaking is usually related to phase transitions, superfluid to normal fluid in the particle number case and spherical to deformed shape in the angular momentum one. In view of enormous number of configurations involved, a statistical description becomes necessary. However, microscopic statistical descriptions of highly excited nuclei are usually based on

conventional single particle treatments such as the Fermi gas model or the more microscopic finite temperature self consistent mean field approximations such as the thermal HF and HFB.

Heating can have a dramatic effect upon nuclear deformations, producing a variety of shape transitions. Rotation also has a significant effect upon nuclear deformation. For example, increasing the temperature of a nonrotating nucleus can change a prolate shape into a spherical and oblate shape and heating can also change a spherical shape to a prolate shape. When a nucleus is simultaneously heated and rotated, the variety of shape transitions will surely proliferate. The finite temperature Hartree – Fock – Bogoliubov (FTHFB) formalism has determined the impact of temperature on the shapes of nonrotating nuclei. Later, the finite temperature Hartree – Fock – Bogoliubov cranking (FTHFBC) theory provides a fully self consistent microscopic treatment of single – particle, shape, pairing, rotational and thermal degrees of freedom.

FTHFBC formalism when applied to hot rotating nuclei, properties such as pair gaps and deformation have been determined as a function of temperature and angular momentum. Besides this it also envisages that rotation can induce a sharp first order transition from superfluid to normal fluid for temperatures below T_c . Concerning the shapes of hot non-rotating nuclei, the FTHFB approach and Landau theory describes a transition from deformed to spherical shape, when temperature reaches T_c at zero angular momentum. As regards the shapes of hot rotating nuclei, the FTHFBC model elucidates a transition from prolate – collective to oblate – noncollective shape as temperature increases at fixed angular momentum. Hence a precise classification of phase transitions is necessary.

Normally, all these types of phase transitions fall into two categories (i) pairing – phase transitions (superfluid to normal fluid) and (ii) shape – phase transitions (deformed to spherical shapes for example). There are many theoretical and experimental supports for the appearance of these phase transitions in finite nuclei. Evidences include the vanishing of gap parameter in superconducting nuclei for pairing – phase transition and the quadrupole moment in deformed nuclei for shape – phase transition.

The phase transition from superfluid to normal nuclear matter has been elaborately investigated in the determination of single particle level density parameter as a function of angular momentum and temperature [Rajasekaran 2008]. In the present study, we have extended our investigation of nuclear phase transitions in light nuclei, with particular focus to its geometrical forms. The nuclear specific heat is also one among them to study the existence of phase transition.

One important parameter to study the phase transition is the specific heat. The specific heat is a quantity which indicates the occurrence of phase transition in nuclei. The nuclear specific heat of a fused compound system formed in heavy ion collision can be estimated if the excited states spectrum is known. Elementary examples of this are stated by Pathria [Pathria 1972], including the free particle, the harmonic oscillator and rigid rotor. The behavior of nuclear specific heat at high temperature directly yields the formation about the relevant degrees of freedom in the spectrum of Dulong and Petit's law. Tanabe [Tanabe 1980], Goodman [Goodman 1984], Cole [Cole 1989], Miller [Miller 1989] and others [Bhaduri 1988, Dukelsky 1991 and Civitarese 1994] have emphasized the role of nuclear specific heat in the determination of important properties of the nuclei. One motivating feature is the peak structure in specific heat which endorses the existence of phase transition.

Several authors have extensively investigated [Tanabe 1982, Goodman 1984, Bhaduri 1988 and Cole 1989] the existence of phase transition in finite nuclei. Miller et al. [Miller 1989] have investigated the occurrence of phase transition using finite temperature Hartree – Fock approximation and in the exact canonical ensemble. Rossignoli et al. [Rossignoli 1999] have studied the correlation between thermal effects and two of the crucial ingredients of the many body problems, via super conductivity and deformation due to a long- range residual force. Their finite temperature method exhibits important shortcomings such as the prediction of sharp phase transition [Rossignoli 1999].

Various cranking Hartree – Fock – Bogliubov (CHFB), provide a reliable analysis for medium and heavy systems. Self-consistent mean field calculations combined with the random phase approximation (RPA) analysis are beneficial to detect quantum phase transitions. In contrary, analogous investigations have shown that the proposed phase transition does not occur for some nuclei belonging to the 2s-1d shell [Dukelsky 1991].

The appearance of peaks in the specific heat at temperatures $T = 1.7$ MeV and 3.1 MeV for the nuclei ^{24}Mg corresponding to average change in shape of the nucleus from ellipsoidal to axially symmetric and from axially symmetric, spherically symmetric shapes, emerge as a signal for phase transitions [Miller 1989]. Hasagawa et al. [Hasagawa 2007] have reported shape phase transition in $A \approx 70$ nuclei along the $N = Z$ line. This occurrence of phase transition to deformed nuclei due to the strong proton-neutron correlations in these nuclei. Civitarese et al. [Civitarese 1990] have witnessed the occurrence of a bump in the specific heat of some of the light nuclei belonging to the 2s-1d shell using nuclear SU_3 model, may be due to finite size effect rather to a phase transition.

It is really interesting and open question whether or not phase transitions do occur in finite nuclear system at finite temperatures and signatures of these phase transitions remain despite of fluctuations. The finite temperature mean field theories such Bardeen – Cooper – Schrieffer (BCS) [Bardeen 1957], Hartree – Fock (HF) [31], and Hartree – Fock – Bogoliubov [HFB] [Goodman 1983] have been addressed the phase transition from super fluid to normal fluid nuclear matter. Danilo et al. [Danilo 2013] have studied the influence of number and number parity projections on heat capacities of nuclear systems ^{161}Dy and ^{161}Dy using finite temperature BCS theory and found S-Shaped heat capacity at temperature T less than the critical temperature T_c , that corresponds to the super fluid to normal phase transition. The quantal and statistical fluctuations are necessary in identifying phase transitions in light nuclear systems. Within the framework of static path approximation (SPA) plus random phase approximation (RPA) treatment, Rossignoli et al. [Rossignoli 1998] have investigated thermal ad quantal fluctuations and even-odd effects in nuclear systems ^{164}Er and ^{165}Er at finite temperature. Liu and Alhassid [Liu 2001] have developed a new method for calculating the heat capacity using the shell model Monte Carlo (SMMC) approach, for iron isotopes $^{52-62}\text{Fe}$, and identified a signature of phase transition in the heat capacities despite the large fluctuations. Strictly speaking, quantal and statistical fluctuations are of essential importance since they smooth out the singularities allied with phase transitions [Kanthimathi 2011]. In the statistical theory, the equilibrium shape of the nucleus at given angular momentum and temperature has been obtained by minimizing the free energy as a function of deformation.

The specific heat C_V as a function of angular momentum M and temperature T is given as,

$$C_V(M, T) = \frac{dE(M, T)}{dT}, \quad (5.1)$$

Or

$$C_V(M, T) = T \frac{dS(M, T)}{dT} \quad (5.2)$$

where $S(M, T)$ is the entropy of the finite nuclear system and $E(M, T)$ is the total energy of the system.

5.3. Results and discussion

In this section, the discussions on C_V as a function of T , obtained from the statistical theory of hot rotating nucleus by incorporating the degrees of freedom such as deformation and collective rotation of the system are presented. The calculations were performed for rare earth nuclei such as ^{141}Ce , ^{142}Ce , ^{141}Ba , ^{142}Ba , ^{141}Xe , ^{142}Xe , ^{145}Nd , ^{146}Nd , ^{150}Sm and ^{151}Sm . The results obtained from our calculations are similar to those reported in [Danilo 2013] and show the presence of bump at $T = 0.5$ to 1.0 MeV for all heavy nuclei. The theoretical discussions, reveals that the occurrence of bump in the specific heat might be due to a nuclear structure effect leading to a phase transition.

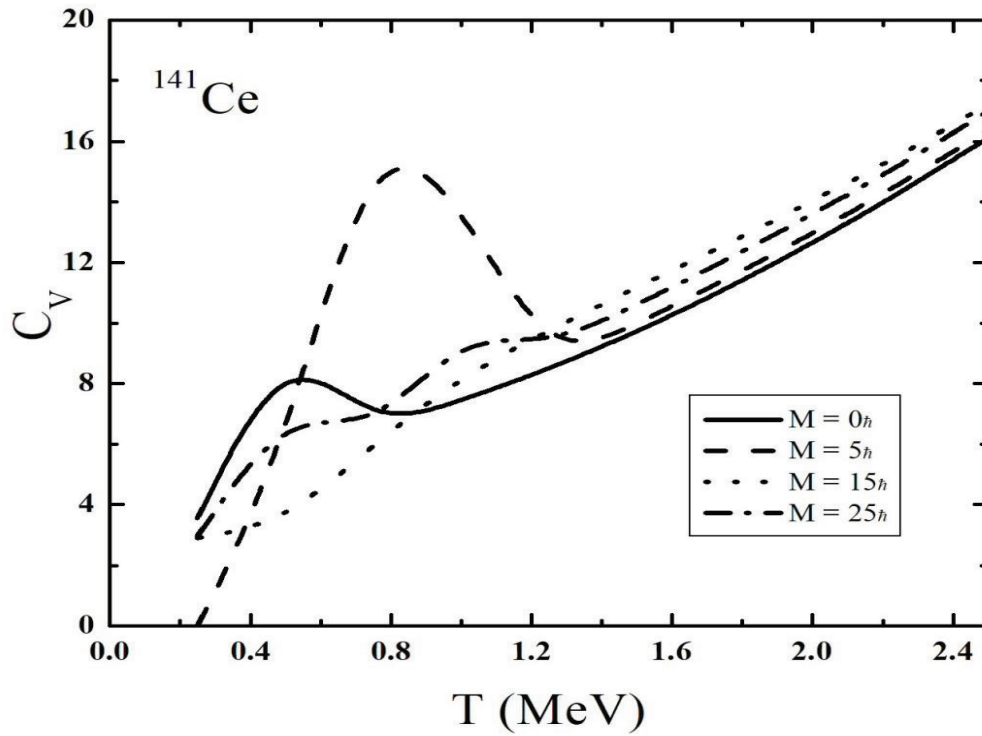


Fig. 5.1: The S-shape nuclear specific heat capacity (C_V) as a function of temperature T (MeV) and angular momentum M (\hbar) for ^{141}Ce .

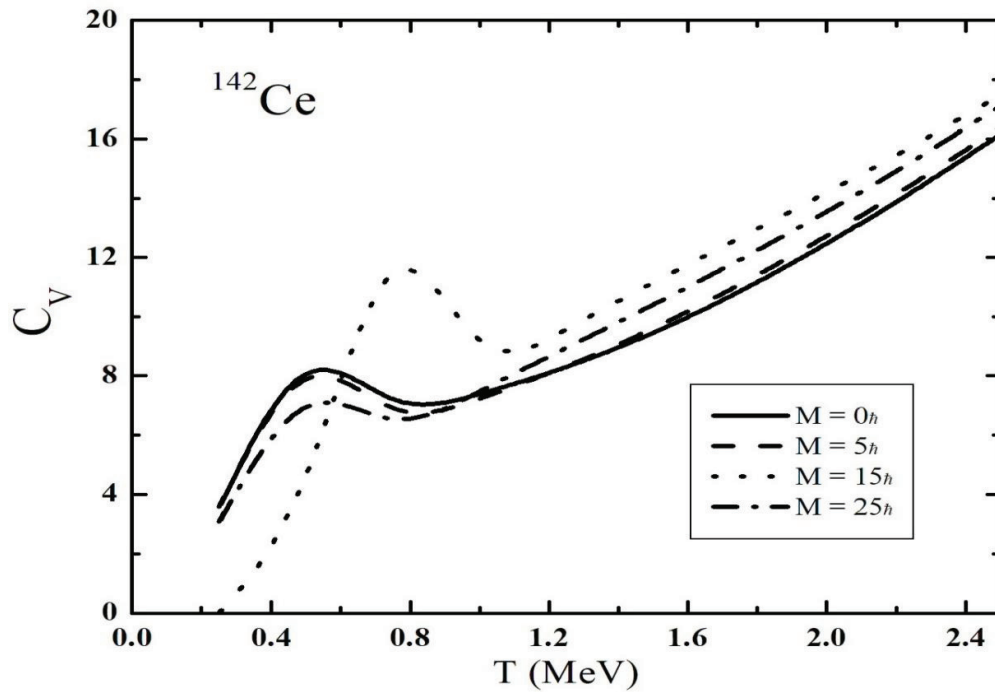


Fig.5.2: The S - shape nuclear specific heat capacity (C_V) as a function of temperature T (MeV) and angular momentum M (\hbar) for ^{142}Ce .

Figures 5.1 and 5.2 shows S - shape specific heat capacity as a function of temperature for varying angular momentum for ^{141}Ce and ^{142}Ce . The effects of pairing correlation on the specific heat for this system is pronounced in the C_V plot as a S – shape curve. Below $T \approx 0.5$ MeV, the C_V is strongly suppressed by pairing correlations. Above $T \approx 0.5$ MeV, the C_V becomes larger than the results for noninteracting particles and then it becomes smaller. This dependence of the specific heat on temperature is commonly referred to as “S – shape” behavior.

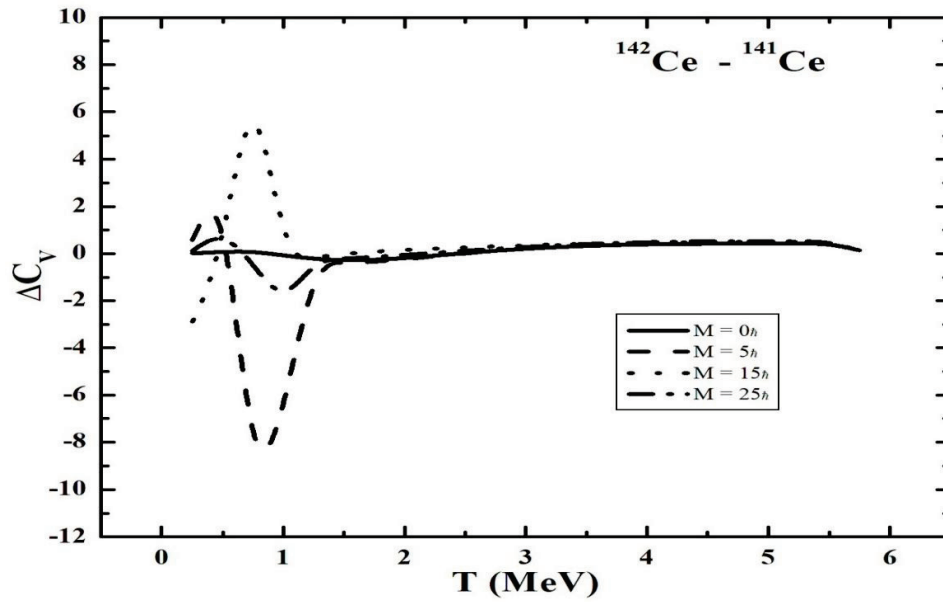


Fig.5.3: The difference in specific heat capacity (ΔC_V) as a function of temperature T (MeV) and angular momentum M (\hbar) for ^{141}Ce and ^{142}Ce isotopes.

$$[\Delta C_V = C_V^{even} - C_V^{odd}]$$

From fig.5.3 it is observed that for even number of neutrons or protons there is a large difference between the noninteracting and interacting system. However, the difference in C_V for ^{142}Ce and ^{141}Ce is almost zero for $M = 0\hbar$. As M increases, the change in C_V is exhibited in ΔC_V plot as a hump in low temperature range. For $M = 15\hbar$, the ΔC_V value is found to be maximum and it is considered to be a signature of phase transition from superfluid to normal system.

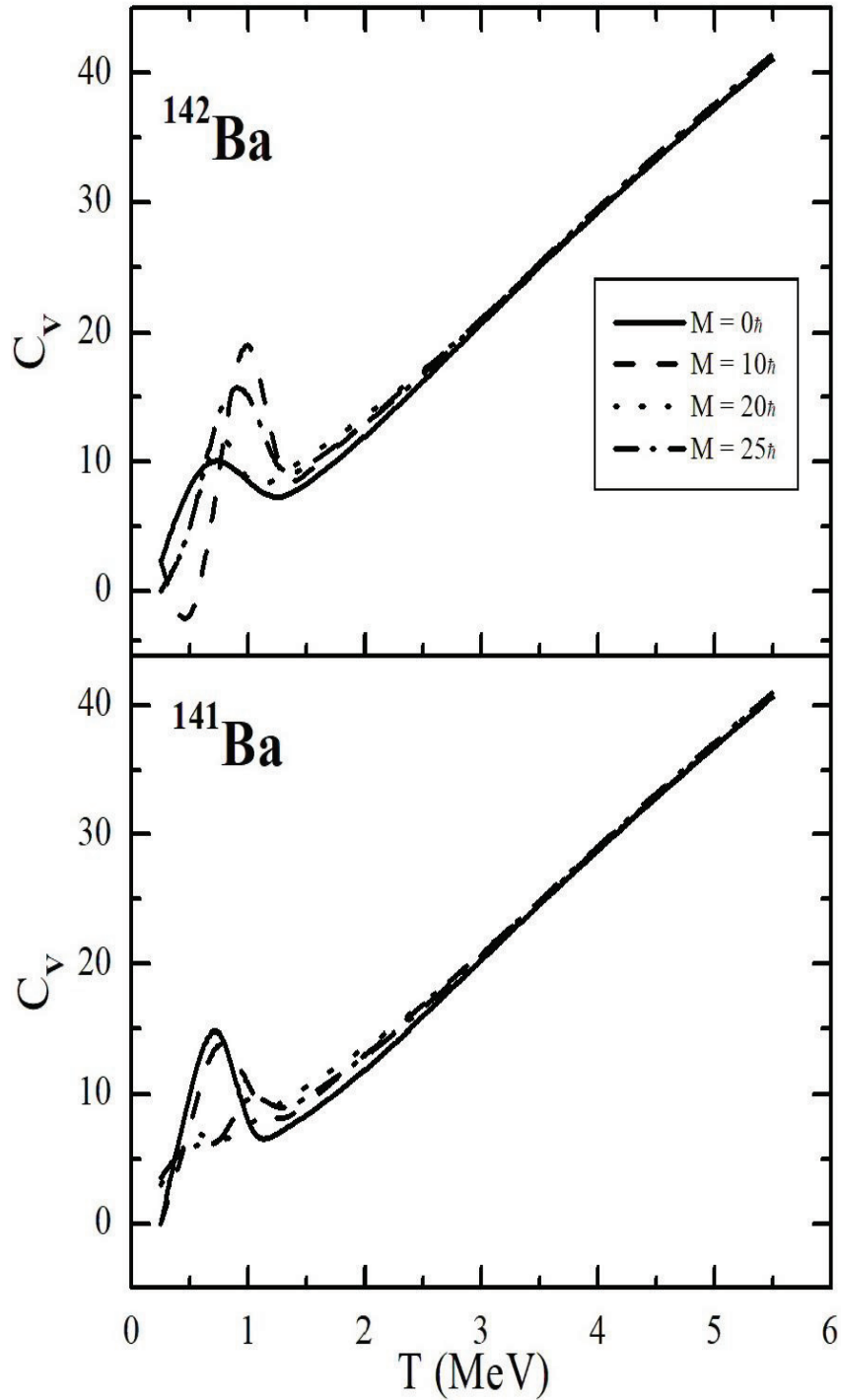


Fig.5.4: The S - shape nuclear specific heat capacity (C_V) as a function of temperature T (MeV) and angular momentum M (\hbar) for (a) ^{141}Ba and (b) ^{142}Ba nuclei.

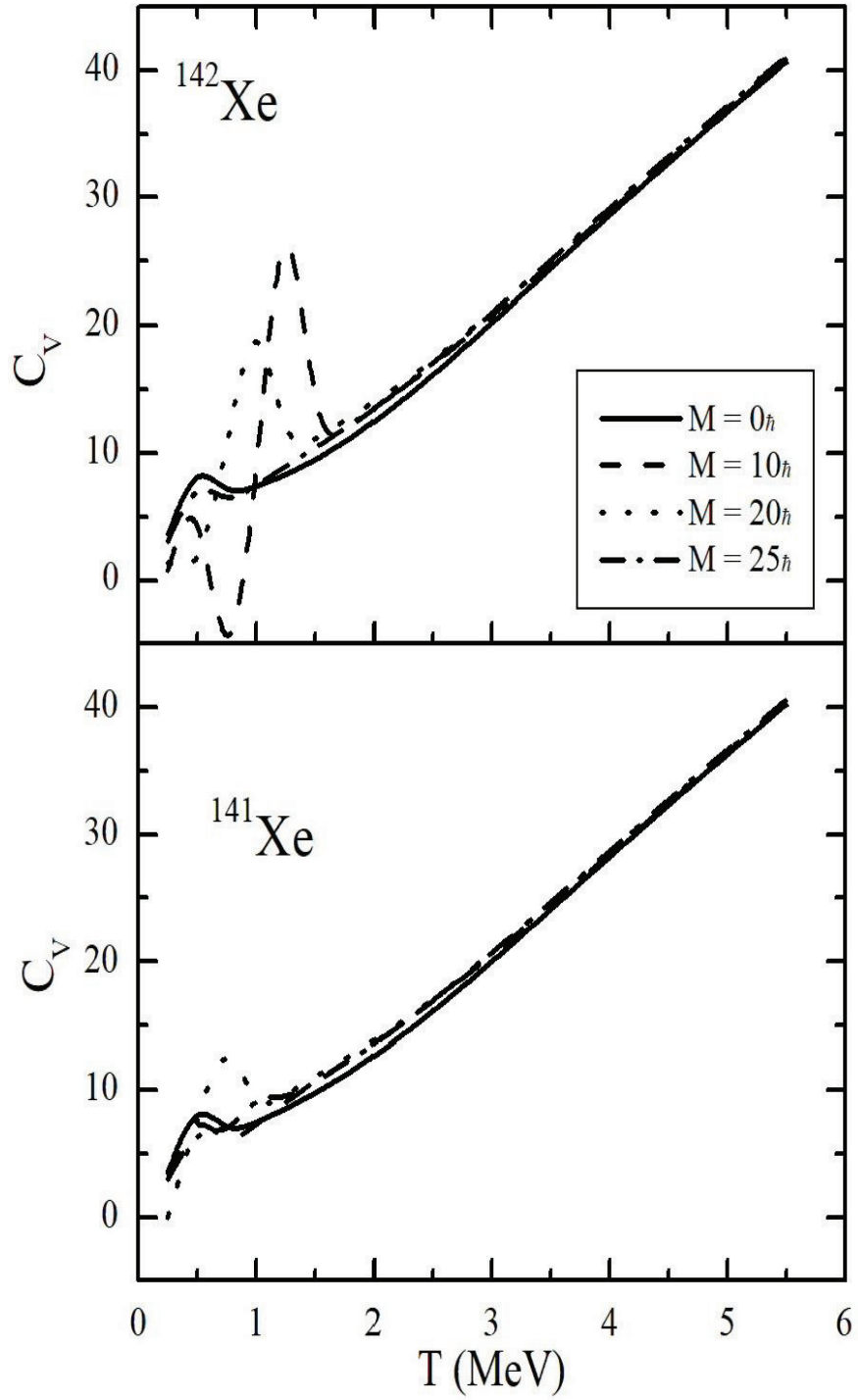


Fig.5.5: The S - shape nuclear specific heat capacity (C_V) as a function of temperature T (MeV) and angular momentum M (\hbar) for (a) ^{141}Xe and (b) ^{142}Xe nuclei.

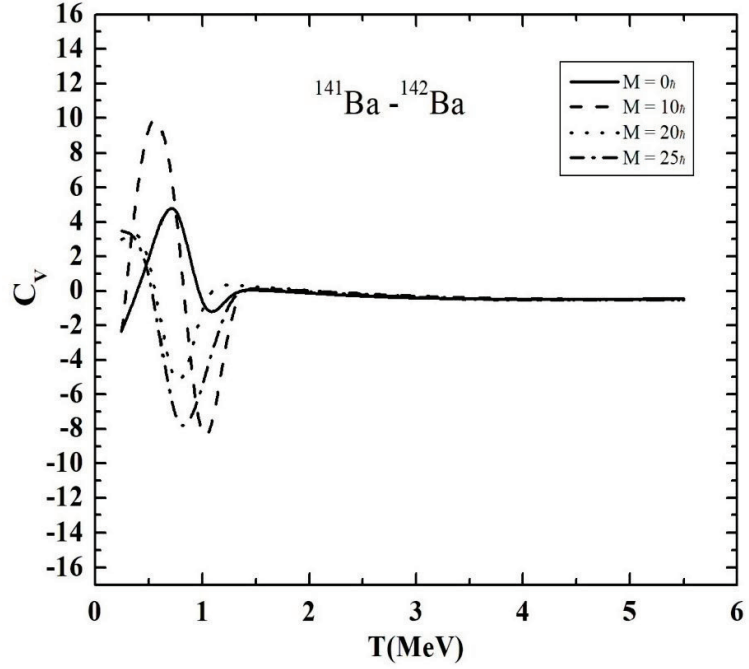


Fig.5.6: The difference in specific heat capacity (ΔC_V) as a function of temperature T (MeV) and angular momentum M (\hbar) for ^{141}Ba and ^{142}Ba isotopes.

$$[\Delta C_v = C_v^{even} - C_v^{odd}]$$

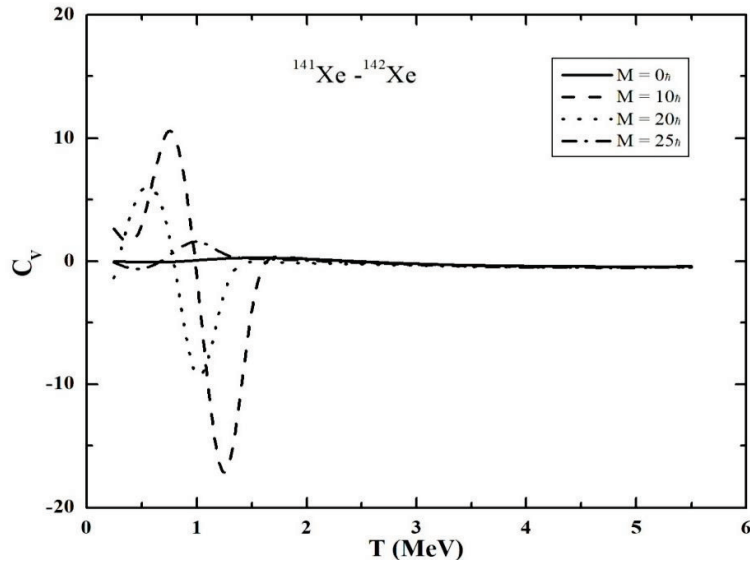


Fig.5.7: The difference in specific heat capacity (ΔC_V) as a function of temperature T (MeV) and angular momentum M (\hbar) for ^{141}Xe and ^{142}Xe isotopes.

$$[\Delta C_v = C_v^{even} - C_v^{odd}]$$

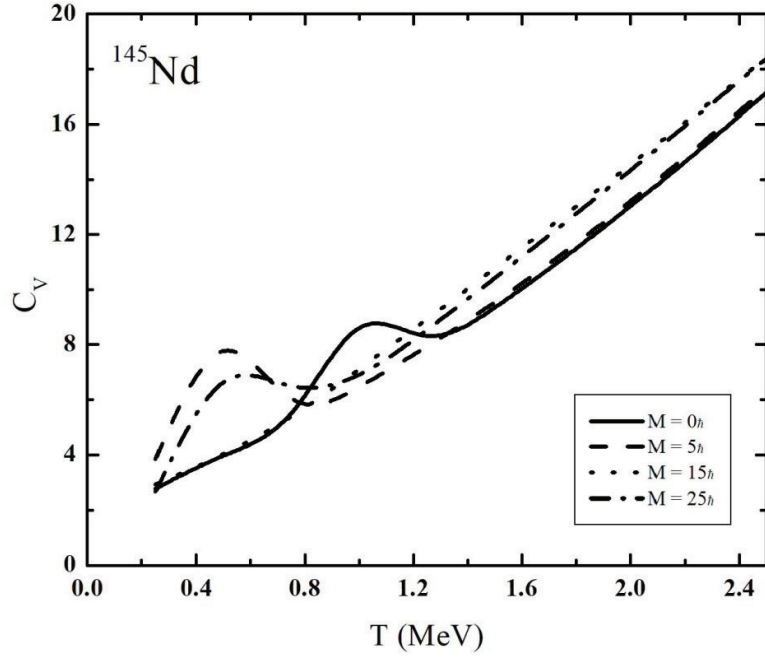


Fig.5.8: The nuclear specific heat capacity (C_V) as a function of temperature T (MeV) and angular momentum M (\hbar) for ^{145}Nd .

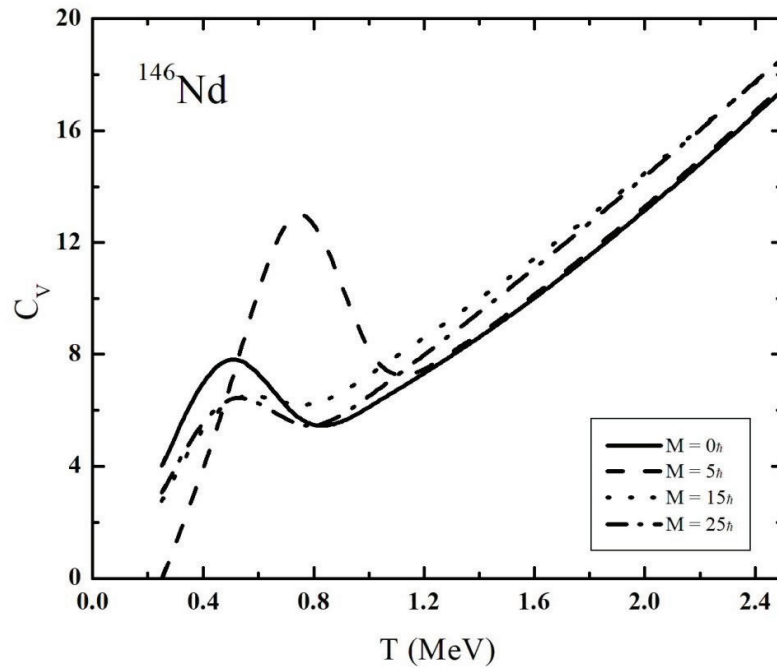


Fig.5.9: The nuclear specific heat capacity (C_V) as a function of temperature T (MeV) and angular momentum M (\hbar) for ^{146}Nd .

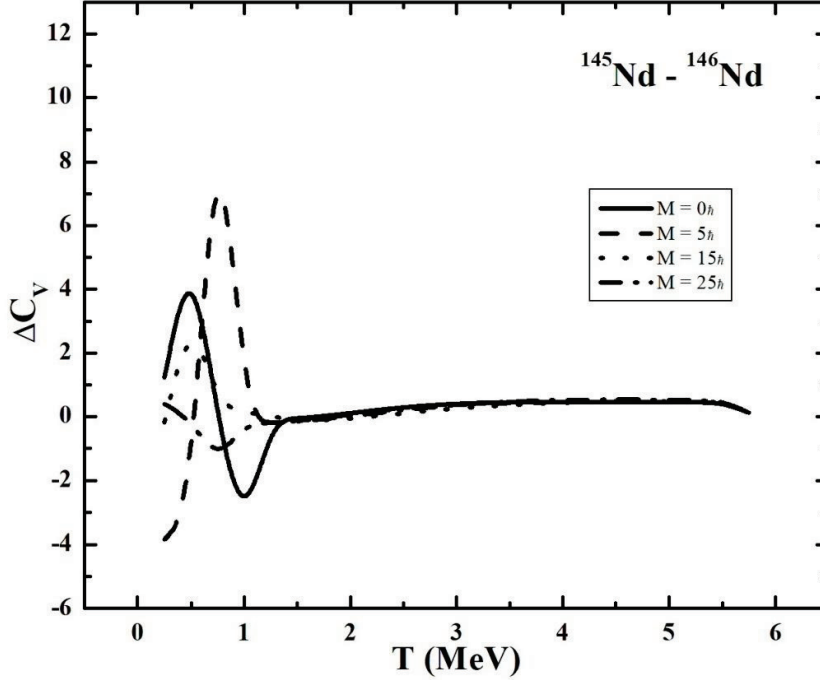


Fig.5.10: The difference in specific heat capacity (ΔC_v) as a function of temperature $T(\text{MeV})$ and angular momentum M (\hbar) for ^{145}Nd and ^{146}Nd isotopes. $[\Delta C_v = C_v^{\text{even}} - C_v^{\text{odd}}]$

As expected at large temperatures, the pairing correlations are found to be ineffective and the difference between even – even and odd – even system is becoming very small. It is thus shown that the pairing correlations have a significant influence on the specific heat, especially for temperatures below $T = 1$ MeV. The calculated ΔC_v between the two isotopes of Ce shows clearly that the pairing correlations contribute to the S – shaped behavior of the specific heat.

As discussed in fig.5.1, 5.2 and fig.5.3 a similar behavior is observed in $^{141}, ^{142}\text{Ba}$ which is shown in fig.5.4 and fig.5.6 and in $^{141}, ^{142}\text{Xe}$ in fig.5.5 and fig.5.7 and also for difference mass number in $^{145}, ^{146}\text{Nd}$ from fig.5.8 to fig.5.10. The appearance of hump in the specific heat capacity at low temperature is also influenced

by the low – lying collective states. There is a general tendency for all the nuclei to exhibit a abrupt change in the specific heat beyond temperature $T = 1$ MeV. These specific heat fluctuations occur at different temperatures for different nuclei. From the ΔC_V plot for $^{145, 146}\text{Nd}$, the maximum value occurs for $M = 5\hbar$.

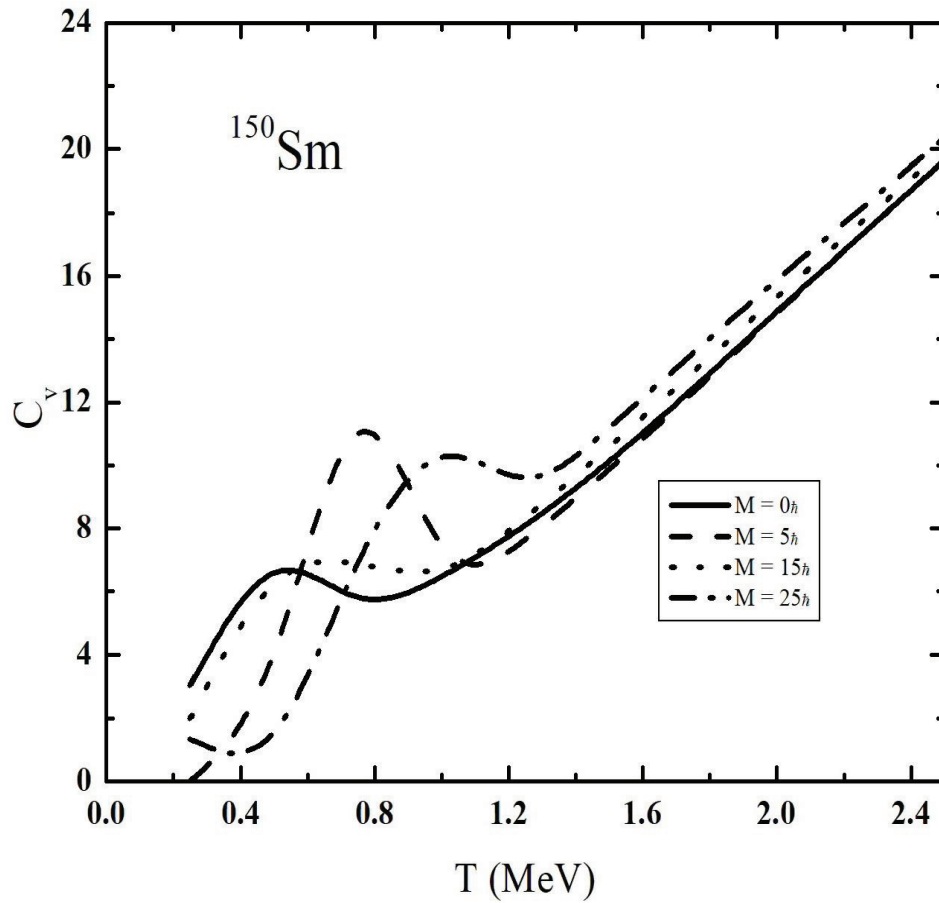


Fig.5.11: The nuclear specific heat capacity (C_V) as a function of temperature $T(\text{MeV})$ and angular momentum M (\hbar) for ^{150}Sm .

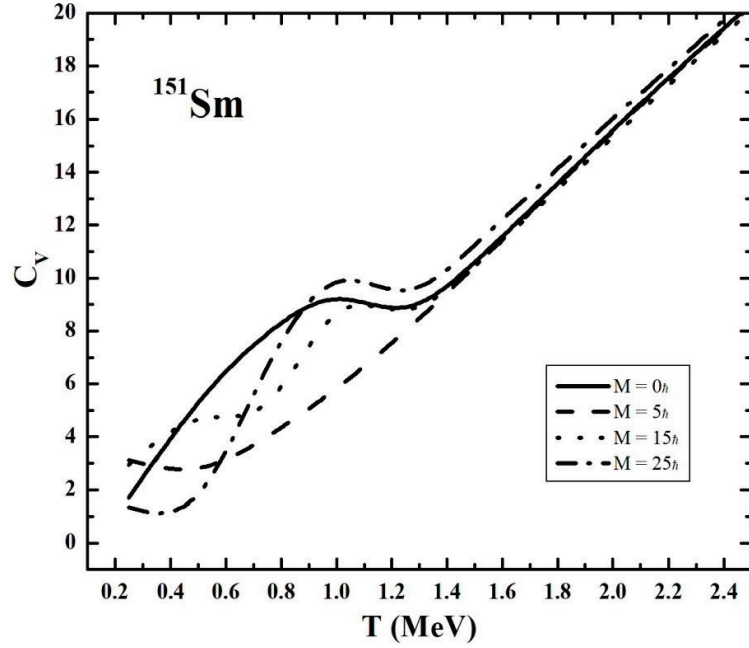


Fig.5.12: The nuclear specific heat capacity (C_V) as a function of temperature T (MeV) and angular momentum M (\hbar) for ^{151}Sm .

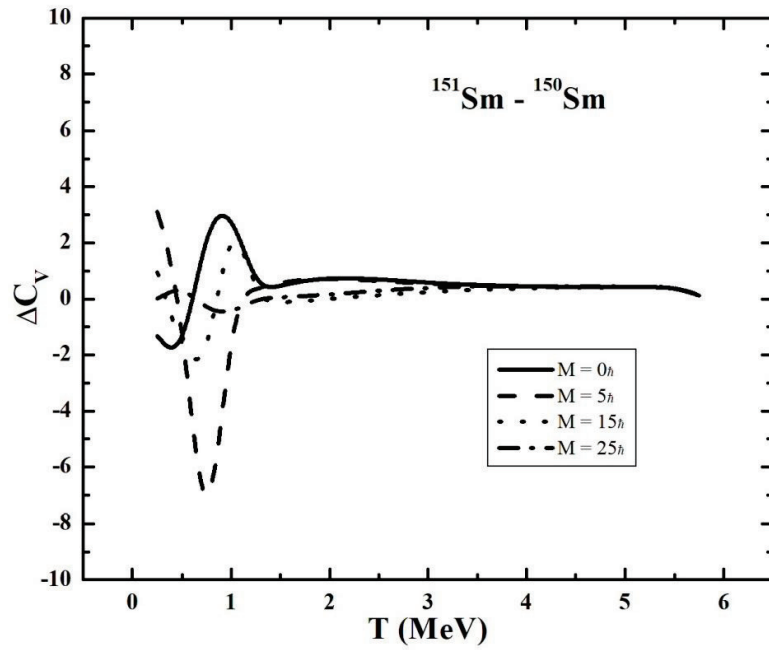


Fig.5.13: The difference in specific heat capacity (ΔC_V) as a function of temperature T (MeV) and angular momentum M (\hbar) for ^{150}Sm and ^{151}Sm isotopes.

$$[\Delta C_v = C_v^{odd} - C_v^{even}]$$

Similar discussions have been carried out for ^{150}Sm and for ^{151}Sm , with an increase in neutron number. Figures 5.11 and 5.12 represents the C_V for the isotopes ^{150}Sm and ^{151}Sm with an increasing M . It is also noted that the occurrence of the peak in the specific heat at low temperature is a contribution of the ground state rotational band which is associated with a superfluid to normal phase transition. The effect of angular momentum on specific heat is very much pronounced at low temperatures which is also observed in fig.5.13 with an increasing value of ΔC_V at $M = 0\hbar$.

5.4 Conclusion

The interplay between pairing phase transition has been studied using the statistical theory with the idea of gaining some insight into the behavior of nuclear specific heat as a function of temperature and angular momentum. The occurrence of phase transition is predicted in three rare nuclei along with their isotopes such as $^{141, 142}\text{Ce}$, $^{145, 146}\text{Nd}$ and $^{150, 151}\text{Sm}$. The results of our calculations on specific heat capacity shows a predominant appearance of a hump in the low temperature region which is considered as the suppression of pairing correlation and it is an indication of phase transition. It is also noted that the occurrence of the peak in the specific heat at low temperature is a contribution of the ground state rotational band. From the ΔC_V plot, it is observed that the maximum difference in C_V occurs at $M = 15\hbar$ for $^{141, 142}\text{Ce}$ and $M = 5\hbar$ for $^{145, 146}\text{Nd}$ followed by $M = 0\hbar$ for $^{150, 151}\text{Sm}$. At large temperatures, as expected the pairing correlations are found to be ineffective and the difference in C_V becomes negligibly small.

CHAPTER VI
A COMPARATIVE STUDY OF NUCLEAR STRUCTURE
PROPERTIES WITH AND WITHOUT PAIRING CORRELATIONS

6.1 Introduction

Pairing correlations play an essential role in many fermion systems [Guttormsen 2000] and have a strong influence on nuclear thermal quantities. Bardeen–Cooper–Schrieffer (BCS) theory of Superconductivity [Bardeen 1957] for infinite Fermi system of electrons play the vital role in explaining the sharp phase transitions which is connected to the breakdown of pairing correlations. The pairing correlation in the BCS theory vanishes suddenly at critical temperature and is observed as a discontinuity in the heat capacity. The S shape of the heat capacity has been found experimentally by the Oslo group [Melby 1999 and Schiller 2001] and in recent theoretical approaches such as the shell-model Monte Carlo (SMMC) calculations [Liu 2001, Rombouts 1998 and Alhassid 2003], the static-path plus random-phase approximation (SPA+RPA) [Rossignoli 1998] and the number projected SPA (NPSPA) [Kaneko 2007]. The Fermi – Dirac statistics was able to reproduce the thermal quantities at high nuclear temperature [Langanke 1996 and Mocalj 2007].

Nuclear properties at the low energy region show strong dependence to the pairing correlations between nucleons. It is important to take into account the pairing effects in theoretical nuclear structure studies. The BCS model, is used in describing many characteristics of the finite system of the paired nucleons inside nucleus. The sudden decrease in the pairing gap parameter at the critical temperature is an indication of second – order phase transition in the BCS model. This sharp phase

transition leads to a discontinuity in the heat capacity. The extracted semi-empirical thermal quantities by the use of the experimental data on the nuclear level densities for some nuclei show a smooth behavior for the excitation energy and entropy and a smooth S-shaped curve for the heat capacity around the critical temperature [Rahmatinejad 2015].

Pairing phase transition in nuclei, the S - shaped heat capacity and the relation between the pairing gap parameter at zero temperature and the critical temperature have been discussed within various approaches in recent studies [Liu 2015, Li 2015 and Niu 2013]. The SPA method which is based on the path integral representation of partition function, is a microscopic framework to deal with large amplitude static fluctuations around the mean field [Rossingoli 1999]. The extracted pairing gap parameter in the SPA method for heavy nuclei is a non-vanishing function of temperature and leads to a smooth S-shaped heat capacity. In the case of light nuclei, the pairing gap parameter decreases very gradually resulting in the S-shape of the heat capacity approximately disappears [Ginzburg 1950]. In the MPBCS method, the pairing gap parameter is assumed to be a Fermi function of temperature at the vicinity of the critical point. This method improves the extracted results for thermal quantities within the BCS model. The Ginzburg–Landau model is a phenomenological method to describe the first and second-order phase transitions near the critical temperature [Ginzburg 1950 and Rahmatinejad 2016].

In the last decade there has been a renewed interest for studying the fingerprints of pairing correlations in the thermodynamic properties of excited nuclei. This interest was triggered by the new accurate measurements of level density at low excitation energies. The possible thermal signatures of pairing correlations in these rare-earth isotopes have been studied either with schematic models or employing

various approximations which go beyond the standard BCS approach. The finite temperature (FT-VAP) approach will be applied here to investigate the effect of pairing on the thermal properties of the Dy and Yb isotopes. Schiller [Schiller 2001] argued that the S-shaped form of the specific heat in Dy and Yb isotopes is generated by the transition from the superfluid to the normal phase. The competition between temperature and pairing correlations in nuclei at low excitation energies has been studied for several decades and it was predicted that the critical temperature T_c for pair correlation quenching could be expressed. In addition, pairing correlations are expected to play an important role in the decay of compound nuclei formed in heavy-ion collisions. The BCS and HFB methods have been extended to self-consistent mean-field models to improve the description of the pairing transition in spherical nuclei as well as in deformed nuclei where shape transitions have been predicted.

At zero temperature i.e., the ground states of most nuclei are superfluid states, but in warm nuclei [Guttormsen 2000] the super-fluidity tends to vanish when the temperature increases. Such a transition from superfluid to normal has attracted wide attentions in the past decades. From these investigations, the S-shaped curve of heat capacity has been found as a function of temperature. This was regarded as a fingerprint of the superfluid to normal (pairing) phase transition. Based on this picture, the critical temperature has been estimated from the experimental data as $T_c \approx 0.5$ MeV for $^{161,162}\text{Dy}$, $^{171,172}\text{Yb}$ [Dean 2003] and $^{166,167}\text{Er}$ [Bardeen 1957].

Clear signatures of pairing phase transition is provided by the mean-field calculations including finite temperature BCS (FT-BCS), finite-temperature HFB (FT-HFB) with a pairing – plus – quadrupole Hamiltonian, as well as the self-consistent mean-field models in both non-relativistic and relativistic form. With a variety of quantum fluctuations, it has been found that the critical temperatures for the

pairing phase transition given by most mean-field models locate in the interval of $0.5-0.6\Delta(0)$, where $\Delta(0)$ is the pairing energy gap at zero temperature. For the pairing phase transition, the particle number conservation is violated in the superfluid phase while preserved in the normal-fluid phase. Due to the restoration of particle number conservation, the calculated heat capacity varies smoothly with the temperature, indicating a gradual transition from the superfluid to the normal phase. Therefore, it is imperative to investigate the pairing transition in hot nuclei and the nature of the S-shaped heat capacity curve by the shell model like approach. In this approach, the particle number is strictly conserved and the blocking effects are also treated exactly.

6.2 Pairing phase transition

To have a complete and comprehensive picture of pairing – phase transition and other intrinsic properties of nuclei, effects of pairing correlations are needed. Pairing correlations at finite temperature have been the subject of peculiar interest since the early 1960s. The theory of nuclear superfluid pairing correlations was developed about 50 years ago by Belyaev [Belyaev 1965]. The first studies were carried on within the framework of FT-BCS theory. It was clearly recognized then that the pairing field is an important component of the nuclear mean-field potential and the interplay between deformation driving forces and the pairing field determines most of the properties of a nuclear system.

Many attempts have been made to describe and understand the response of the nuclear pairing in the superfluid system. The finite temperature mean field description of heavy nuclei has provided the theoretical support for the study of nuclear properties at high excitation energy and angular momentum. The pairing correlations existing in nuclei are counteracted by interactions induced in nuclear rotation. Indeed a short range monopole pairing force, i.e., an attractive two body

nucleon – nucleon force tends to couple nucleons in pairs resulting in zero angular momentum. On the other hand, the Coriolis force exhibits a direct tendency to align the angular momentum of the nucleons with rotation axis. It has been expected that with increasing angular momentum the pairing correlations will gradually collapse. This has been explained by BCS formalism introduced to investigate the theory of superconductors and modified to finite nuclear system by Bohr [Bohr 1958]. The overall pairing collapse takes place in nuclei at high spins due to the breaking of individual pairs by Coriolis force and by high temperature.

Tanabe [Tanabe 1982] have extracted the average properties of the deformed nuclei in excited system, employing temperature dependent HFB equations where the effects of pairing are important and have predicted a possible first order phase transition. Agarwal et al. [Agarwal 2000] have made a detailed study of the temperature dependence of pairing gap using relativistic Hartree-BCS theory. Further Skyrme's interaction is used in deformed HF calculations that includes pairing correlation in a self-consistent way by considering energy functional depending on occupational probabilities. Recently density functional theory of nuclear structure provides a many particle wave function which is very useful to study the static properties. However, the study of quantum phase transitions in rotating nuclei involves the interplay between static and dynamic properties. This interplay determines the type of shape – phase transitions in rotating nuclei. It also elucidates the behavior of low – lying excitations specifically related to the shape transitions at high spins. We have also analyzed the shapes of hot rotating nuclei and the intention is to find out how the deformation varies with temperature and angular momentum.

In this work, thus special attention is paid to the influence of pairing on the low-temperature behavior of the specific heat, nuclear level density parameter,

excitation energy, entropy and pairing gap for $^{161,162}\text{Dy}$ and $^{171,172}\text{Yb}$ nuclei within the superconducting BCS model.

6.3 Formalism

The physical quantity of heat capacity is calculated by using the following relation

$$C_{pair} = T dS_{pair}/dT. \quad (6.1)$$

In order to study the clearest picture of phase transition, the partition function is also calculated without incorporating pairing correlation and heat capacity is defined by,

$$C = T dS/dT. \quad (6.2)$$

Further, the influence of pairing on level density parameter (a_{pair}) with pairing correlation is defined with the following equations:

$$a_{pair} = \frac{S_{pair}^2}{4E_{pair}^*}, \quad (6.3)$$

where, S_{pair} is entropy and E_{pair}^* is the excitation energy of the system. The entropy and excitation energy are calculated using the statistical formalism with pairing correlation given in chapter II.

6.4 Results and discussion

The influence of pairing in the atomic nucleus is studied by employing statistical theory of hot rotating nuclei under extreme temperature for the isotopes $^{161, 162}\text{Dy}$ and $^{171, 172}\text{Yb}$. Due to the particle number fluctuation and quasiparticle parity mixing, the BCS theory is not well suited to describe pairing effects in hot nuclei. An alternative method to overcome these drawbacks is to use the particle number projected BCS approximation extended to finite temperature. The statistical properties of pairing interaction are investigated in the framework of FT-BCS approximation. The variation of the pairing correlations with the temperature is characterized by the pairing gap. The pairing gap as a function of temperature shows

that at a critical temperature T_c the pairgap vanishes and the fermion system predicts a sharp second – order transition from superfluid to normal fluid. The sharp transition predicted by FT-BCS is connected to the breaking of particle number conservation.

In principle the effect of pairing correlations can be studied with any energy as to preserve the amount of pairing correlations, however this cannot be applied for too large energy windows because the number of excited states which can be built on from the single particle levels becomes too large to be handled in calculation. The thermal quantities such as level density parameter, excitation energy, entropy and heat capacity has been calculated for the above mentioned isotopes and it is compared with the thermal parameters calculated without the inclusion of pairing correlations. The results show a considerable effect of pairing phenomenon in the thermal quantities. The S – shape heat capacity as a function of temperature is considered as an indication of phase transition in the nucleus. The results are compared with the available experimental data and other available theoretical data.

Figure 6.1 illustrates the pairing gap (Δ) as a function of temperature (T) for ^{161}Dy and ^{162}Dy . It is observed that the pairing gap vanishes at a critical temperature $T_c \approx 0.6$ MeV for ^{161}Dy and ^{162}Dy . As mentioned earlier the critical temperature at which the pairgap vanishes is the occurrence of phase transition of the nuclear system from superfluid to normal phase.

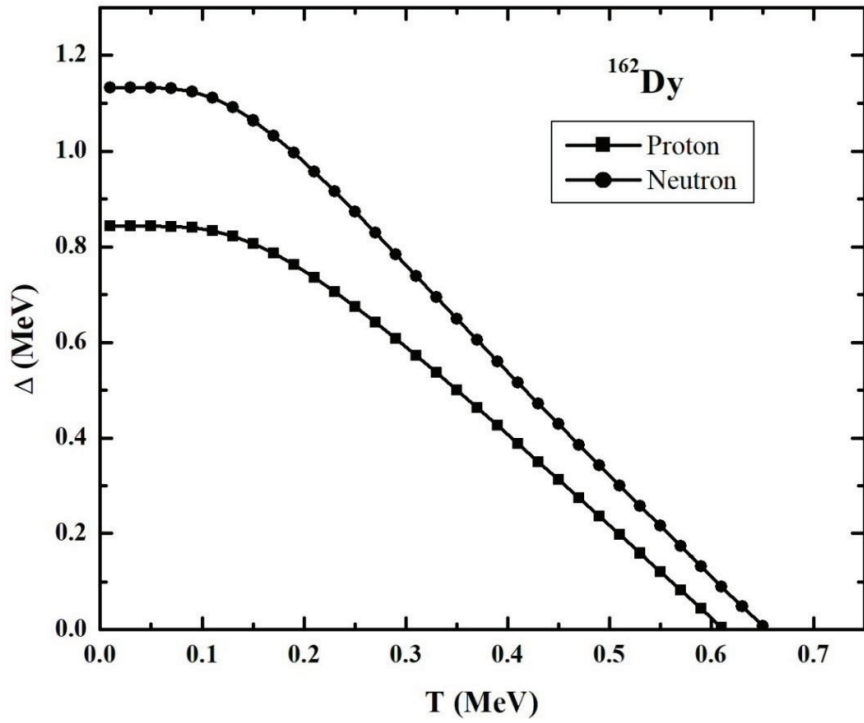
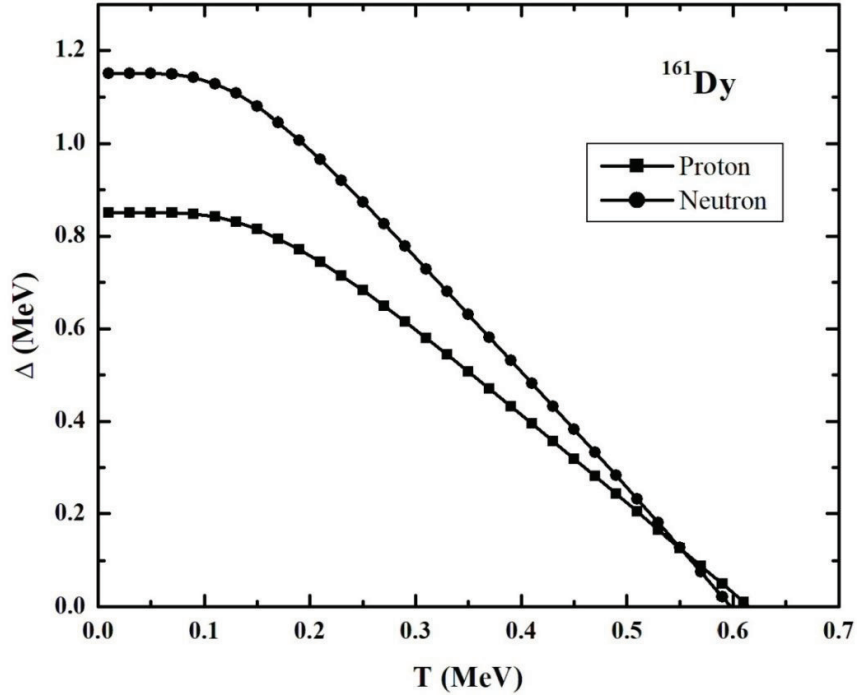


Fig. 6.1: Pairing gap Δ (MeV) as a function of temperature T (MeV) for (a) ^{161}Dy and (b) ^{162}Dy isotopes.

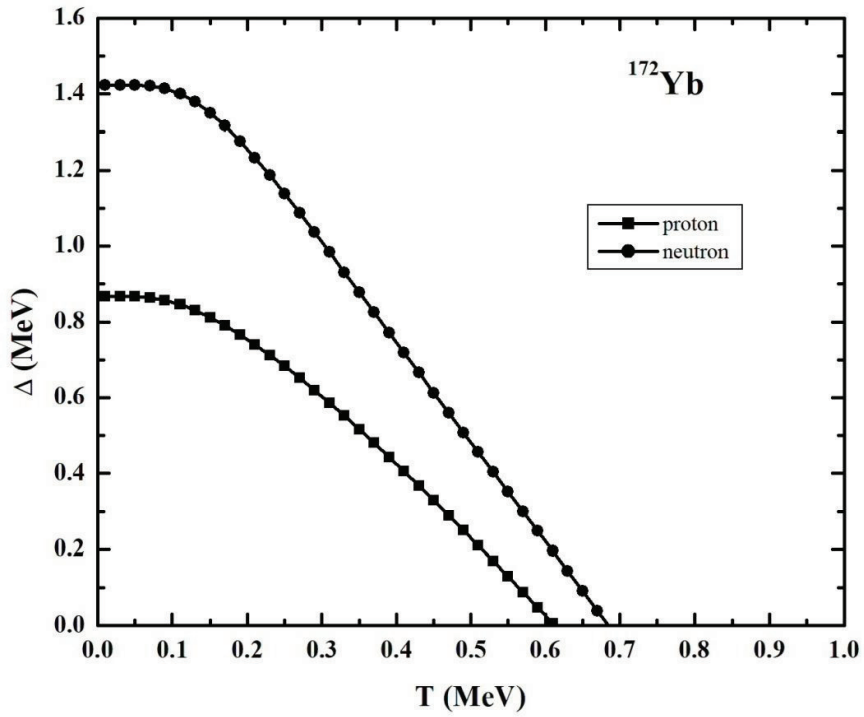
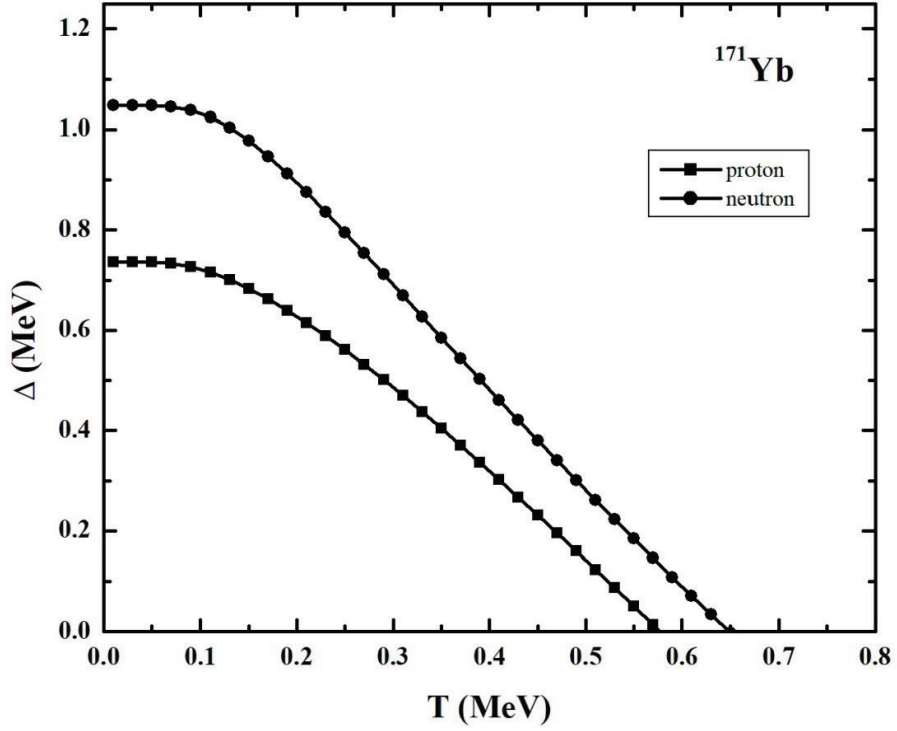


Fig. 6.2: Pairing gap Δ (MeV) as a function of temperature T (MeV) for (a) ^{171}Yb and (b) ^{172}Yb isotopes.

Table 6.1 : Neutron and Proton pairgap as a function of temperature for ^{161}Dy , ^{162}Dy , ^{171}Yb and ^{172}Yb .

T (MeV)	Pairing Gap (Δ) (MeV)											
	^{161}Dy		^{162}Dy		^{171}Yb		^{172}Yb					
	Δ_N	Δ_P	Δ_N	Δ_P	Δ_N	Δ_P	Δ_N	Δ_P				
0.01	0.85139	1.15075	0.84361	1.1324	0.73642	1.04700	0.86762	1.42304				
0.05	0.85136	1.15057	0.84358	1.13221	0.73610	1.04679	0.86762	1.42304				
0.10	0.84167	1.12837	0.83385	1.11058	0.71584	1.02405	0.84558	1.39966				
0.15	0.81481	1.07946	0.80697	1.06425	0.68313	0.97780	0.81106	1.35011				
0.20	0.74376	0.96517	0.73599	0.95761	0.61531	0.87508	0.74002	1.23328				
0.25	0.68267	0.87413	0.67503	0.87317	0.5610	0.79518	0.68299	1.13812				
0.30	0.57985	0.72914	0.57248	0.73939	0.46985	0.66958	0.58645	0.98363				
0.35	0.50716	0.63066	0.50000	0.64935	0.40450	0.58541	0.51653	0.87766				
0.40	0.39504	0.48235	0.38819	0.51594	0.30196	0.46114	0.40571	0.71839				
0.45	0.31915	0.38294	0.31251	0.42863	0.23152	0.38016	0.32886	0.61293				
0.50	0.20433	0.23168	0.19800	0.30007	0.12369	0.26166	0.21023	0.45604				
0.55	0.12728	0.12825	0.12116	0.21571	0.05067	0.18453	0.12930	0.35203				
0.60	0.01105	-0.03311	0.00522	0.09064	-0.06023	0.07138	0.00553	0.19611				
0.65	-0.6692	-0.14635	-0.07255	0.00792	-0.135	-0.00251	-0.07844	0.09171				

The pairing gap is almost constant below $T \approx 0.2$ MeV and above $T \approx 0.2$ MeV, the neutron and proton pairing gap calculated decreases smoothly with the temperature, while it does not vanish up to 0.6 MeV. This indicates a gradual pairing transition from the superfluid state to the normal state in the hot nucleus. The drop of the pairing gap results in an increasing number of the Cooper-pair-broken excited states, and thus a rapid increase of the heat capacity. In this way, the S shape of heat capacity curves shown in fig.6.9 and fig.6.10 is provided by the competition between the effects from temperature and pairing correlations.

The thermodynamic properties of hot nuclei are convenient to study in terms of excitation energies. The excitation energies (E_{pair}^*) defined in Eq. (2.24) for $^{161, 162}\text{Dy}$ and $^{171, 172}\text{Yb}$ calculated with (dashed line) and without (solid line) pairing correlations as functions of the temperature are shown in fig.6.3 and fig.6.4, which exhibits directly the correspondence between the temperature and the excitation energy. From the fig.6.2 and 6.4 it is observed that the excitation energy with the inclusion of pairing correlation shows a higher value compared to the excitation energy calculated without incorporating pairing phenomenon.

The sensitivity of thermodynamic quantities such as entropy S , level density parameter a and specific heat C_V with and without pairing correlations are studied for $^{161, 162}\text{Dy}$ and $^{171, 172}\text{Yb}$. The quantities such as entropy and specific heat are the first and second derivatives of the free energy F with respect to the temperature, and thus sensitive to thermal changes of the ground state.

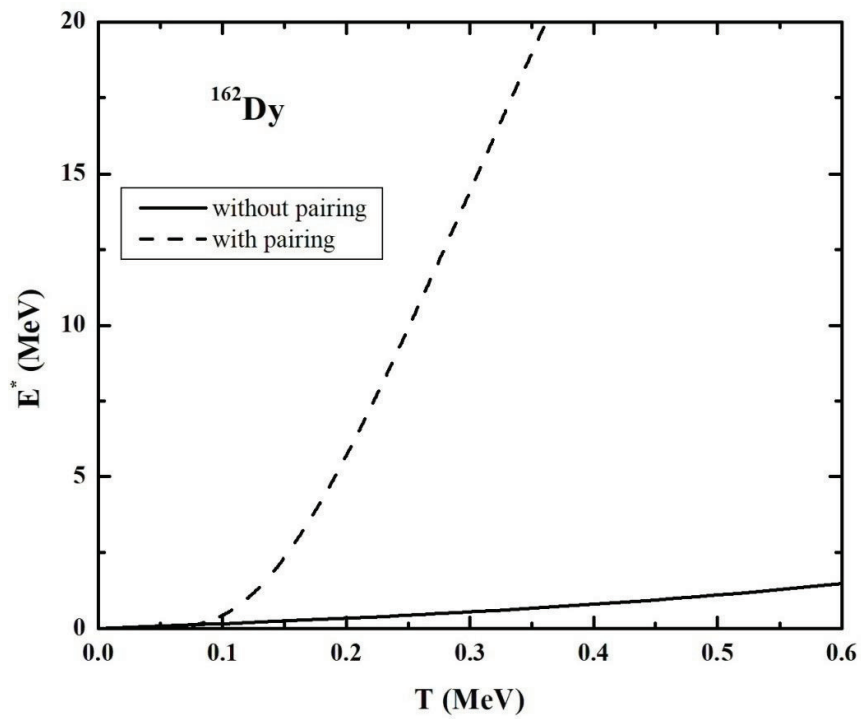
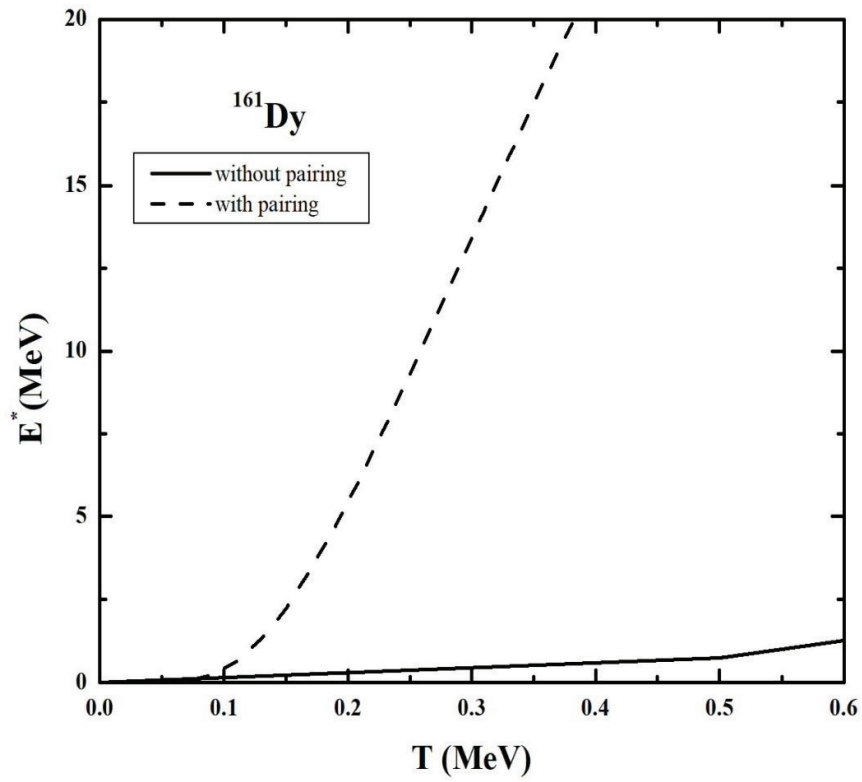


Fig.6.3: Excitation energy E^* (MeV) as a function of temperature with inclusion of pairing and without pairing for (a) ^{161}Dy and (b) ^{162}Dy isotopes.

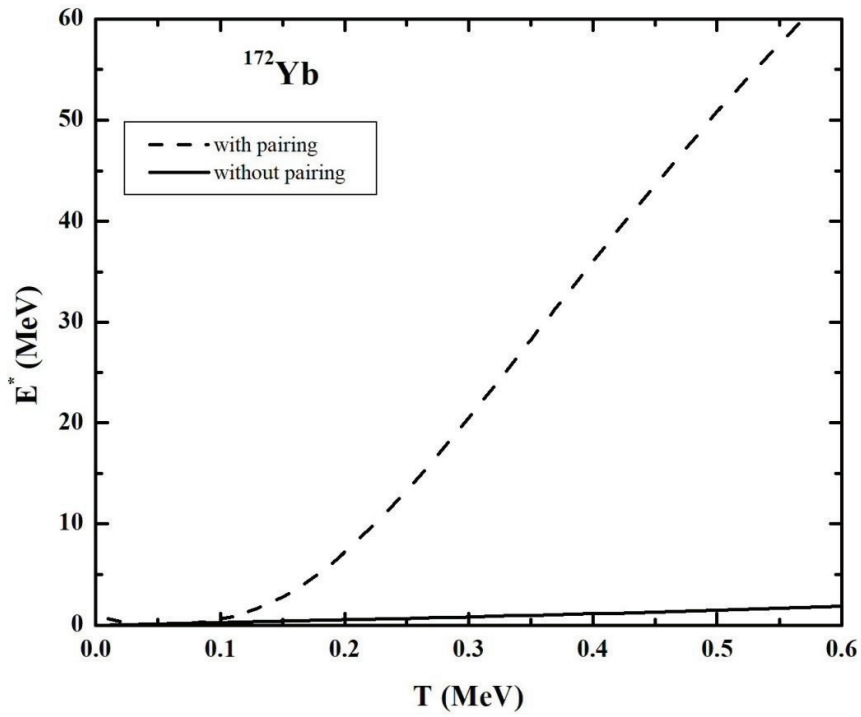
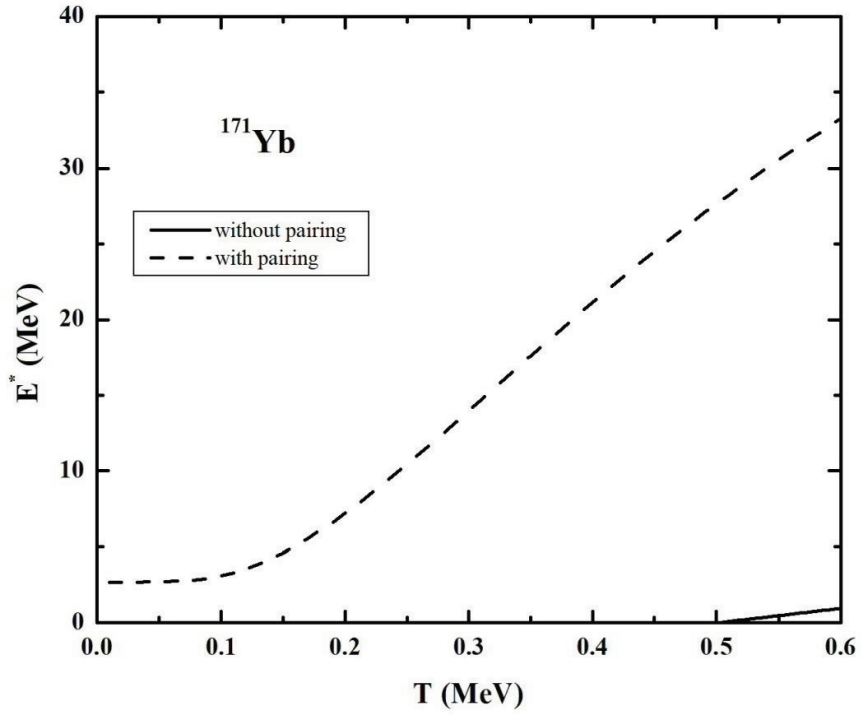


Fig.6.4: Excitation energy E^* (MeV) as a function of temperature with inclusion of pairing and without pairing for (a) ^{171}Yb and (b) ^{172}Yb isotopes.

In fig.6.5 and fig.6.6 are shown the entropy S as functions of the temperature calculated by the finite temperature BCS formalism. The entropy calculated with the pairing correlations is compared with the entropy calculated without the inclusion of pairing correlations. At low temperature, if the pairing effects are ignored it leads to larger single particle level spacing on the average, presents smaller entropy (dashed black line). At low temperature, without pairing correlations, the entropy is largely determined by the few states around the Fermi energy, and the number of the involved states is essentially determined by the detailed single particle spectrum therefore leading to increase in entropy as shown in fig.6.5 and fig.6.6 (solid black line). Both temperature and pairing correlations can disperse the particle over the states beyond the Fermi level.

As the temperature increases, and as the pairing correlations are enhanced, more single particle states will get involved to contribute to the entropy. As expected, the effect of the pairing correlations is clearly visible below the critical temperature ($T_C \approx 0.6$ MeV), inducing a strong reduction of the entropy calculated without the inclusion of pairing correlation. Figure 6.5 and 6.6 gives a comparison of entropy (S) as a function of temperature including and excluding the pairing phenomenon. From the fig.6.5 it is observed that the entropy of an unpaired fermion system shows a linear increase with temperature whereas the paired system shows an abrupt increase in entropy. The level density parameter (a) as a function of temperature in fig. 6.4 also indicates the impact of pairing at a low temperature region.

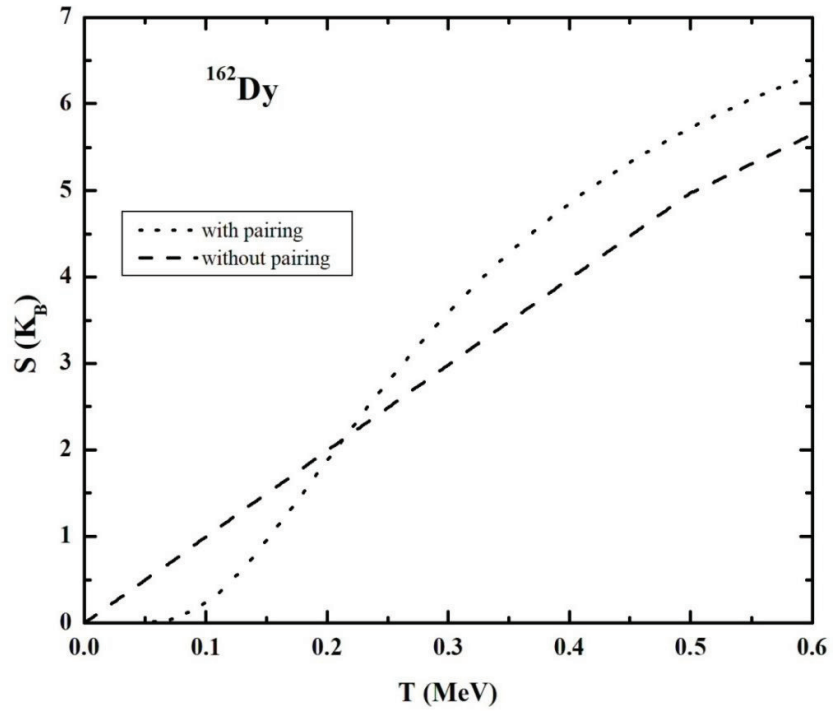
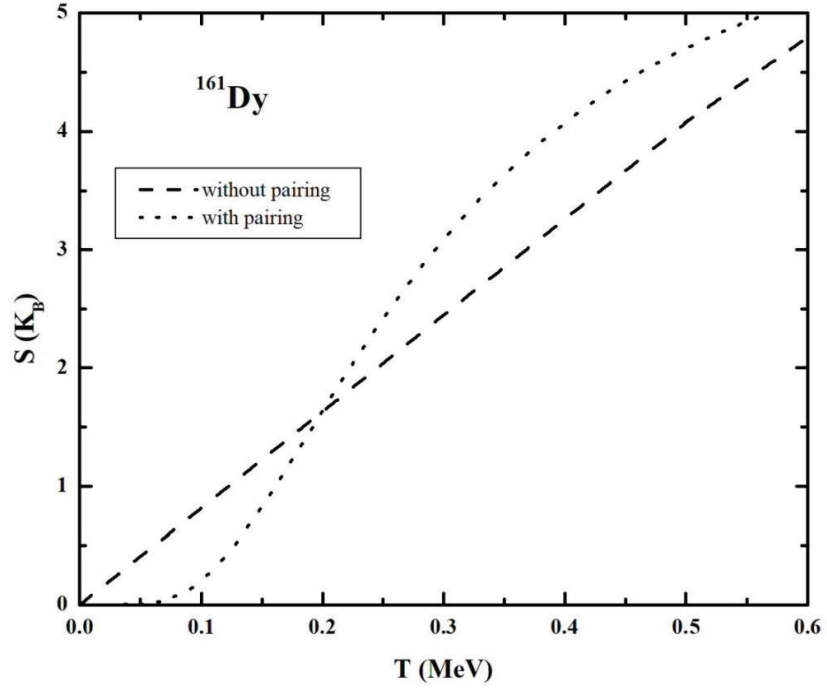


Fig.6.5: Entropy (S) as a function of temperature T (MeV) with inclusion of pairing and without pairing for (a) ^{161}Dy and (b) ^{162}Dy isotopes.

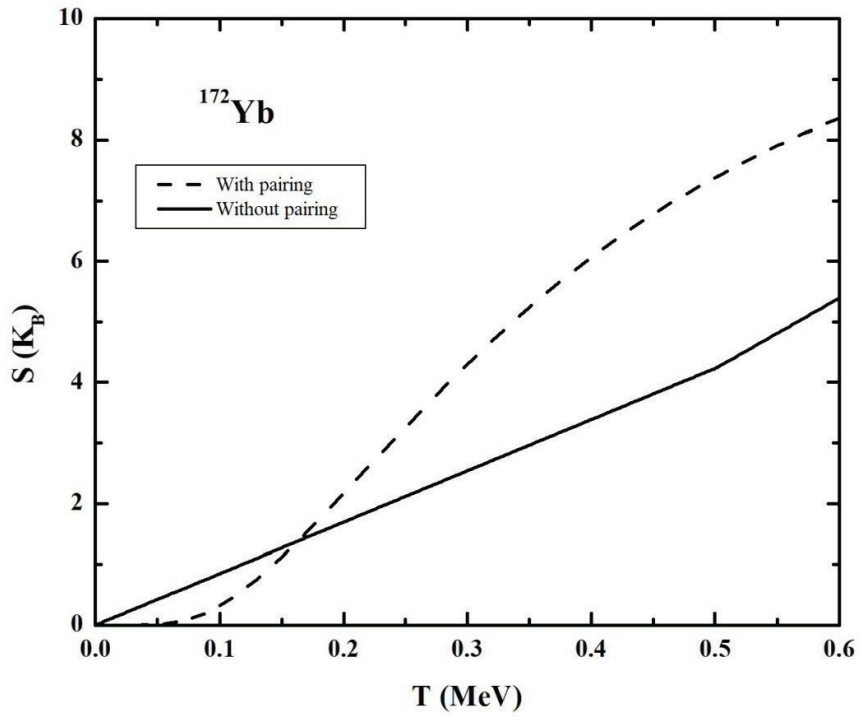
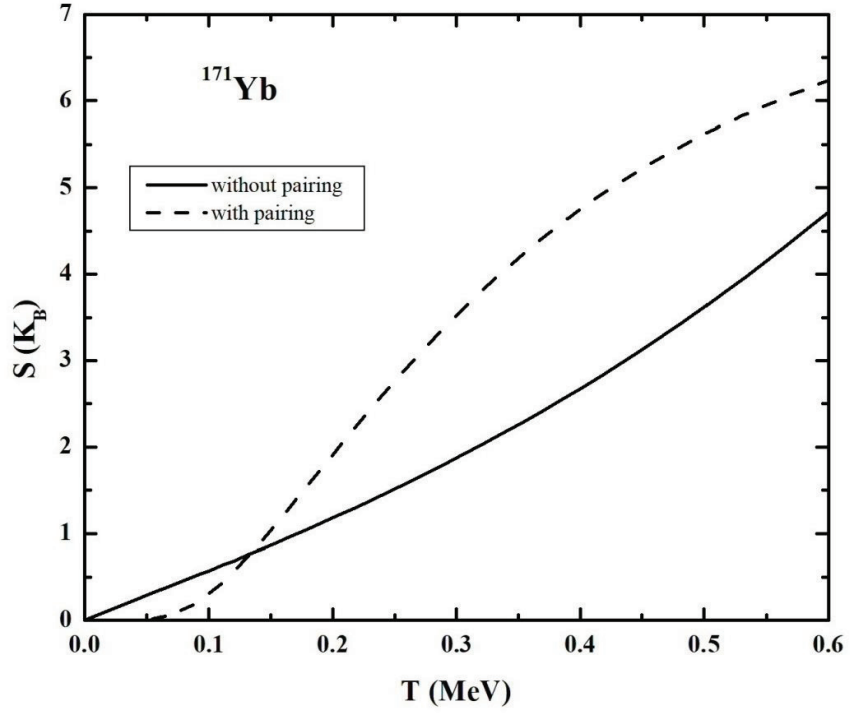


Fig.6.6: Entropy (S) as a function of temperature with inclusion of pairing and without pairing for (a) ^{171}Yb and (b) ^{172}Yb isotopes.

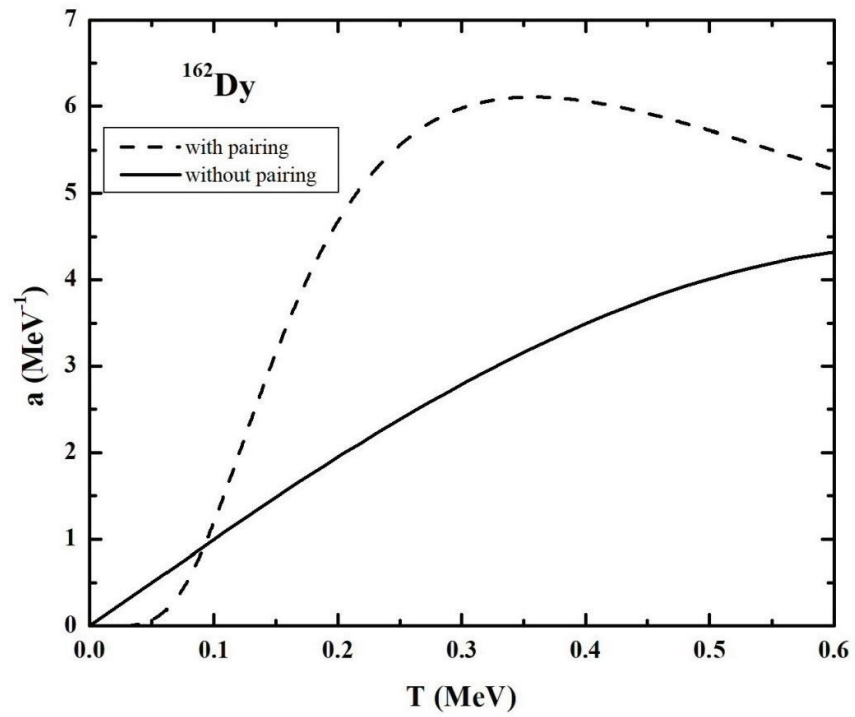
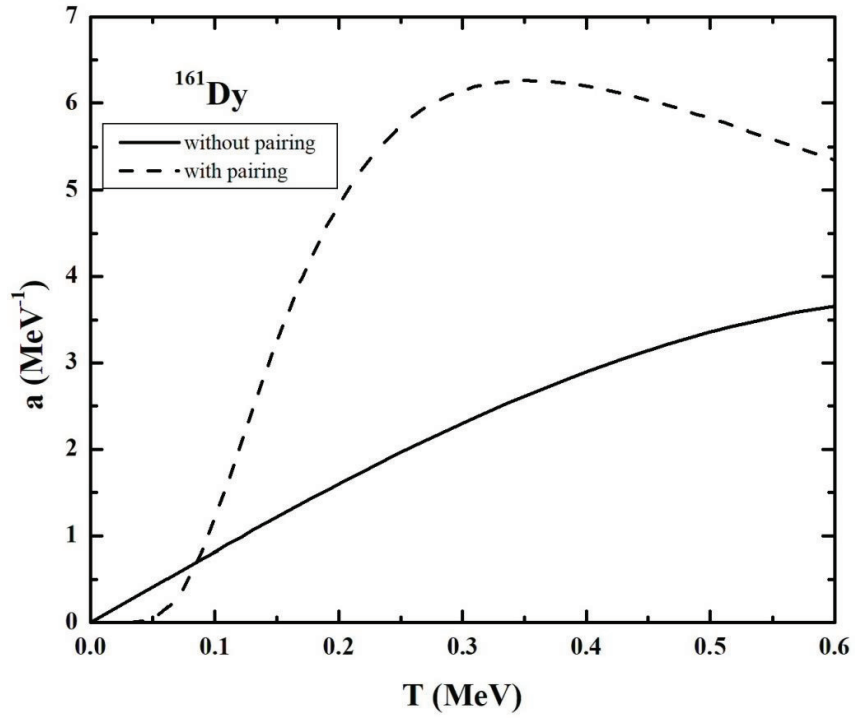


Fig.6.7: Level density parameter a (MeV^{-1}) as a function of temperature T (MeV) with inclusion of pairing and without pairing for (a) ^{161}Dy and (b) ^{162}Dy isotopes.

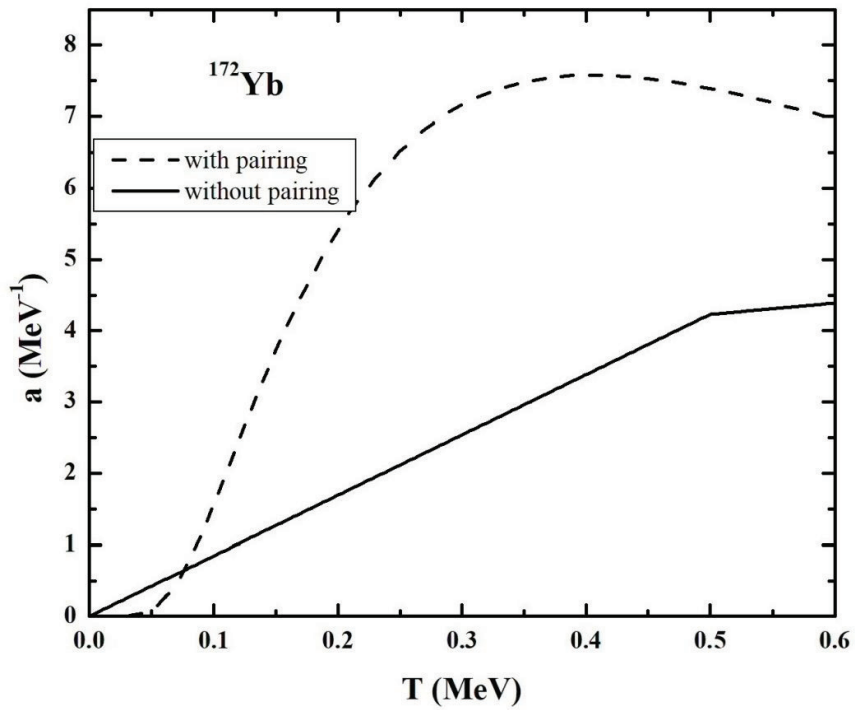
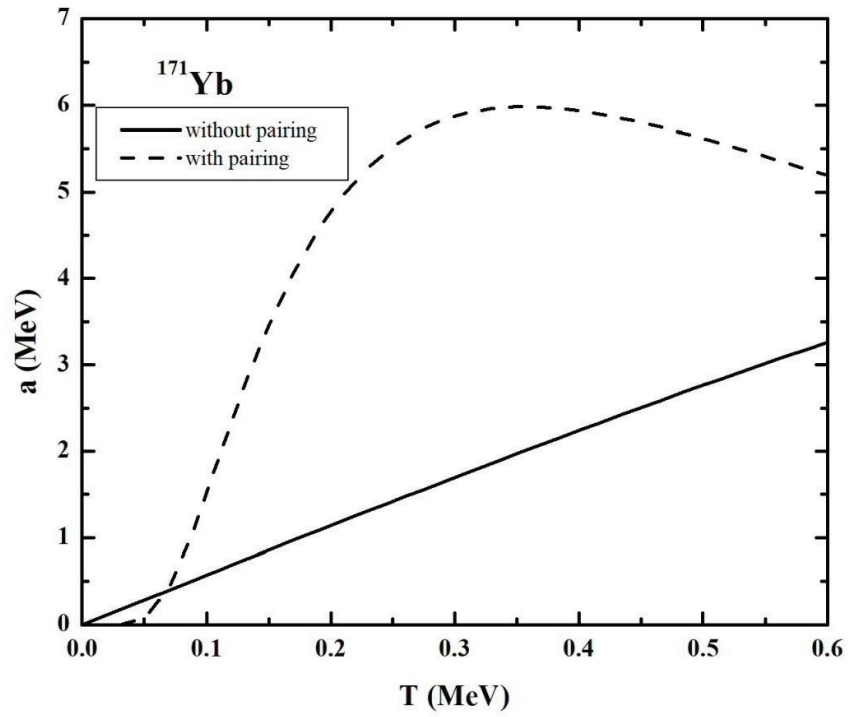


Fig.6.8: Level density parameter a (MeV^{-1}) as a function of temperature T (MeV) with inclusion of pairing and without pairing for (a) ^{171}Yb and (b) ^{172}Yb isotopes.

Figure 6.9 indicates the specific heat capacity (C_V) as a function of temperature for ^{161}Dy and ^{162}Dy . The observed S – shape heat capacity curve is found to be an indication of the occurrence of phase transition from superfluid to normalfluid system. The observed S-shape heat capacity C_V is found to be a remarkable signature of phase transition and it is found to occur around the critical temperature $T_C = 0.6$ MeV. The heat capacity without the inclusion of pairing correlation is found to have a linear increase as a function of temperature. In the absence of pairing, there is no notable change or peak in the specific heat which means it exhibits a very gradual spherical to deformed transition.

The nonlinearity of the specific heat around T_C might be related to shell effects. The results thus clearly show that the pairing correlations contribute to the S-shaped behavior of the specific heat in thermally excited nuclei. A realistic description of the smooth S-shaped behavior in finite nuclei requires a more elaborated model including particle number projection. It is shown that the smooth S-shaped behavior may be even washed out in some rare-earth nuclei [Danilo 2013]. The predictions for the critical temperature, associated to the discontinuity in the specific heat of fig.6.9 and fig.6.10, vary among the models to a much larger extent since this phenomenon is strongly related to the position of resonance states in the continuum, we expect to observe deviations among models predicting different positions of these states.

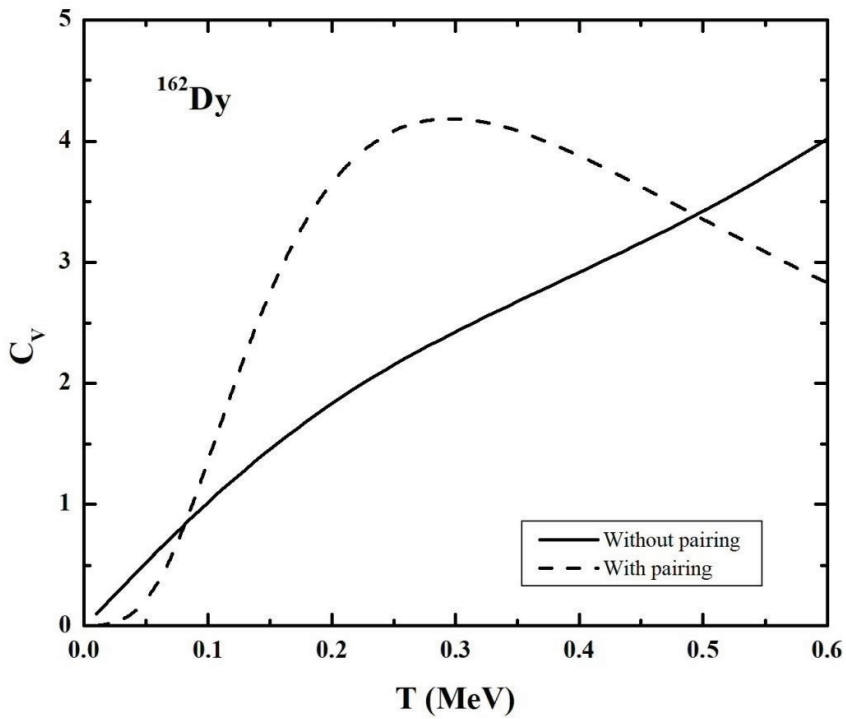
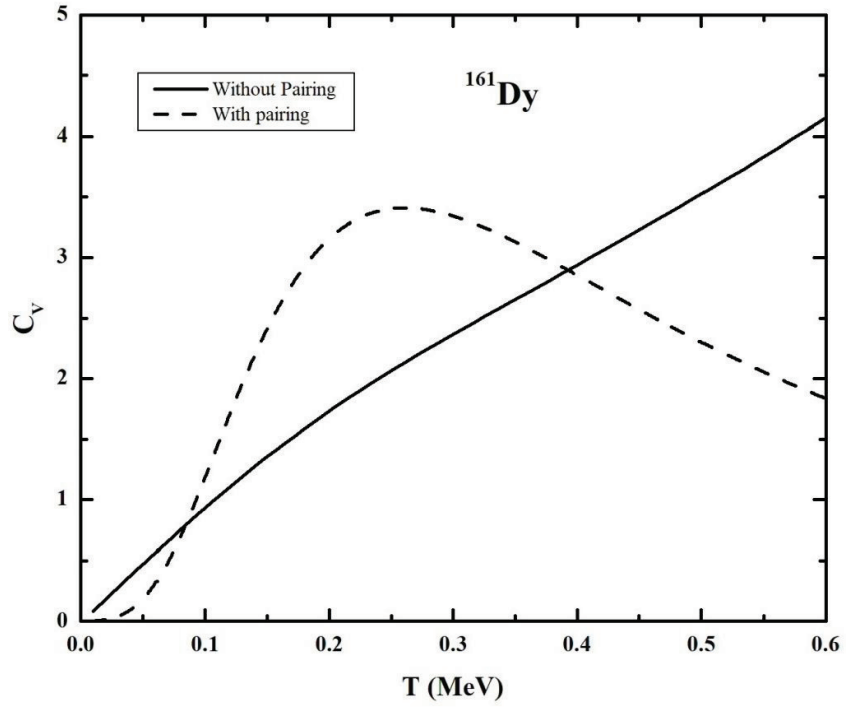


Fig.6.9: S-shape heat capacity (C_V) as a function of temperature T (MeV) with inclusion of pairing and without pairing for (a) ^{161}Dy and (b) ^{162}Dy isotopes.

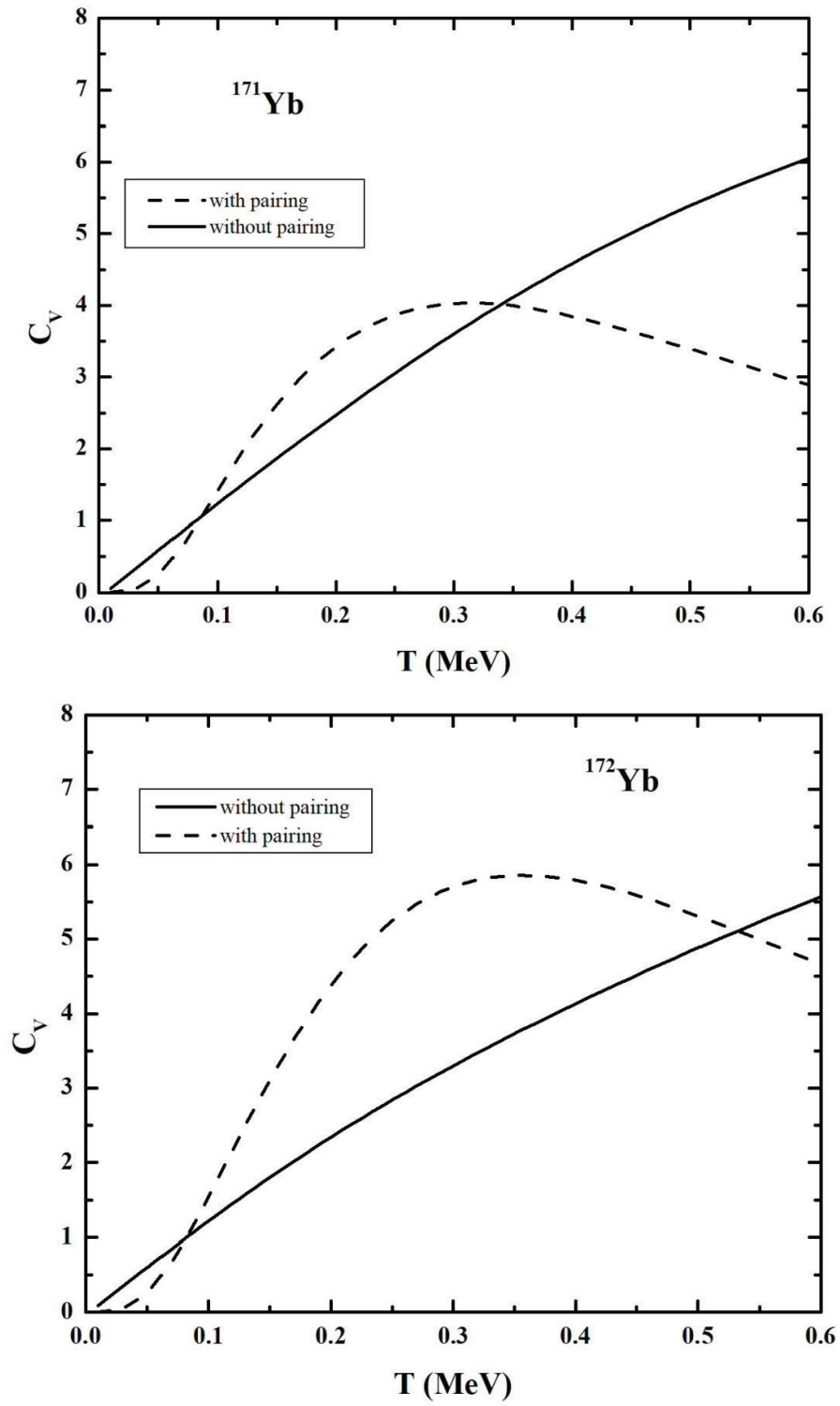


Fig.6.10: S-shape heat capacity (C_V) as a function of temperature T (MeV) with inclusion of pairing and without pairing for (a) ^{171}Yb and (b) ^{172}Yb isotopes.

Figure 6.10 indicates the specific heat capacity (C_V) as a function of temperature for ^{171}Yb and ^{172}Yb . The observed S – shape heat capacity curve is found to be an indication of the occurrence of phase transition from superfluid to normalfluid system. The observed S- shape heat capacity C_V is found to be a remarkable signature of phase transition and it is found to occur around the critical temperature $T_C = 0.7$ MeV. The heat capacity without the inclusion of pairing correlation is found to have a linear increase as a function of temperature. In the absence of pairing, there is no notable change or peak in the specific heat which means it exhibits a very gradual spherical to deformed transition.

6.5 Conclusion

The calculations performed using STHR method was able to predict the pairing phase transition from superfluid to normal and the pairing gap vanishes around a critical temperature (T_c) = 0.6 MeV for angular momentum $M = 0\hbar$. Role of pairing has significant effects on the evaluated thermodynamical parameters at a low temperature region. The thermodynamical parameter that are evaluated without incorporating pairing correlation shows a linear response for increasing temperature while from pairing correlation they show a pronounceable change due to the presence of pairing. The impact of pairing correlation is observed only in low temperature region i.e., for $T < 1$ MeV.

CHAPTER VII

SUMMARY AND CONCLUSION

The shape-phase transition and shape evolution in hot rotating nuclei are studied using the statistical model incorporating deformation, collective and non-collective rotational degrees of freedom and shell effects.

Nuclei in the region $110 \leq A \leq 142$ have been investigated which involve shape changes associated with temperature and angular momentum. The nuclear properties that are studied in detail are nuclear level density, level density parameter, spin cut-off parameter, kinematic and dynamic moments of inertia, single neutron and single proton separation energies, excitation energy and so on. Excitation energies calculated for Te were compared with experimental values and shell model values. Excitation energy calculated from statistical model agreed with the experimental values at higher angular momenta. The same behavior was also shown by ^{74}Se nuclei whose excitation energy calculated matched closely with the available experimental data. The shape of the nuclei ^{110}Te , ^{114}Te , ^{116}Te , ^{122}Te , ^{124}Te and ^{130}Te are found to change from spherical to oblate non-collective. The spin cut-off parameter values are found to increase sharply at $6\hbar$ and $8\hbar$ respectively for ^{70}Se and ^{74}Se which shows the shape transition from spherical to non-collective oblate.

The calculations were performed for rare earth nuclei such as ^{141}Ce , ^{142}Ce , ^{141}Ba , ^{142}Ba , ^{141}Xe , ^{142}Xe , ^{145}Nd , ^{146}Nd , ^{150}Sm and ^{151}Sm . The theoretical discussions, reveals that the occurrence of bump in the specific heat might be due to a nuclear structure effect leading to a phase transition. As expected at large temperatures, the pairing correlations are found to be ineffective and the difference between even – even and odd – even system is becoming very small. It is thus shown that the pairing correlations have a significant influence on the specific heat, especially for

temperatures below $T = 1$ MeV. The appearance of hump in the specific heat capacity at low temperature is also influenced by the low – lying collective states. There is a general tendency for all the nuclei to exhibit a abrupt change in the specific heat beyond temperature $T = 1$ MeV. These specific heat fluctuations occur at different temperatures for different nuclei. It is also noted that the occurrence of the peak in the specific heat at low temperature is a contribution of the ground state rotational band which is associated with a superfluid to normal phase transition. The occurrence of phase transition is predicted in three rare nuclei along with their isotopes such as $^{141, 142}\text{Ce}$, $^{145, 146}\text{Nd}$ and $^{150, 151}\text{Sm}$. The results of our calculations on specific heat capacity shows a predominant appearance of a hump in the low temperature region which is considered as the suppression of pairing correlation and it is an indication of phase transition. It is also noted that the occurrence of the peak in the specific heat at low temperature is a contribution of the ground state rotational band.

REFERENCES

- 1) Agarwal B.K, Tapas Sil, De J.N & Samaddar S.K, 2000, 'Nuclear shape transition at finite temperature in a relativistic mean field approach', Physical Review C, Vol. 62, No.044307, pp. 1-16.
- 2) Agarwal B.K, Tapas Sil, Sumaddar S.K & De J.N, 2001, 'Temperature induced shell effects in deformed nuclei', Physical Review C, Vol. 64, No. 017304, pp. 1-6.
- 3) Agrawal B. K, Samaddar S. K, Ansari A & De J. N, 1999, 'Influence of pairing correlations on the excitation energy, angular momentum, and parity dependence of nuclear level densities', Physical Review C, Vol.59, No.6, pp. 3109-3115.
- 4) Algin E, Agvaanluvsan U, Guttormsen M, Larsen A.C, Mitchell G.E, Rekstad J, Schiller A, Siem S & Voinov A, 2008, 'Thermodynamic properties of $^{56,57}\text{Fe}$ ', Physics Review C, Vol. 78, No. 054321, pp.1-23.
- 5) Alhassid Y, 1994, 'The Giant Dipole Resonance in Hot Rotating Nuclei', Nuclear Physics A, Vol. 569, No.1-2, pp. 37-50.
- 6) Alhassid Y, Bertsch G. F, Liu S & Nakada H, 2000, 'Parity dependence of Nuclear level densities', Physical Review Letters, Vol.84, No.19, pp.4313 – 4316.
- 7) Alhassid Y, Bush B & Levit S, 1988, 'Thermal Shape Fluctuations, Landau Theory, and Giant Dipole Resonances in Hot Rotating Nuclei', Physical Review Letters, Vol.61, No.17, pp.1926-1929.
- 8) Alhassid Y, G.F. Bertsch & L. Fang, 2003, 'Nuclear level statistics: Extending shell model theory to higher temperatures', Physical Review C, vol.68, No.044322, pp.1 -11.

- 9) Alhassid Y, Levit S & Zingman J, 1986, 'Universal features of shape transitions in hot rotating nuclei', *Physics Review Letter*, Vol. 57, No. 5, pp.539 – 542.
- 10) Andersson C.G, Bengtsson R, Bengtsson T, Krumlinde J, Leander G, Neergard K, Olenders P, Pinsto J.A, Ragnarrson I, Szymanski Z & Aberg S, 1981, 'Survey of Collective and Single-Particle Features in the Yrast Domain of the $A \sim 150$ Nuclei', *Physica Scripta*, Vol. 24, No.1B, pp.266-282.
- 11) Andersson G, Larsson S.E, Leander G, Moller P, Nilsson S.G, Ragnarrson I, Aberg S, Bengtsson R, Dudek J, Nerlo-Pomorska B, Pomorski K & Szymanski Z, 1976, 'Nuclear shell structure at very high angular momentum', *Nuclear Physics A*, Vol.268, No. 2, pp. 205-256.
- 12) Ansari A, 1976, *Frontiers of Nuclear Structure Physics* (Indian Physics Association) edited by B. K. Jam, pp.110.
- 13) Arunachalam N, Alli Periyanyaki P & Illangovan K, 1996, 'Structural properties of hot rotating ^{40}Ca ', *Physical Review C*, Vol. 55, No. 4, pp.1826-1831.
- 14) Bahri C, Rowe D.J & Wijesundera W, 'Phase transition in the pairing plus – quadrupole model', *Physical Review C*, Vol.58, No.3, pp.1539-1550.
- 15) Bardeen J, Cooper LN & Schrieffer JR, 1957, 'Theory of Superconductivity'. *Physical Review*, Vol.108, No.108, pp.1175 - 1203.
- 16) Barranco F, Bortignon P.F, Broglia R.A, Colo G & Vigezzi E, 2001, 'The halo of the exotic nucleus ^{11}Li : a single cooper pair', *European Physics Journal A*, Vol.11, No.4, pp.385-392.
- 17) Bartel J & Quentin P, 1985, 'Fission barriers of excited nuclei', *Physics Letters B*, Vol.152, No.1-2, pp.29 – 34.

- 18) Behkami A.N & Kargar Z, 1992, 'Nuclear level densities and spin cut-off factors deduced from microscopic theory for nuclei from ^{20}F to ^{244}Am ', Journal of Physics G: Nuclear and Particle Physics, Vol.18, No.6, pp.1023-1037.
- 19) Behkami A.N, Kargar Z & Nasrabadi N, 2002, 'Level density parameter study using a microscopic model', Physical Review C, Vol.66, No.064307, pp.1-6.
- 20) Behkami, A.N & Soltani, M, 2005, 'Spin Cut-off Parameter of Nuclear Level Density and Effective Moment of Inertia', Communications in Theoretical Physics, Vol. 43, pp. 709-719.
- 21) Belyaev S.T, 1965, 'Time dependent self consistent field and collective nuclear Hamiltonian', Nuclear Physics, Vol.64, No.1, pp.17-54.
- 22) Bengtsson B, Larsson S.E, Leander G, Moller P, Aberg S, Nilsson S.G and Szymanski A, 1975, 'Yrast bands and high-spin potential-energy surface', Physics Letter, Vol.57, No.4, pp. 301-305.
- 23) Bengtsson R Moller P, Nix J.R & Jing-ye Zhang, 1984, 'Nuclear Shapes and Shape Transitions', Physica Scripta, Vol. 29, No.5, pp. 402-430.
- 24) Bernstein L.A, Hughes J.R, Becker J.A, Farrdis L.P, Henry E.A, Asztablos S.J, Cederwall B, Clark R.M, Deleplangue M.A, Diamond R.M, Faloon P, Lee I.Y, Macchiavelli A.O, Stephens F.S, Cizewski J.A & Younes W, 1995, 'Superdeformation in ^{154}Er ', Physical Review C, Vol. 52, No.3, pp.R1171 – R1174.
- 25) Bethe H.A, 1936, 'An Attempt to Calculate the Number of Energy Levels of a Heavy Nucleus', Physical Review, Vol.50, No. 4, pp.332-341.
- 26) Bhaduri R.K & Van Dijk W, 1988, 'Nuclear specific heat and effective degrees of freedom', Nuclear Physics A, Vol. 485, No. 1, pp. 1-15.

- 27) Bhuyan M, Patra S.K & Raj K Gupta, 2011, 'Relativistic mean-field study of the properties of $Z=117$ nuclei and the decay chains of the $^{293,294}117$ isotopes', *Physical Review C*, Vol. 84, No. 014317, pp. 1-6.
- 28) Blatt J.M & Weisskopf V. F, 1979, *Theoretical Nuclear Physics*, Springer, NewYork, First Edition.
- 29) Bohr A & Mottelson B.R, 1975, 'The structure of angular momentum in rapidly rotating nuclei', *Nuclear Physics A*, Vol. 354, No.1-2, pp. 303-316.
- 30) Bohr A, Mottelson B.R & Pines D, 1958, 'Possible analogy between the excitation spectra of nuclei and those of the superconducting metallic state', *Physical Review*, Vol. 110, No. 4, pp. 936-938.
- 31) Boomadevi N, Dhivya Saranya J, Selvaraj S & Rajasekaran T.R, 2014, 'Nuclear Specific heat and Phase Transition in Finite Nuclear Systems', *Acta Physica Polonica B*, Vol.45, No.5, pp.989 - 1013.
- 32) Bromley, D.A, 1985, 'Treatise on Heavy-Ion Science, Compound System Phenomena', Plenum, New York, Vol. 3, pp. 313.
- 33) Brookhaven National Nuclear Data Center, <<http://www.nndc.bnl.gov>>
- 34) Castanos O, Frank A, & Federman P, 1979, 'The shape transition in the Sm isotopes and the structure of the IBA Hamiltonian', *Physical Letters B*, Vol. 88, No. 3-4, pp. 203-206.
- 35) Cerny, J, 1974, *Nuclear Spectroscopy and Reactions*, Vol. 1-3 (Academic Press, NewYork.)
- 36) Chakraborty D.R, Datar V.M, Suresh Kumar, MishraG, Mirgule E.T, Mitra A, Rout P.C, Nanal V, Deepak Pandit, Mukhopadhyay S & Srijit Bhattacharya, 2012, 'Exclusive giant dipole resonance measurement on the Jacobi transition in the $^{19}\text{F}+^{27}\text{Al}$ system', *Physical Review C*, Vol. 85, No. 044619, pp. 1-10.

- 37) Chomaz Ph, Gulminelli F, 2005, 'Phase transition in small system', Proceedings of the 18th Nuclear Physics Division Conference of the EPS – (NPDC18), Nuclear Physics A, Vol. 749, pp.3-13.
- 38) Civitarese O & De Paoli A.L, 1985, 'The nuclear level-density parameter and temperature-dependent effects in finite nuclei', Nuclear Physics A, Vol. 440, No. 3, pp. 480-492.
- 39) Civitarese O, Dumrauf A.G & Reboiro M, 1990, 'Renormalized particle-particle and particle-hole random-phase approximation correlations at finite temperature: Effects upon the nuclear level density parameter', Physical Review C, Vol.41, No.4, pp. 1785-1791.
- 40) Civitarese O, Dussel G.G & Perazzo R.P.J, 1983, 'Thermal aspects of the pairing correlations in finite nuclei', Nuclear Physics A, Vol. 404, No.1, pp.15-28.
- 41) Civitarese O, Peter O. Hess & Jorge G. Hirsch, 1989, 'Low temperature S – shaped heat capacities in finite nuclei', Rev. Mex. Fis, Vol. 40, No.4, pp.406 – 411.
- 42) Cohen S, Plasil F & Swiatecki W. J, 1979, 'Equilibrium configurations of rotating charged or gravitating liquid masses with surface tension – II', Annals of Physics, Vol.82, No.2, pp.557 - 596.
- 43) Cole B.J, Quick R.M & Miller H.G, 1989, 'Shape of ²⁴Mg at zero and finite temperature', Physical Review C, Vol. 40, No.1, pp. 456-458.
- 44) Cooper Leon N, 1956, 'Bound Electron Pairs in a Degenerate Fermi Gas, Physical Review', Vol. 104 , No. 4, pp. 1189-1190.
- 45) Cranmer-Gordon H.W, Forsyth P.D, Elenkov D.V, Howe D, Sharpey-Schafer J.F, Riley M.A, Sletten G, Simpson J, Ragnarsson I, Xing Z & Bengtsson T,

- 1987, 'Discrete levels in ^{154}Dy above spin 30h: Evidence for terminating band structures', Nuclear Physics A, Vol. 465, No. 3, pp. 506-528.
- 46) Danilo Gambacurta, Denis Lacroix & N. Sandulescu, 2013, 'Pairing and specific heat in hot nuclei', Physical Review C, Vol.88, No.034324, pp.1–9.
- 47) Dean DJ & Hjorth-Jensen M, 2003, 'Pairing in nuclear systems: from neutron stars to finite nuclei'. Reviews of Modern Physics, Vol.75, pp.607 - 656.
- 48) Dhivya Saranya J, Boomadevi N & Rajasekaran T.R, 2016, 'Particle entropy and depairing in hot nuclei'. International Journal of Modern Physics E, Vol.25, No.11, pp.1 - 10.
- 49) Dinh Dang N & Quang Hung N, 2008, 'Pairing within the self-consistent quasiparticle random-phase approximation at finite temperature', Physics Review C, Vol. 77, No.064315, pp.1-31.
- 50) Dukelsky J, Poves A & Retamosa J, 1991, 'Phase transitions in light nuclei' Phys. Rev. C, Vol.44, No.6, pp.2872 – 2874.
- 51) Egidio J.L, Ring P, Iwasaki S & Mang H.J, 1985, 'On the validity of the mean field approach for the description of pairing collapse in finite nuclei', Physics Letters B, Vol. 154, No.1, pp. 1-15.
- 52) Egidy T.V & Bucurescu D, 2005, 'Systematics of nuclear level density parameters', Physical Review C, Vol.72, No.044311, pp.1-22.
- 53) Eisenberg, J.M, Greiner, W, 1975, Nuclear Models, North-Holland, New York, pp.451.
- 54) Ericson Torleif, 1960, 'The statistical model and nuclear level densities', Advanced Physics, Vol. 9, No.36, pp.425-511.
- 55) Faber M, Poloszajctak M & Amand Faessler, 1979, 'Fission instability of nuclei at very high angular momenta', Nuclear Physics A, Vol. 326, No. 2, pp.129-160.

- 56) Faessler A, Hilton R.R & Sandhya Devi K.R, 1976, 'Microscopic determination of nuclear deformation energy surfaces at very high spins', *Physics Letters B*, Vol. 61, No. 2, pp.133-138.
- 57) Faessler A, Sandhya Devi K. R, Grumer F, Schmid K. W & Hilton R. R, 1976, 'Backbending: Coriolis antipairing or rotational alignment', *Nuclear Physics A*, Vol. 256, No. 1, pp.106-126.
- 58) Feynmann, R.P, 1972, *Statistical Mechanics*, Benjamin, Massachusetts, 1.
- 59) Fotiadis N, Cizewski J.A, Krucken R, Clark R.M, Fallon P, Lee I.Y, Macchiavelli A.O & Younes W, 2014, 'High-spin states in ^{124}Te ', *Physical Review C*, Vol. 89, No.017303, pp.1-4.
- 60) Fu Y, Mei H, Xiang J, Li Z. P, Yao J.M & Meng J, 2013, 'Beyond relativistic mean-field studies of low-lying states in neutron-deficient krypton isotopes', *Physical Review C*, Vol. 87, No.054305, pp. 1-9.
- 61) Gaardhoje, J. J, 1992, 'Nuclear Structure at high excitation energy studied with Giant Resonances', *Annual Review of Nuclear and Particle Science*, Vol. 42, pp.483-536.
- 62) Ginzburg V.L & Pitaevskii L.P, 1950, 'On the theory of Superconductivity', *Soviet Physics JETP*, Vol.34, No.5, pp.1064 -1082.
- 63) Goldenfeld, N, 1992, 'Lectures on Phase Transitions and Renormalization Group', Westview Press, USA, 1st Edition.
- 64) Goodman A.L, 1983, 'Landau-Ginzburg theory of phase transitions in heated rotating nuclei', *Nuclear Physics A*, Vol.406, No.1, pp. 94-108.
- 65) Goodman A.L, 1984, 'Statistical fluctuations in the $i_{13/2}$ model', *Physical Review C*, Vol. 29, No.5, pp.1887-1896.

- 66) Goodman A.L, 1989, 'Shapes and shape fluctuations in hot rotating ^{158}Yb nuclei', *Physical Review C*, Vol. 39, No.5, pp.2008-2017.
- 67) Goriely S, Hilaire S & Girod M, 2012, 'Latest development of the combinatorial model of nuclear level densities', *Journal of Physics: Conference Series*, Vol. 337, No.012027, pp. 1-3.
- 68) Gupta Y. K, Bency John, Biswas D.C, Nayak B.K, Saxena A & Choudhery R.K, 2008, 'Angular momentum dependence of the nuclear level-density parameter around $Z\sim 50$ ', *Physical Review C*, Vol. 78, No.054609, pp. 1-12.
- 69) Guttormsen M, Hjorth-Jensen H, Melby E, Rekstad J, Schiller A & Siem S, 2001, 'Heat capacity and pairing transition in nuclei', *Physical Review C*, Vol. 64, No. 034319, pp. 1-14.
- 70) Guttormsen M, Hjorth-Jensen M, Melby E, Rekstad J, Schiller A & Siem S, 2000, 'Energy shifted level densities in rare earth region', *Physical Review C*, Vol.61, No.067302, pp.1 – 4.
- 71) Hamamota Ikuko, 1983, 'Single-Particle and Collective Aspects of Rotating Nuclei', *Physica Scripta*, Vol. 5, No.T5, pp.10-15.
- 72) Hasegawa M, Kaneko K, Mizusaki T & Sun Y, 2007, 'Phase transition in exotic nuclei along the $N=Z$ line', *Physics Letters B*, Vol. 656, No.1-3, pp.51-55.
- 73) Henss S, Ruckelshausen A, Fischer R.D, Kuhn W, Metag V, Novotny R, Janssens R.V.F, Khoo T.L, Habs D, Schwalm D, Freeman D, Duchene G, Haas B, Haas F, Hlavac S & Simon R.S, 1988, 'Measurement of the Nuclear Level Density at High Spins', *Physical Review Letters*, Vol. 60, No. 1, pp.11-13.
- 74) Hersking B, 1986, *Nuclear structure at high spin, Heavy ion collisions*, NATO ASI Series (Series B : Physics), Vol.130, Springer, Boston, Plenum Press, Newyork.

- 75) Hossaina I, Mubaraka A.A, Sharradb F.I & Abdullahc H.Y, 2015, ‘Moments of inertia for even-even $^{120-124}\text{Te}$ isotopes’, Armenian Journal of Physics, Vol. 8, No.1, pp. 7-16.
- 76) Hua H, Wu C.Y, Cline D, Hayes A.B, Teng R, Clark R.M, Fallon P, Macchiavelli A.O & Vetter K, 2002, High-spin states in $^{103,105}\text{Mo}$, ^{103}Nb , and the $\nu_{h_{11/2}}$ alignment, Physical Review C, Vol. 65, No. 064325, pp. 1-5.
- 77) Huang Po-lin, Grim, S.M & Massey T.N, 2002, ‘Level densities for nuclei with $20 < A < 41$ ’, Physical Review C, Vol. 62, No.024002, pp. 1-12.
- 78) Huizenga, J.R & Moretto L.G, 1972, ‘Nuclear Level Densities’, Annual Review of Nuclear and Particle Science, Vol. 22, pp. 427-464.
- 79) Iachello F, Leviatan A, & Petrellis D, 2011, ‘Effect of a fermion on quantum phase transitions in bosonic systems’, Physics Letters B, Vol. 705, No.4, pp.375-378.
- 80) Ignatyuk A.V & , 1969, ‘Even-odd differences and structure of the fission barrier’, Physics Letters B, vol.29, No.3, pp.159-161.
- 81) Inglis D.R, 1954, ‘Particle derivation of nuclear rotation properties associated with a surface wave’, Physical Review, Vol. 96, No.4, pp.1059-1065.
- 82) Irvine, J.M, 1972, Nuclear Structure Theory, Pergamum Press, Oxford, New York, 1st Edition, pp.319.
- 83) Jian-You Guo, Peng Jiao, & Xiang-Zheng Fang, 2010, ‘Microscopic description of nuclear shape evolution from spherical to octupole-deformed shapes in relativistic mean-field theory’, Physical Review C, Vol. 82, No. 047301, pp. 1-4.
- 84) Jing-ye-zhang, Xu Y, Fossan D.B, Liang Y, Ma R & Paul E.S, 1989, ‘Nilsson parameter set in the $A \approx 120-140$ region’, Physical Review C, Vol.39, No.2, pp.714-716.

- 85) Johnson A, Ryde H, Sztarkier J, 1971, 'Evidence for a singularity in the nuclear rotational band structure', *Physics Letters B*, Vol.34, No.7, pp. 605 – 608.
- 86) Kaneko K & Schiller A, 2007, 'Particle number conservation in static – path approximation for thermal superfluid systems', *Physical Review C*, Vol.76, No.064306, pp.1 - 6.
- 87) Kanthimathi G, Boomadevi N & Rajasekaran T.R, 2011, 'Influence of quantal and statistical fluctuations on phase transitions in finite nuclei', *Communications in Theoretical Physics*, Vol. 56, No. 4, pp. 718-726.
- 88) Kargar Z & Dehghani V, 2013, 'Statistical pairing fluctuation and phase transition in ^{94}Mo ', *Journal of Physics G : Nuclear Particle Physics*, Vol.40, No.4, pp.1-8.
- 89) Kargar Z & Mosaleh F, 2011, 'Thermal Phase transition in $^{93-98}\text{Mo}$ nuclei', *Physica Scripta*, Vol. 83, No. 035201, pp.1-5.
- 90) Lagergren K, Cederwall B, Bäck T, Wyss R, Ideguchi E, Johnson A, Atac A, Axelsson A, Azaiez F, Bracco A, Cederkäll J, Dombrádi Z, Fahlander C, Gadea A, Million B, Petrache C.M, Rossi-Alvarez C, Sampson J.A, Sohler D & Weiszflog M, 2001, 'Coexistence of Superdeformed Shapes in ^{154}Er ', *Physical Review Letters*, Vol. 87, No.022502, pp.1 - 4.
- 91) Landau L.D & Lifshitz E.M, 1980, *Statistical Physics – Course of theoretical physics*, Vol.5, Institute of Physical Problems, USSR Academy of Sciences, Moscow, Pergamon Press, Oxford, 3rd revised edition.
- 92) Langanke K, D.J. Dean, P.B. Radha & S.M. Koonin, 1996, 'Temperature dependence of pair correlations in nuclei in the iron region', *Nuclear Physics A*, Vol.602, pp.244 - 262.

- 93) Langanke K, Maruhn, J. A. & Koonin, S. E, 1991, Computational Nuclear Physics I – Nuclear Structure, Springer - Verlag, Berlin Heidelberg, New York, Ist Edition.
- 94) Lauritzen B, Arve P & Bertsch G. F, 1988, ‘Nuclear Level Densities in the Static-Path Approximation’, Physics Review Letter, Vol. 61, No. 25, pp. 2835-2838.
- 95) Leander G, Nilsson B.S & Chen Y.S, 1976, ‘Nuclear Structure and the Quasi-Continuum Gamma Rays’, Physica Scripta, Vol. 24, pp:164-183.
- 96) Levit S, Alhassid Y & Wright A.W, 1984, ‘Phenomenology of shape transitions in hot nuclei’, Nuclear Physics A, Vol. 413, No.3, pp.439-474.
- 97) Li Jia Jie, Jerome Margueron, Wen Hui Long & Nguyen Van Giai, 2015, ‘Pairing phase transition: A finite – temperature relativistic Hartree – Fock – Bogoliubov study’, Physical Review C, Vol.92, No.014302, pp.1 – 13.
- 98) Li Z.P, Niksic T, Vretenar D, & Meng J, 2010, ‘Microscopic description of spherical to γ -soft shape transitions in Ba and Xe nuclei’, Physical Review C, Vol. 81, No.034316, pp. 1-22.
- 99) Li Z.P, Niksic T, Vretenar D, Meng J, Lalazissis G.A & Ring P, 2009, ‘Microscopic analysis of nuclear quantum phase transitions in the $N \approx 90$ region’, Physical Review C, Vol.79, No.054301, pp.1-14.
- 100) Liu L, Zhen-Hua Zhang & Peng – Wei Zhao, 2015, ‘Thermodynamics of pairing transition in hot nuclei’. Physical Review C, Vol. 92, No.044304, pp.1 - 7.
- 101) Liu S & Alhassid Y, 2001, ‘Signature of a pairing transition in the heat capacity of finite nuclei’, Physical Review Letter, Vol.87, No.022501, pp.1 - 4.
- 102) Maj A, Kmiecik M, Krolas W, Styczen J, Bracco A, Camera F, Million B, Gaardhøje J.J, Herskind B, Kicinska-Habior M, Kownacki J & Ormand W.E,

- 2001, 'Search for the Jacobi instability in rapidly rotating ^{46}Ti nuclei', *Acta Physica Polonica B*, Vol. 32, No.2433, pp. 1-7.
- 103) Mamta Agarwal & Mazumdar I, 2009, 'Deformation and shape transitions in hot rotating neutron deficient Te isotopes', *Physical Review C*, Vol.80, No.024322, pp. 1-7.
- 104) Melby E, Bergholt L, Guttormsen M, Hjorth – Jensen M, Ingebretsen F , Messelt S, Rekstad J, Schiller A, Siem S & Odegard SW, 1999, 'Observation of thermodynamical properties in the ^{162}Dy , ^{166}Er and ^{172}Yb Nuclei'. *Physical Review Letter*, Vol.82, No.16, pp.3150 - 3153.
- 105) Miller H.G, Cole B.J & Quick R.M, 1989, 'Evidence for phase transitions in finite systems', *Physical Review Letters*, Vol. 63, No.14, pp.1922-1925.
- 106) Miller H.G, Quick R. M & Cole B.J, 1989, 'Nuclear shape transitions at finite temperature', *Physical Review C*, Vol. 39, No.4, pp. 1599-1603.
- 107) Mocalj D, Rauscher T, Martinez – Pinedo, Langanke K, Pacearescu L, Faessier F K, Thielemann & Alhassid Y, 2007, 'Large scale prediction of the parity distribution in the nuclear level density and application to astrophysical reaction rates', *Physical Review C*, Vol.75, No.045805, pp.1-15,
- 108) Moller P & Nix, J. R, 1992, 'Nuclear pairing models', *Nuclear Physics A*, Vol. 536, No.1, pp. 20-60.
- 109) Moller P, Arnold J. Sierk, Ragnar Bengtsson, Hiroyuki Sagawa & Takatoshi Ichikawa, 2009, 'Global Calculation, of Nuclear Shape Isomers', *Physics Review Letters*, Vol.103, No.212501, pp.1-4.
- 110) Moller P, Nix J. R, Myers W.D & Swiatecki W. J, 1995, 'Nuclear Ground State Masses and Deformations at Data Nuclear Data Tables', Vol.59, pp.185-381.

- 111) Moretto L. G, 1971, 'Pairing correlation in excited nuclei with non-zero angular momentum', Physics Letters B, Vol. 35, No. 5, pp.379-382.
- 112) Moretto L. G, 1972, 'Statistical description of deformation in excited nuclei & disappearance of shell effects with excitation energy', Nuclear Physics A, vol.182, pp.641- 668.
- 113) Moretto L.G, 1972, 'Pairing fluctuations in excited nuclei and the absence of a second order phase transition', Physics Letters B, Vol.40, No.1, pp.1-4.
- 114) Moretto L.G., 1974, 'Influence of pairing and of the spin projection distribution on the Classical isothermal rotations of a nucleus'. Nuclear Physics A, Vol. 226, pp.9-30.
- 115) Nanal A.V, Back B.B, Hofman D.J, Hackman G, Ackermann D, Fischer S, Henderson D, Janssens R.V.F, Khoo T.L, Sonzogni A.A & Alhassid Y, 1999, 'Exclusive studies of the GDR in excited nuclei', Nuclear Physics A, Vol. 649, No.1-4, pp.153-156.
- 116) Nazarewicz W, Dudek J, Bengtsson R, Bengtsson T & Ragnarsson I, 1985, 'Microscopic study of the high - spin behaviour in selected $A \approx 80$ nuclei' Nuclear Physics, A, Vol. 435, No. 2, pp. 397- 447.
- 117) Neergard K & Pashkevich V.V, 1975, 'Shell corrections to the deformation energies of very high spin nuclei ($I \lesssim 100$)', Physics Letters B, Vol. 59, No.3, pp.218-222.
- 118) Neergard K, Pashkevich V.V. & Frauendorf S, 1976, 'Shell energies of rapidly rotating nuclei', Nuclear Physics A, Vol. 262, No.1, pp. 61-90.
- 119) Newton J.O, Sie S. H, Leigh J. R & Diamond R.M, 1981, 'Multiplicity of the statistical γ -rays following ($^{16}\text{O},xn$) reactions', Physics Review Letters, Vol.46, No. 6, pp.405 - 408.

- 120) Nguyen Dinh Dang & Nguyen Zuy Thang, 1990, 'Fluctuations in the thermal superfluid model for heated spherical nuclei'. *Journal of Physics G : Nuclear Particle Physics*, Vol.16, No.2, pp.231–244.
- 121) Nilsson S.G & Ragnarsson I, 2005, 'Shapes and Shells in Nuclear Structure. New York : Cambridge University Press', 1st print, pp.110-118.
- 122) Nilsson S.G, Chin Fu Tsang, Adam Sobiczewski, Zdzislaw Szymanski, Slawomir Wycech, Christer Gustafson, Inger-Lena Iamm, Peter molle & Bjorn Nilson, 1969, 'On the nuclear structure and stability of heavy and superheavy elements', *Nuclear Physics A*, Vol.131, No.1, pp.1-66.
- 123) Niu Y.F, Niu Z.M, Paar N, Vretenar D, Wang G.H, Bai J.S & Meng J, 2013, 'Pairing transitions in finite temperature relativistic Hartree – Bogoliubov theory', *Physical Review C*, Vol.88, No.034308, pp.1 - 8.
- 124) Nix J.R, 1972, 'Calculation of Fission Barriers for Heavy and Superheavy Nuclei', *Annual Review Nuclear Science*, Vol. 5525, No.22, pp. 65-120.
- 125) Nomura K, Rodríguez-Guzmán R & Robledo L.M, 2017, 'Structural evolution in germanium & selenium nucleus within the mapped interacting boson model based on the Gogny energy density functional', *Physical Review C*, Vol. 95, No. 064310, pp.1-15.
- 126) Nomura K, Rodríguez-Guzmán R, Humadi Y.M, Robledo L.M & Abusara H, 2017, 'Structure of krypton isotopes within the interacting boson model derived from the Gogny energy density functional', *Physical Review C*, Vol.96, No.034310, pp. 1-12.
- 127) Pathria R. K., 1972, *Statistical Mechanics*, Pergamon, Oxford, pp. 76, 159 & 195.

- 128) Poloszajctak M, Sandhya Devi K.R & Faessler Amand, 1977, 'Microscopic determination of energy surfaces at very high spin states', *Zeitschrift für Physik A Atoms and Nuclei*, Vol. 282, No.3, pp. 267-276.
- 129) Quentin P & Flocard H, 1978, 'Self consistent calculations of nuclear properties with phenomenological effective forces', *Annual Review of Nuclear Particle Science*, Vol.28, pp.523 – 594.
- 130) Rahmatinejad A, Razavi R & Kakavand T, 2015, 'Thermal quantities of ^{46}Ti ', *Nuclear Physics A*, Vol. 939, pp.46-52.
- 131) Rahmatinejad A, Razavi R & Kakavand T, 2016, 'Studying temperature dependence of pairing gap parameter in a nucleus as a small superconducting system', *International Journal of Modern Physics E*, Vol.25, No.8, pp.1 - 12.
- 132) Rajasekaran M, Arunachalam N, Rajasekaran T.R & Devanathan V, 1988, 'Shell effects in hot isobaric nuclei', *Physical Review C*, Vol.38, No. 4, pp. 1926 - 1981.
- 133) Rajasekaran M, Rajasekaran T.R & Arunachalam N, 1988, 'Nuclear level density parameter—its dependence on spin and temperature', *Physical Review C*, Vol.37, No. 1, pp.307-313.
- 134) Rajasekaran M, Rajasekaran T.R, Arunachalam N & Devanathan V, 1988, 'Neutron separation energy and emission probability at high spins', *Physical Review Letters*, Vol. 61, No. 18, pp. 2077-2080.
- 135) Rajasekaran T. R, Selvaraj S & Santhosh Kumar S, 2003, 'The phenomenon of nucleon emission at high angular momentum states of fused compound systems', *Pramana Journal of Physics*, Vol.60, No.1, pp.75-93.

- 136) Rajasekaran T.R & Kandhimathi G, 2008, 'Investigation on phase and shape transitions in the hot rotating nucleus ^{154}Dy ', European Physical Journal A, Vol. 35, pp.57-68.
- 137) Rajasekaran T.R & Kanthimathi G, 2008, 'A comparative study of superdeformation in the $A \approx 150$ and $A \approx 60$ nuclei', Acta Physica Polonica B, Vol. 39, No. 6, pp.1391-1404.
- 138) Ramamurthy V. S, Kapoor S. S & Kataria S. S, 1970, 'Excitation energy dependence of shell effects on nuclear level densities and fission fragment anisotropies', Physical Review Letters, Vol. 25, No.6, pp.386-390.
- 139) Rombouts S, Heyde K & Jachowicz N, 1998, 'Thermodynamical properties of a mean field plus pairing model and applications for the Fe nuclei', Physical Review C, Vol.58, No.6, pp.3295 - 3304.
- 140) Rossignoli R, Canosa N & Ring P, 1998, 'Thermal and quantal fluctuations for fixed particle number in finite superfluid systems', Physics Review Letters, Vol. 80, No.9, pp.1853 - 1856.
- 141) Rossignoli R, Canosa N & Ring P, 1999, 'Fluctuations and odd-even effects in small superfluid systems', Annals of Physics, Vol. 275, No.1, pp.1-26.
- 142) Saxena, M, Kumar R, Jhingan A, Mandal S, Stolarz A, Banerjee A, Bhowmik R.K, Dutt S, Kaur J, Kumar V, Modou Mbaye M, Sharma V.R & Wollersheim H.J, 2014, 'Rotational behavior of $^{120,122,124}\text{Te}$ ', Physical Review C, Vol.90, No.024316, pp.1-5.
- 143) Schiller A, Agvaanluvsan U, Algin, E, Bagheri, A, Chankova, R, Guttormsen M, Hjorth-Jensen M, Rekstad J, Siem S, Sunde A.C & Voinov A, 2005, 'Nuclear thermodynamics below particle threshold', AIP Conference Proceedings. Vol.777, No.1, pp.216-228.

- 144) Schiller A, Bjerve A, Guttormsen M, Hjorth – Jensen M, Ingebretsen F , Melby E , Messelt S, Rekstad J, Siem S & Odegard SW, 2001, ‘Critical temperature for quenching of pair correlations’, *Physical Review C*, Vol.63, No.021306(R), pp. 1-5.
- 145) Scholes, D.T, Cullen D.M, Kondev F.G, Janssens R.V.F, Carpenter M.P, Hartley D.J, Djongolov M.K, Sletten G, Hagemann G, Wheldon C, Walker P.M, Abu Saleem K, Ahmad I, Balabanski D. L, Chowdhury P, Danchev M, Dracoulis G. D, El-Masri H. M, Goon J, Heinz A, Kaye R. A, Khoo T. L, Lauritsen T, Lister C. J, Moore E. F, Riedinger L. L, Riley M. A, Seweryniak D, Shestakova I, Wiedenhöver I, Zeidan O & Jing-ye Zhang, 2004, ‘Highly deformed Bands in ^{175}Hf ’, *Physical Review C*, Vol.70, No.054314, pp.1-8.
- 146) Simpson J, 1988, ‘Nuclear shapes and phases at very high spin’, *Physica Scripta*, Vol. 23, pp. 37 - 42.
- 147) Sofia Karampagia & Vladimir Zelevinsky, 2017, ‘Nuclear shell model and phase transition’, *Proceedings of Nuclei and Mesoscopic Physics (NMP17)*; 2017 March 6 to 10; Michigan, USA.
- 148) Stephens F.S, Diamond R.M and Nilsson S.G, 1972, ‘A coupling scheme relevant to high angular momenta and intermediate nuclear deformations’, *Physics Letters B*, Vol.44, No.5, pp.429-432.
- 149) Strutinsky V. M, 1967, ‘Shell effects in nuclear masses and deformation energies’, *Nuclear Physics A*, Vol.95, No.2, pp.420-442.
- 150) Stuchberyet. A.E, Allmond J.M, Galindo-Uribarri A, Padilla-Rodal E, Radford D.C , Stone N. J, BatchelderJ. C, Beene J. R, Benczer-KollerN, Bingham C. R, Howard M. E, Kumbartzki G. J, Liang J. F, Manning B, Stracener D. W & Yu C.H, 2013, ‘Electromagnetic properties of the 2^+_1 state in ^{134}Te : Influence of

- core excitation on single-particle orbits beyond ^{132}Sn ', *Physical Review C*, Vol. 88, No. 051304, pp.1-5.
- 151) Sulaksono A, Mart T & Bahri C, 2005, 'Nilsson parameters κ and μ in relativistic mean field models', *Physical Review C*, Vol. 71, No.034312, pp.1-9.
- 152) Svensson C.E, Rudolph D, Baktash C, Bentley M.A, Cameron J.A, Carpenter M.P, Devlin M, Eberth J, Flibotte S, Galindo-Uribarri A, Hackman G, Haslip D.S, Janssens R.V.F, Lafosse D.R, Lampman T.J, Lee I.Y, Lerma F, Macchiavelli A.O, Nieminen J.M, Paul S.D, Radford D.C, Reiter P, Riedinger L.L, Sarantites D.G, Schaly B, Seweryniak D, Thelen O, Thomas H.G, Waddington J.C, Ward D, Weintraub W, Wilson J.N, Yu C.H, Afanasjev A.V & Ragnarsson I, 1999, 'Decay Out of the Doubly Magic Superdeformed Band in the N=Z Nucleus ^{60}Zn ', *Physical Review Letters*, Vol.82, No.17, pp. 3400-3403.
- 153) Svensson, C. E, Macchiavelli A. O, Juodagalvis A, Poves A, Ragnarsson I, Aberg S, Appelbe D. E, Austin R. A. E, Ball G. C, Carpenter M. P, Caurier E, Clark R. M, Cromaz M, Deleplanque M. A, Diamond R. M, Fallon P, Janssens R. V. F, Lane G. J, Lee I. Y, Nowacki F, Sarantites D. G, Stephens F. S, Vetter K, and Ward D, 2001, 'Lifetimes of superdeformed rotational states in ^{36}Ar ', *Physical Review C*, Vol. 63, No.061301, pp.1-5.
- 154) Svensson, C. E, Baktash C, Cameron J.A, Devlin M, Eberth J, Flibotte S, Haslip D.S, LaFosse D.R, Lee I.Y, Macchiavelli A.O, MacLeod R.W, Nieminen J.M, Paul S.D, Riedinger L.L, Rudolph D, Sarantites D.G, Thomas H.G, Waddington J.C, Weintraub W, Wilson J.N, Afanasjev A.V and Ragnarsson I, 1997, 'Observation and Quadrupole-Moment Measurement of the First Superdeformed

- Band in the A~60 Mass Region', Physical Review Letters, Vol. 79, No.7, pp. 1233-1236.
- 155) Szymanski Z, 1983, Fast Nuclear Rotation, Clarendon Press, Oxford.
- 156) Tanabe S.K and Akito Arima ,1982, 'Particle pairs in the cranked Hartree-Fock-Bogoliubov approximation and the interacting boson model', Physics Letters, B Vol. 110, No. 2, pp. 87-91.
- 157) Tanabe S.K, Tanabe K, & Mang H.J, 1981, 'Theory of the cranked temperature-dependent Hartree-Fock-Bogoliubov approximation and parity projected statistics', Nuclear Physics A, Vol. 357, No. 1, pp. 20-44.
- 158) Tanabe, K & Sugawara-Tanabe, K 1982, 'Phase transitions along and off the yrast line', Nuclear Physics A, Vol.390, No.3, pp. 385-412.
- 159) Tavukcu E, 2002, 'Ph.D. thesis – Level densities and radiative strength functions in ^{56}Fe and ^{57}Fe ', North Carolina State University.
- 160) Varley B. J, Campbell M, Chishti A.A, Gelletly W, Goettig L, Lister C. J, James A.N & Skeppstedt O, 1987, 'Evidence for Shape Coexistence in the N = Z Nucleus Kr_{36} ', Physics Letters B, Vol. 194, pp.463 – 467.
- 161) Vikas Kumar, Srivastava P.C, Ermamatov M.J & Irving O Morales, 2015, 'Analysis of proton and neutron pair breakings: High-spin structures of $^{124-127}\text{Te}$ isotopes', Nuclear Physics A, Vol. 942, pp. 1-17.
- 162) Werner V, Pietralla N, Von Brentano P, Casten R.F & Jolos R.V, 2000, 'Quadrupole shape invariants in the interacting boson model', Physical Review C, Vol. 61, No.021301, pp.1-10.
- 163) Yu C. H, Baktash C, Dobaczewski J, Cameron J.A, Chitu C, Devlin M, Eberth J, Galindo-Uribarri A, Haslip D.S, Lafosse D.R, Lampman T.J, Lee I.Y, Lerma F, Macchiavelli A.O, Paul S.D, Radford D.C, Rudolph D, Sarantites D.G,

Svensson C.E, Waddington J.C & Wilson J.N, 1999, 'Comparison of superdeformed bands in ^{61}Zn and ^{60}Zn : Possible evidence for $T = 0$ pairing', Physical Review C, Vol. 60, No.031305, pp.1-5.

164) Zelevinsky V, Brown B. A, G Frazier N & Horoi M, 1996, 'The nuclear shell model as a testing ground for many-body quantum chaos', Physics Reports, Vol. 276, No.2-3, pp.85-176.